MICROCOPY RESOLUTION TEST CHART
NATIONAL BUREAU OF STANDARDS-1963-A

AD-A189 156

DNA-TR-86-169

INVESTIGATION OF THE CREDIBILITY OF IN-SITU MEASUREMENTS OF RADIAL AND TANGENTIAL STRESS IN A SALT TEST BED

D. D. Keough, et al.
SRI International
333 Ravenswood Avenue
Menlo Park, CA 94025-3493

DTIC
ELECTE
DEC 0 8 1987
S D
D

31 May 1986

Technical Report

CONTRACT No. DNA 001-82-C-0248

Prepared for
Director
DEFENSE NUCLEAR AGENCY
Washington, DC 20305-1000

87 11 2.0 1

DISTRIBUTION LIST UPDATE

This mailer is provided to enable DNA to maintain current distribution lists for reports. We would appreciate your providing the requested information.

☐ Add the individual listed to your distribution list.

☐ Delete the cited organization/individual.

☐ Change of address.

NAME: _____

ORGANIZATION: _____

OLD ADDRESS	CURRENT ADDRESS
_____	_____
_____	_____
_____	_____

TELEPHONE NUMBER: ( ) _____

SUBJECT AREA(s) OF INTEREST:

_____	_____
_____	_____
_____	_____

DNA OR OTHER GOVERNMENT CONTRACT NUMBER: _____

CERTIFICATION OF NEED-TO-KNOW BY GOVERNMENT SPONSOR (if other than DNA):

SPONSORING ORGANIZATION: _____

CONTRACTING OFFICER OR REPRESENTATIVE: _____

SIGNATURE: _____

Director
Defense Nuclear Agency
ATTN: ▮▮▮ TITL
Washington, DC 20305-1000

REPORT DOCUMENTATION PAGE

1a. REPORT SECURITY CLASSIFICATION UNCLASSIFIED		1b. RESTRICTIVE MARKINGS		
2a. SECURITY CLASSIFICATION AUTHORITY N/A since Unclassified		3. DISTRIBUTION / AVAILABILITY OF REPORT Approved for public release; distribution is unlimited.		
2b. DECLASSIFICATION / DOWNGRADING SCHEDULE N/A since Unclassified				
4. PERFORMING ORGANIZATION REPORT NUMBER(S) SRI Project PYU-4460		5. MONITORING ORGANIZATION REPORT NUMBER(S) DNA-TR-86-169		
6a. NAME OF PERFORMING ORGANIZATION SRI International	6b. OFFICE SYMBOL (If applicable)	7a. NAME OF MONITORING ORGANIZATION Director Defense Nuclear Agency		
6c. ADDRESS (City, State, and ZIP Code) 333 Ravenswood Avenue Menlo Park, CA 94025-3493		7b. ADDRESS (City, State, and ZIP Code) Washington, DC 20305-1000		
8a. NAME OF FUNDING / SPONSORING ORGANIZATION	8b. OFFICE SYMBOL (If applicable) SPSS/Couch	9. PROCUREMENT INSTRUMENT IDENTIFICATION NUMBER DNA 001-82-C-0248		

8c. ADDRESS (City, State, and ZIP Code)	10. SOURCE OF FUNDING NUMBERS			
	PROGRAM ELEMENT NO	PROJECT NO	TASK NO	WORK UNIT ACCESSION NO
	62715H	Y99QAXS	A	DH007070

11. TITLE (Include Security Classification)
INVESTIGATION OF THE CREDIBILITY OF IN-SITU MEASUREMENTS OF RADIAL AND TANGENTIAL STRESS IN A SALT TEST BED

12. PERSONAL AUTHOR(S)
Keough, D. D.; DeCarli, P.; Florence, A. L.; Mak, R.; Walter, D. F.; Rosenberg, J. T.

13a. TYPE OF REPORT Technical	13b. TIME COVERED FROM 820519 TO 851231	14. DATE OF REPORT (Year, Month, Day) 860531	15. PAGE COUNT 105

16. SUPPLEMENTARY NOTATION
This work was sponsored by the Defense Nuclear Agency under RDT&E RMSS Code B344083466 Y99QAXSA00053 H2590D.

17.	COSATI CODES		18. SUBJECT TERMS (Continue on reverse if necessary and identify by block number)
FIELD	GROUP	SUB-GROUP	Ytterbium Piezoresistant Gages HE Test in Salt
08	13		Radial and Tangential Stresses Inclusion Calculations
18	03		In-situ Stress Measurements

19. ABSTRACT (Continue on reverse if necessary and identify by block number)

Eighteen ytterbium piezoresistant sensors in nine Teflon-steel flatpack stress gage-salt core assemblies were fielded in a spherical HE test in a salt medium. The objective was to examine the credibility of in-situ stress measurements by comparing measured stress with stress inferred from independent particle velocity measurements and with stress from computational simulations of the experiment.

Criteria for gage emplacement were examined by finite element computational simulation of the emplacement configuration. This simulation indicated that two critical parameters that influence the relationship between free-field stress and the stress in the core at the plane of the stress gage are the bonding of the cores to the native salt and the size of the gage relative to core diameter.

Static loading calibration of the stress gages yielded a response essentially the same as static calibrations of ytterbium in uniaxial strain loading. Unloading calibration of the

20. DISTRIBUTION / AVAILABILITY OF ABSTRACT ☐ UNCLASSIFIED/UNLIMITED ☒ SAME AS RPT. ☐ DTIC USERS	21. ABSTRACT SECURITY CLASSIFICATION UNCLASSIFIED	
22a. NAME OF RESPONSIBLE INDIVIDUAL Sandra E. Young	22b. TELEPHONE (Include Area Code) (202) 325-7042	22c. OFFICE SYMBOL DNA/CSTI

DD FORM 1473, 84 MAR   83 APR edition may be used until exhausted.   SECURITY CLASSIFICATION OF THIS PAGE
All other editions are obsolete.   UNCLASSIFIED

,cccu ~: Omega/Cmin MPa ,

19. ABSTRACT (Continued)

gages showed no hysteresis, unlike the uniaxial strain response of ytterbium foil.
A gage sensitivity of 0.05 x 10⁻⁴ Ω/Ω/MPa was found to represent the loading and
unloading data and was used to convert the experiment waveforms to stress histories.

The experiment produced radial stress histories that are characterized by a slowly
rising compression, often containing a precursor of approximately 10 bars (1 MPa),
a larger main wave peak of 90 to 350 bars, (9 to 35 MPa), and a release wave to an
apparent tensile stress of 30 to 40 bars, (3 to 4 MPa). Positive offset hysteresis
usually observed with ytterbium-steel flatpacks at somewhat higher peak stresses
was not seen. The loading portions of the observed waveforms were reproducible,
consistent, and reliable enough to be used in determining stress gradients and
differences. The combination of multiple differential amplifiers for noise sup-
pression and a low noise environment in the salt bed permitted the use of DC
rather than pulsed gage power and yielded low noise signals, 2 bars equivalent
(200 kPa).

Because of the unusually high quality of the waveforms obtained in this experiment
and because of the high integrity of the medium, we recommend that posttest gage
locations and orientations be determined and that the comparison of stress gradient,
stress difference, and velocity be completed. Successful completion of this effort
will provide the ground motion community with the only experimental assessment of
the validity of in-situ stress measurement in divergent flow, particularly tangen-
tial stress measurements.

Accession For

NTIS CRA&I   ☑
DTIC TAB   ☐
Unannounced   ☐
Justification

By
Distribution/

Availability Codes

Dist | Avail and/or
     | Special

A-1

DTIC
COPY
INSPECTED
4

SUMMARY

Eighteen ytterbium piezoresistant sensors in nine Teflon-steel flatpack stress gage-salt core assemblies were fielded in a spherical HE test in a uniform natural salt medium. The objective was to examine the credibility of <u>in-situ</u> stress measurements by comparing measured stress with (1) the stress calculated from measured particle velocity flow parameters through the equations of motion for spherical flow and (2) the stress from wave propagation calculations based on assumed constitutive relations for salt.

Gage-core emplacement criteria for maximizing the accuracy of free-field stress measurement were examined by finite element computational simulation of the emplacement con:f· uration. This simulation indicated that bonding of the cores to the native salt and the gage size relative to the core diameter are two critical parameters that influence the relationship between free-field stress and the stress in the core at the planes of the stress gages.

Static loading calibration of the stress gages yielded a response essentially the same as static calibrations of ytterbium foil in uniaxial strain loading. Unloading calibration of the gages showed no hysteresis, unlike the uniaxial strain response of ytterbium foil. A gage sensitivity of $0.054 \pm 10\%$ $\Omega/\Omega/\text{kbar}$ was found to represent the loading and unloading data and was used to convert the experiment waveforms to stress histories.

The combination of multiple differential amplifiers for noise suppression and a low noise environment in the salt bed permitted the use of DC rather than pulsed gage power and yielded low noise (2 bars, or 200 kPa, equivalent) signals. The stress histories determined from these signals using the cited calibration procedures were characterized by a slowly rising compression, often containing a precursor of approximately 10 bars (1 MPa), a larger main wave peak of between 90 and 350 bars (9 and 35 MPa), and a release to an apparent tensile stress of from 30 to 100 bars (3 to 10 MPa). Positive offset hysteresis usually observed with ytterbium-steel flatpacks stressed to somewhat higher peak stresses was not seen.

The loading portions of the observed waveforms were reproducible and consistent and were judged to be reliable enough to be used in determining stress gradients and differences. The unloading portions of the stress histories, particularly the tensile stress portion, were judged to be not credible. Consistency of time-of-arrival data was assumed and used to estimate actual gage locations, which differed from planned locations by as much as 1.25 m at a nominal radial distance of 6 m.

Lack of consistency of peak stress as functions of range and gage orientation forced the conclusion that the uncertainty in gage orientation was considerably larger than that estimated during gage installation, and compromised the primary experiment objectives--correlation of the stress and velocity data through the equations of motion and also with the calculated stresses.

Because of the unusually high quality of the waveforms obtained in this experiment and because of the high integrity of the medium, we recommend that posttest gage locations and orientations be determined and that the comparison of stress gradient, stress difference, and velocity be completed. Successful completion of this effort will provide the ground motion community with the only experimental assessment of the validity of in-situ stress measurement in divergent flow, particularly tangential stress measurement.

PREFACE

TABLE OF CONTENTS

LIST OF ILLUSTRATIONS (Concluded)

LIST OF TABLES

SECTION 1

INTRODUCTION

1.1 BACKGROUND.

The measurement of free-field, in-situ dynamic stress in soils and rocks is an important element in many Defense Nuclear Agency basing studies. Although many types of soil gages and emplacement methods have been studied and used, the inaccuracy caused by perturbation of the local stress by the gage and emplacement materials has been quantified for only very restricted stress ranges, material properties, and geometries, primarily for planar, high-modulus inclusions (gage and coupling material) under static, uniaxial strain, elastic loading with a slip boundary between the inclusion and surrounding medium. For this restricted case, the stress normal to the plane of the inclusion is within <5% of the free-field stress. However, we need to determine whether these results can be applied to the inelastic, triaxial strains encountered in most basing studies. In addition, the validity of measuring tangential stress has never been shown.

To address the measurement of in-situ, dynamic stress, SRI has formulated a combined computational and experimental program (Appendix A). The goal of this program is to provide a predictive capability for assessing the credibility of in-situ stress measurements in divergent flows and at stress ranges where material strengths affect the measurement. The program consists of four elements:

(1) Establishing accuracy requirements for specific applications of the stress data, e.g., material modeling, structure load definition.

(2) Developing and validating a computational model for relating inclusion stress to free-field stress.

(3) Developing hardware (gages and emplacement methods) to minimize local stress perturbations as determined by the computational model.

(4) Performing laboratory and field validation experiments under uniaxial strain and also divergent flows.

Various portions of this program have been addressed in previous efforts. Under Contract DNA001-76-C-0113, SRI performed an error analysis for planar and divergent flows. The effect of random and systematic errors of measurement on the determination of the flow field was examined using the SRI Lagrange Analysis for Stress and Strain (LASS) technique.[1] In an SRI-sponsored project,[2] a method of treating inclusion boundaries was incorporated into a finite element code, and a limited parameter study was conducted to evaluate the relation between inclusion and free-field stress and various boundary conditions and material properties. Under

1

Contract DNA001-80-C-0142, SRI developed a high-modulus, high-aspect-ratio stress gage and tested it under uniaxial strain loading in a sand test bed.[3] The satisfactory results of these tests encouraged the extension of the emplacement methods to divergent flows (CIST 23). However, results of this divergent flow test were inconclusive, primarily because unexpected geologic inhomogeneities at the CIST 23 site prevented duplication of the gage emplacement techniques. Lack of reproducibility in stress histories was attributed to the influence of geologic layering on the flow field.

1.2 OBJECTIVE.

The objective of the current in-situ measurement program was to evaluate the credibility of stress measurement using state-of-the-art methods in a test in which the effects of geologic anisotropies and inhomogeneities would be eliminated. A unique opportunity was presented by a series of high explosive (HE) tests sponsored by the Defense Advanced Research Projects Agency (DARPA) in a homogeneous and isotropic salt dome. In these tests, the velocity flow field and wave symmetry were being measured independently. These data permit an evaluation of the credibility of stress measurement by comparing the stress parameters (stress gradient, radial and tangential stresses) with the mass motion (velocity) through the momentum conservation equation

$$-\rho \left(\frac{\partial u_r}{\partial t}\right)_h = \left(\frac{\partial \sigma_r}{\partial h}\right)_t + \frac{2(\sigma_r - \sigma_\theta)}{r} \tag{1}$$

where u_r is radial particle velocity

ρ is mass at time t

h is Lagrangian distance

t is time

σ_r, σ_θ are radial stress and tangential stress.

As can be seen from this equation, acceleration must correlate with the sum of (1) the radial stress gradient and (2) the difference between the radial and tangential stresses; i.e., the stresses are not uniquely determined from the velocity data in divergent flow. However, the consistency of the stress component measurements can be assessed by comparing the stress and velocity data.

2

1.3 PROGRAM.

The research program undertaken to accomplish our objective consisted of the following four elements:

(1) Computations

- Modeling of the proposed gage installation geometry by finite element (NIKE CODE) calculations.

- Modeling of the proposed HE test in salt by wave propagation calculations (PUFF finite difference code).

(2) Laboratory tests

- Calibration of stress gages.

- Measurement of strength of materials.

(3) Development and implementation of field techniques

- Design and construction of gage assemblies, installation procedures and equipment, and recording equipment.

(4) Data reduction and analysis.

The following sections present the results obtained for each of these program elements. Section 6 gives our overall conclusions and recommendations.

SECTION 2

COMPUTATIONS

2.1 COMPUTATIONAL ANALYSIS OF STRESS PERTURBATION DUE TO GAGE EMPLACEMENT.

To evaluate the effect of various controllable emplacement parameters on the in-situ measurements, we performed finite element calculational simulations of the response of a proposed installation design to stress wave loading. The results of these calculations were used as general guides and were not intended as a means of inferring free-field stress from the measurements.

The configuration of the proposed HE experiment in salt is shown in Figure 1(a) and (b). A chamber containing the explosive was located at the bottom of a 62-m hole drilled vertically from a mining chamber in the salt bed. This geometry required installing the gages as shown, i.e., at the bottom of 62-m vertical drill holes. To minimize the effect of the holes on the free-field stress, we proposed to use gage-salt core assemblies at the bottom of the holes and powdered salt filler above the gages.

The gage-salt core formed a cylindrical inclusion, Figure 1(c), that could perturb the local stresses. Because previous calculations[2] of cylindrical inclusions had indicated that the boundary conditions strongly influence the stress distribution in the cylindrical inclusion, we performed a finite element analysis of our configuration, specifically to examine the degree of bonding required between the core and native salt. We did not treat the effect of the gage, which formed an additional inclusion. Criteria for gage characteristics and emplacement parameters were taken from past studies of soil stress measurement and from a recent analysis by Florence,[4] in which it was determined that thin unbonded planar inclusions of higher compressive modulus than the surrounding medium perturb the free-field stress by < 5%; i.e., the stress normal to the plane of the inclusion is essentially the same as the free-field stress. In our calculations, therefore, we examined the stress perturbations at the planes of measurement, normal and parallel to a radial to the source. These planes were positions of gages oriented to measure radial and tangential stresses, respectively.

Before discussing the numerical results, we describe the material models, finite element model, and interface model.
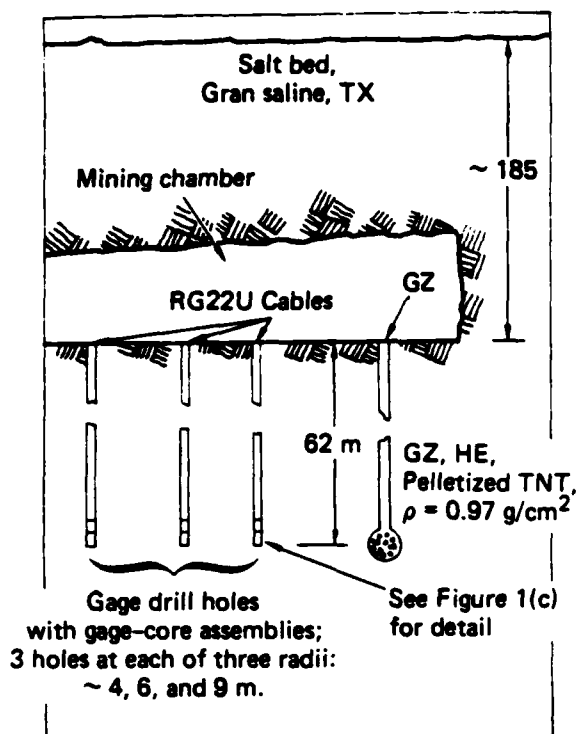
(a) Elevation view
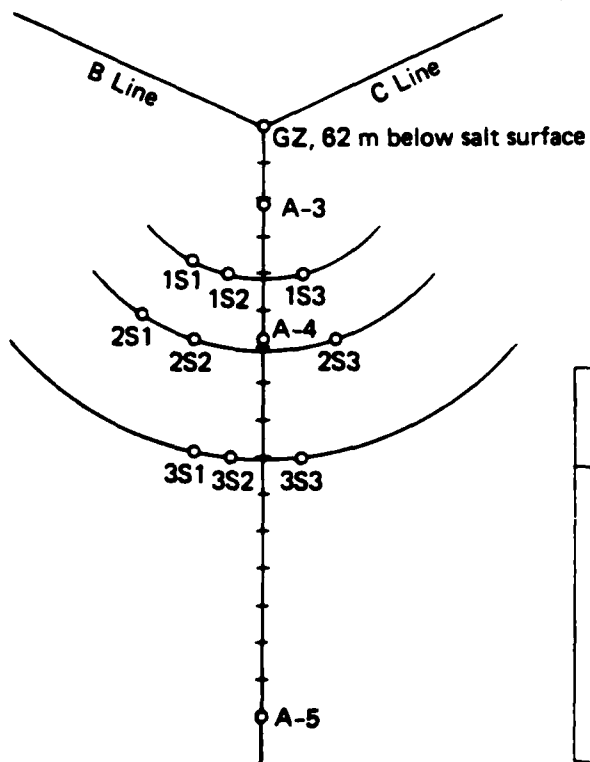
(b) Plan view
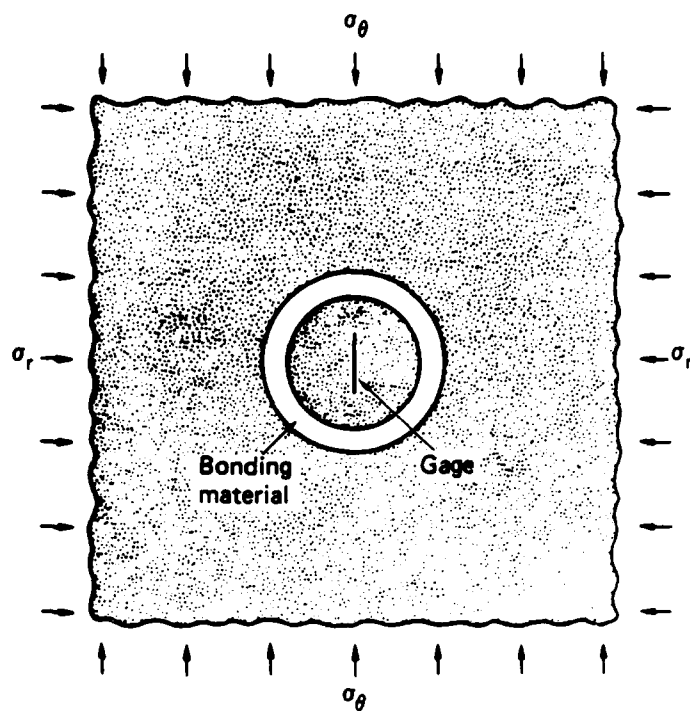
(c)

Range (m)	Depth (m)	Hole No.	Gage No.	Measure	Calc. Peak Stress (MPa)	
					σ_r	σ_θ
4.21	62	1S1	10	σ_θ		3.0
	62	1S2	6	σ_θ		3.0
	62	1S3	8	σ_r	29	
6.17	62	2S1	128	σ_θ		2.0
	62	2S2	11	σ_r	17.5	
	62	2S3	4	σ_r	17.5	
9.07	62	3S1	7	σ_θ		1.0
	62	3S2	1	σ_r	12.5	
	62	3S3	2	σ_r	12.5	

JA-4460-1

Figure 1.   The HE/salt experiment--overall configuration and stress gage information.

5

2.1.1 Material Model.

The salt model was extracted from the work of Gupta and Privitzer,[5] where salt was described as elastic-ductile plastic with strain-hardening (Figure 2), no dilatancy, and low porosity. The low stresses expected at the proposed gage locations allowed considerable simplification of the material model. The applicable pressure-volume relationship in loading, from Reference 6 is shown in Figure 3. The bulk modulus ranges from 11.7 to 16.3 GPa (117 to 163 kbar). The unloading bulk modulus varies linearly from 12.0 to 11.7 GPa (137 kbar) for loading and unloading. Reference 5 gives a ratio of 0.6 between shear and bulk moduli, which corresponds to a Poisson's ratio of 0.25, and a Young's modulus (E) of 20 GPa (200 kbar). A summary of our salt properties is listed in Table 1.

Table 1. Material properties of salt and epoxy.

	Salt	Epoxy (PMMA)
Young's modulus (E)	20 GPa (200 kbar)	5.50 GPa (53.5 kbar)
Poisson's ratio (μ)	0.25	0.37
Yield stress (γ)	25.4 MPa (0.254 kbar)	252 MPa (2.52 kbar)
Hardening modulus (ET)	5.4 GPa	0
Density (ρ)	2.14 g/cm^3	1.18 g/cm^3

The annulus material proposed to bond the salt cores to the native salt was a slow-curing epoxy. For our material model of epoxy, we assumed that its properties would be similar to PMMA for which considerable data existed and a model had been derived.[6] Table 1 also lists the epoxy (PMMA) properties. A perfectly plastic von-Mises material model was used. A yield stress of 152 MPa was obtained from Maiden and Green.[7]

2.1.2 Finite Element Model of Salt-Core Inclusion.

Figures 4 and 5 show the finite element mesh. Because of symmetry, only one-fourth of the gage-core assembly was modeled (Figure 5). The grid extended to 10 times the radius of the core inclusion (Figure 4). Four node plane-strain quadrilateral elements were used. Stresses of interest in the core were those normal to the x and y axes, i.e., the stresses normal to the stress gages in these
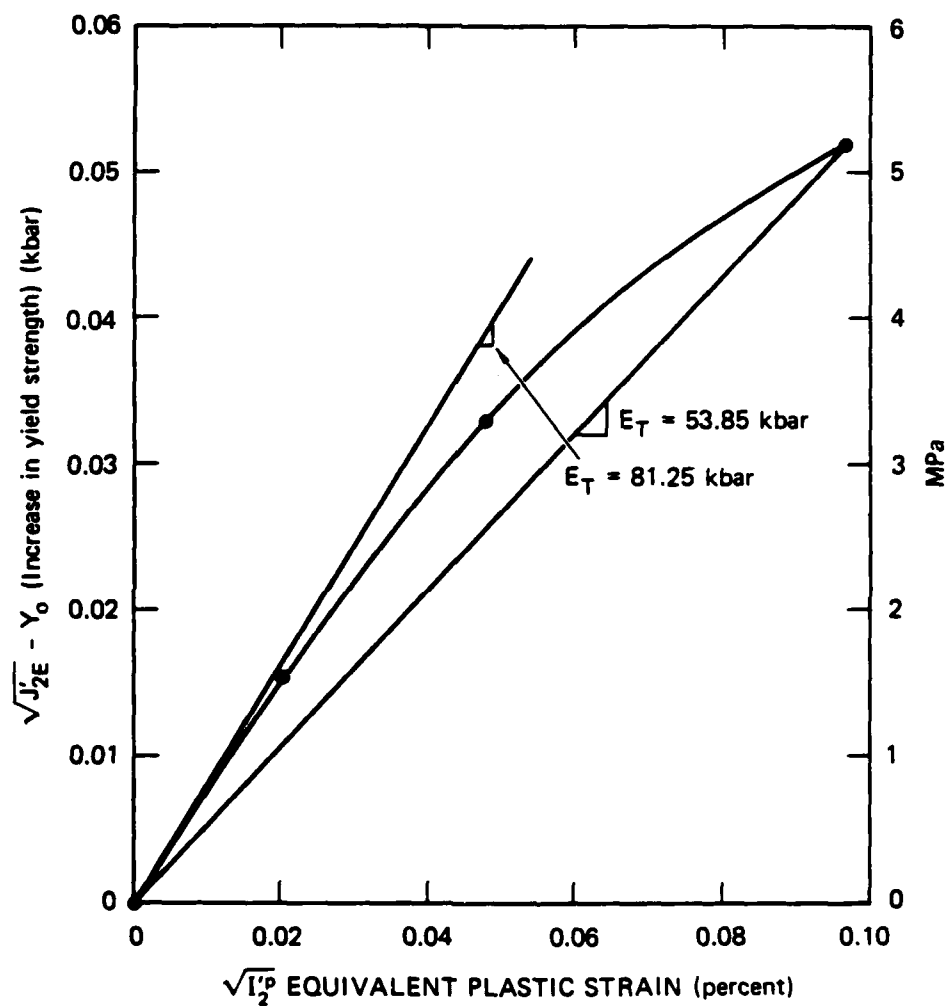
Figure 2.   Strain hardening curve for salt.
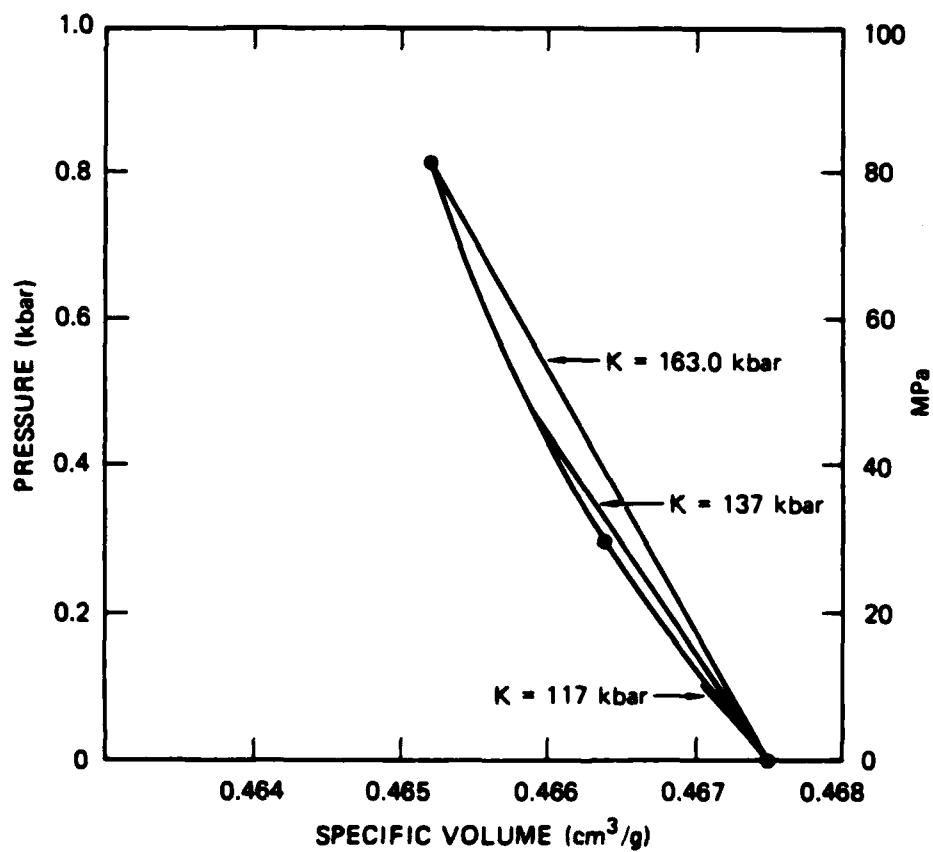
JA-314532-10A

Figure 3.   Pressure-specific volume curve for salt.

8

Figure 4.   Finite element mesh.
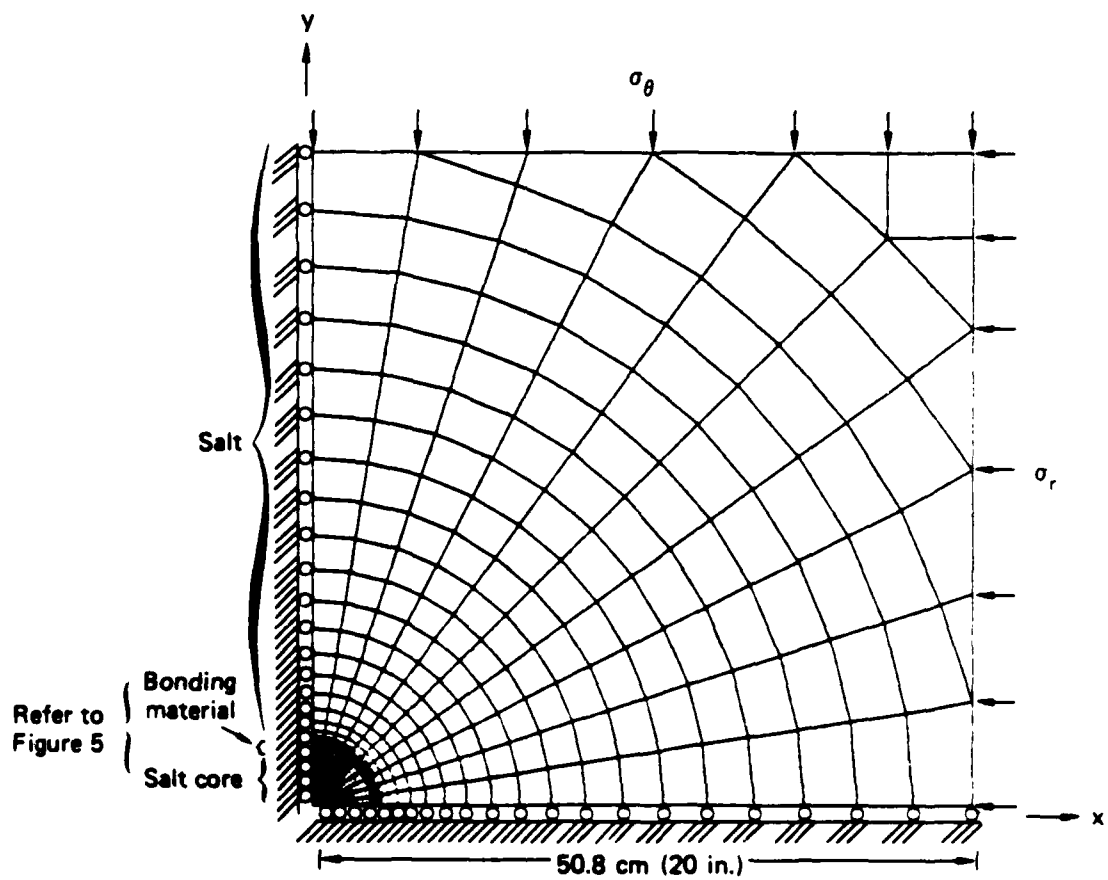
JA-314532-12A
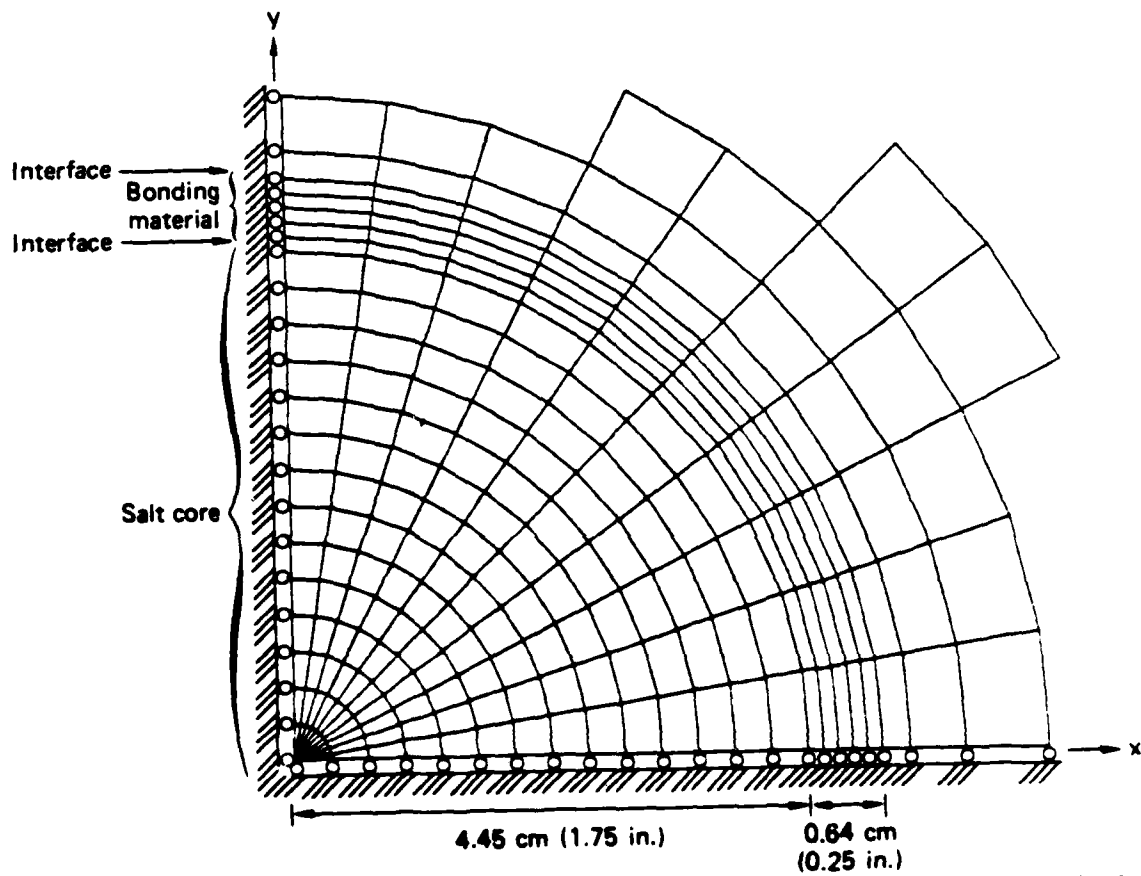
Figure 5.   Finite element mesh--central core.

JA-314532-13A

10

planes. As noted previously, our analysis did not treat the gage as a separate inclusion.

The two-dimentional plane-strain model implies an infinitely long inclusion normal to the plane. Although there is more confinement in the plane-strain model than in the actual three-dimensional test configuration, the plane-strain model provided a practical way to obtain approximate results within a reasonable time and budget.

For numerical stability and accuracy in any dynamic modeling (wave propagation analysis), the integration time step size is controlled by wave transit time across the stiffest element. Wave propagation analyses of the response of materials nearly matched to each other in density, and where the period of the loading wave is long compared with the time steps, have shown that a quasi-static analysis gives reasonable estimates of the dynamic response. In our finite element model, the controlling time step size was 0.166×10^{-3} s. The period of the loading wave was expected to be about 1000×10^{-3}, requiring 6000 time steps or approximately 30 hours on a VAX 11/780 computer. To keep the computer time manageable and because of the results of the wave propagation analogy, we based the present investigation on a quasi-static analysis.

2.1.3 Interface Model.

To bound the probable field conditions, we investigated two core-medium interface conditions (bonded and free-sliding) and compared their influence on x and y stresses. The bonded interface transfers both compressive and shear loads, whereas the free-sliding interface transfers only compressive loads; tensile loads were not considered because typical geologic materials have low tensile strengths.

The perfectly bonded interface was described by the usual finite node-element connectivity. The free-sliding interface was modeled by a layer of two-dimensional Mohr-Coulomb quadrilateral elements to transfer compressive loads; the elements were made weak in shear to eliminate almost entirely the transfer of shearing stress. The model was developed by replacing two thin annuli of the bonding material (at the inner and outer circumferences of this material) with the weak Mohr-Coulomb elements. With two such interfaces, the thickness of the bonding material between them was 0.38 cm (Figure 5). Young's modulus and Poisson's ratio of the Mohr-Coulomb layer were the same as the average of the surrounding material. Numerical tests indicated that a cohesion value of 0.1 MPa and a friction angle of 0.1 degree were satisfactory to represent slip.

11

To investigate the adequacy of the weak Mohr–Coulomb layer, we calculated stresses for the configuration shown in the grid of Figures 4 and 5 (but with the inner sliding interface) and compared our results with the elastic analytical solution values. A comparison of normal stresses (Mohr–Coulomb versus analytical) for an applied stress of 0.1 kbar (1.0 MPa) (elastic state), shown in Figure 6, indicates that the Mohr–Coulomb model adequately represents the free–sliding interface, especially for the central region of the core.

Stresses at the interface for the two cases are shown in Figure 7. Normal stresses compared well, but the finite element model with a Mohr–Coulomb layer generated a small shearing stress. Examination of the shearing stress distribution along a radius, shown in Figure 8 (solid curve), revealed that there was a large change in slope at the interface ($r/r_1 = 1.0$), and suggested that a finer finite element spatial discretization was required for an accurate representation. A finer, but practical discretization was used to obtain the shearing stress of Figure 8 (dashed curve). The values plotted are for the centers of the elements; therefore, the interface shear, by extrapolation on either side, is lower than that shown in Figure 8.

2.1.4 Numerical Results.

Given the adequacy of the Mohr–Coulomb representation of a free–sliding interface in elastic deformation, we applied the model to elastic and elasto–plastic deformation. Two sets of calculations were made. The first, with $\sigma_r/\sigma_\theta = 4$ and a peak σ_r of either –50 MPa (0.5 kbar) (elastoplastic) or –20 MPa (0.2 kbar) (elastic) assessed the effect of the interface in the elastic and in the elasto–plastic regimes. The second set used σ_r and σ_θ histories obtained from the PUFF calculation of the HE/SALT test and had the same implications for the measurements as the first; this second set is not presented here.

Ratios between x and y stresses and the corresponding free–field stresses (σ_r and σ_θ) from the first set of calculations ($\sigma_r/\sigma_\theta = 4$) for the elastic and elasto–plastic regimes are shown for the free–sliding interface in Figure 9 and for the bonded interface in Figure 10. For the elasto–plastic case, extensive yielding occurred for both interface conditions. For the free–sliding interface, the x stress (larger component) matches the free–field closer than the y stress.

The calculations contain three significant conclusions:

(1) The ratio of σ_x/σ_r is within 15% of an ideal value of 1.0 along the x plane over the central portion of the core [x $\leq$ (core radius)/2]

12
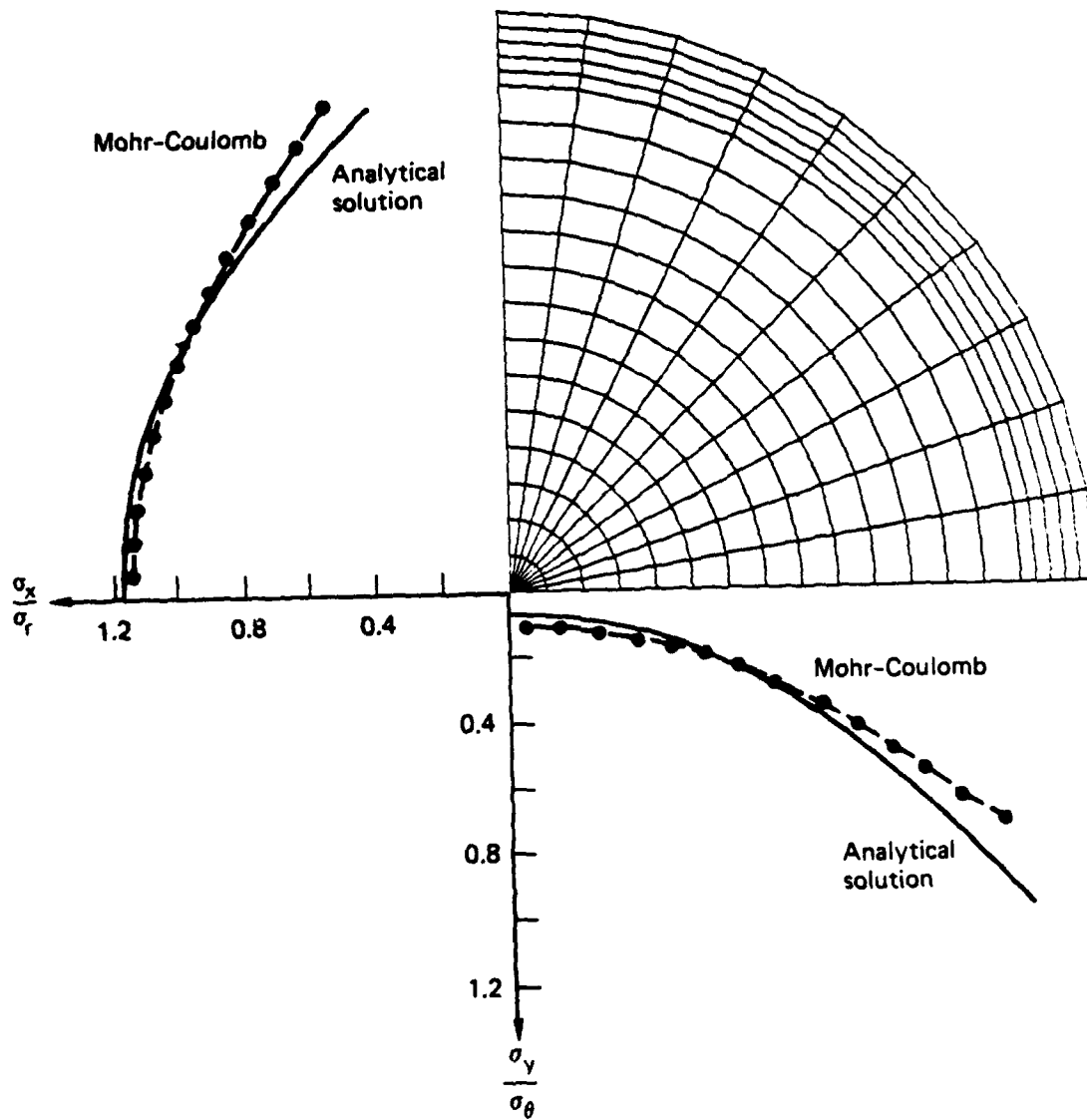
Figure 6. Comparison of Mohr-Coulomb solution against exact solution--
stresses distributions along gage planes.

1.2

1.0

0.8

$\dfrac{\sigma_{\text{interface}}}{\sigma_r}$ 0.6

0.4

0.2

0

—— Analytical solution

--- Finite element solution

Normal stress

Shearing stress

σ_θ

Normal stress

Shearing stress

σ_r

0   20   40   60   80   100

θ (degrees)
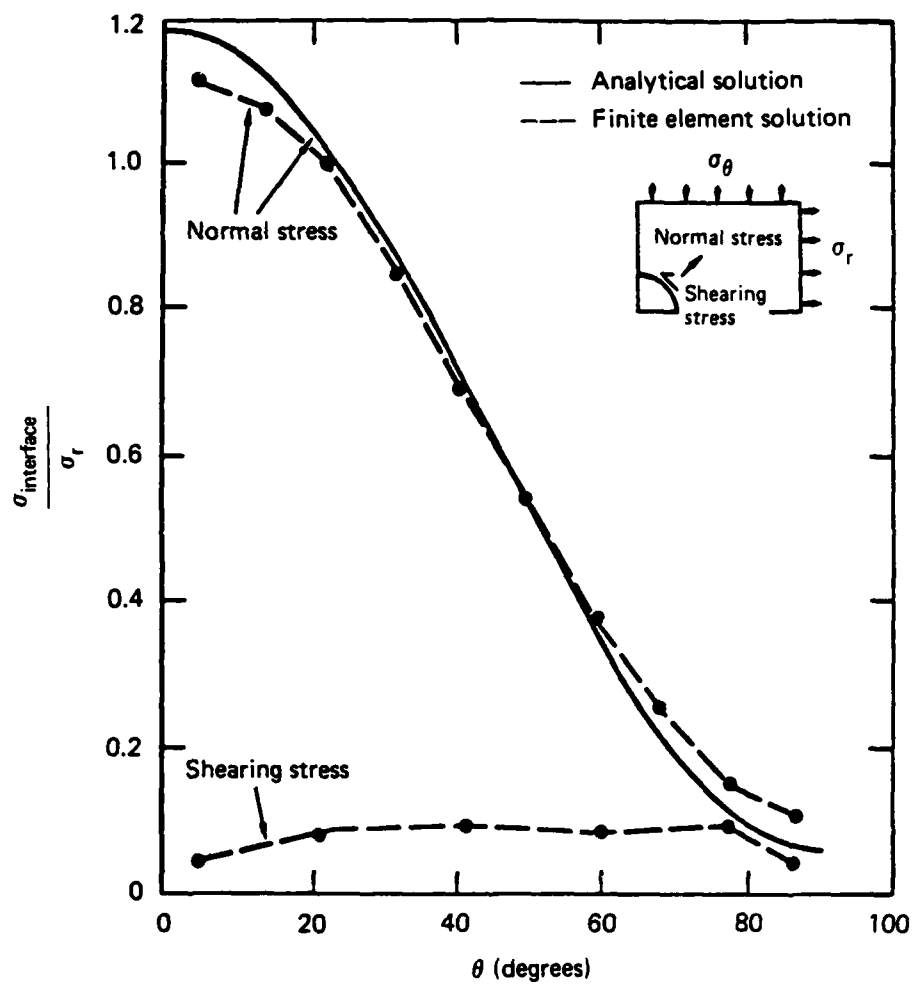
JA-314532-15A

Figure 7. Comparison of Mohr–Coulomb solution against exact solution--
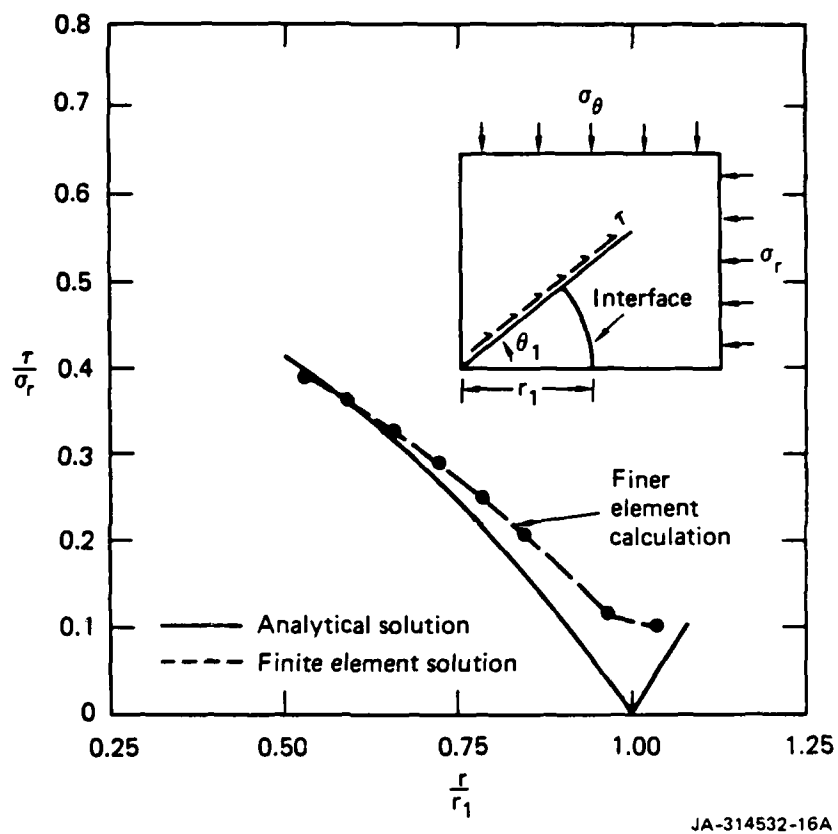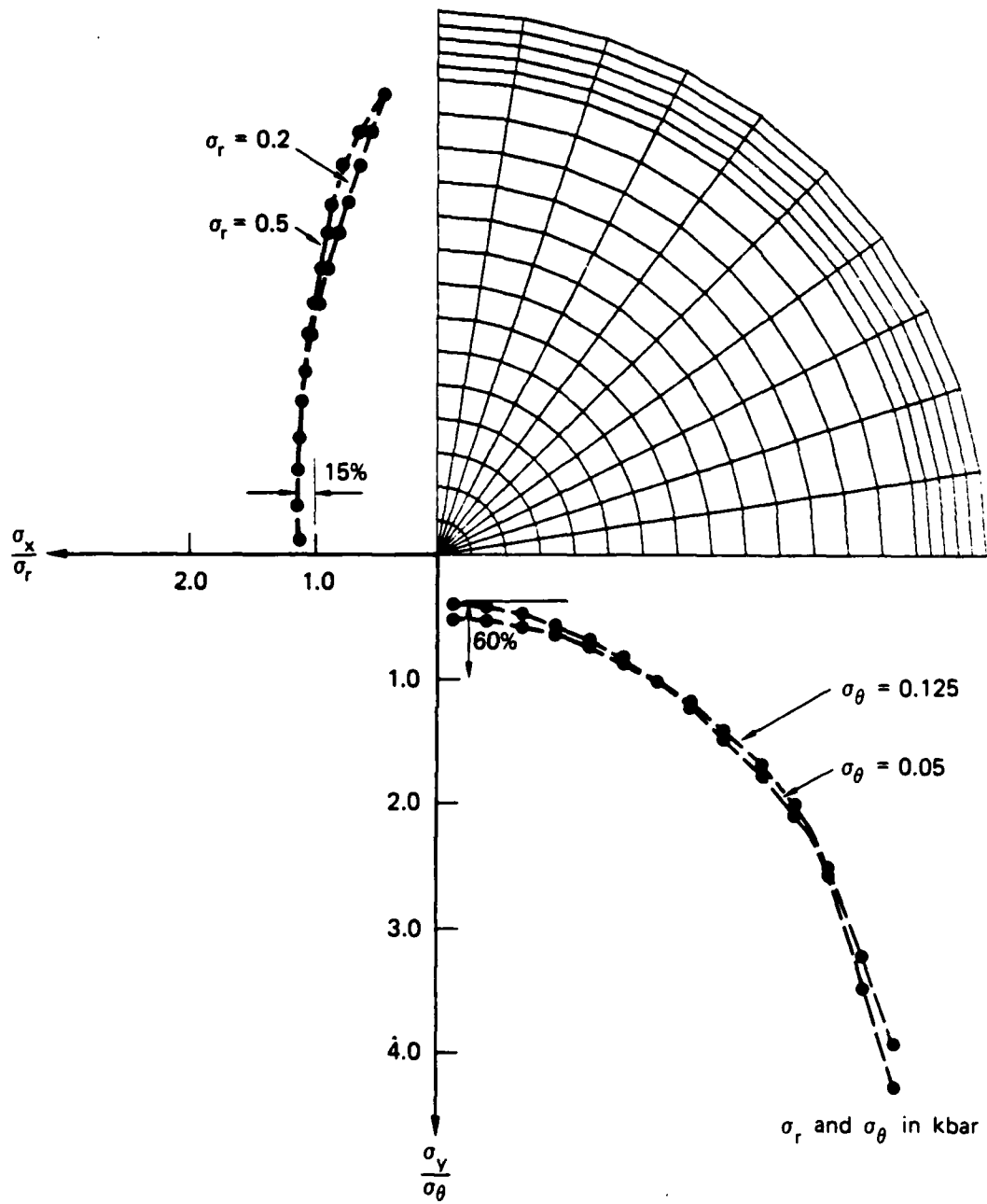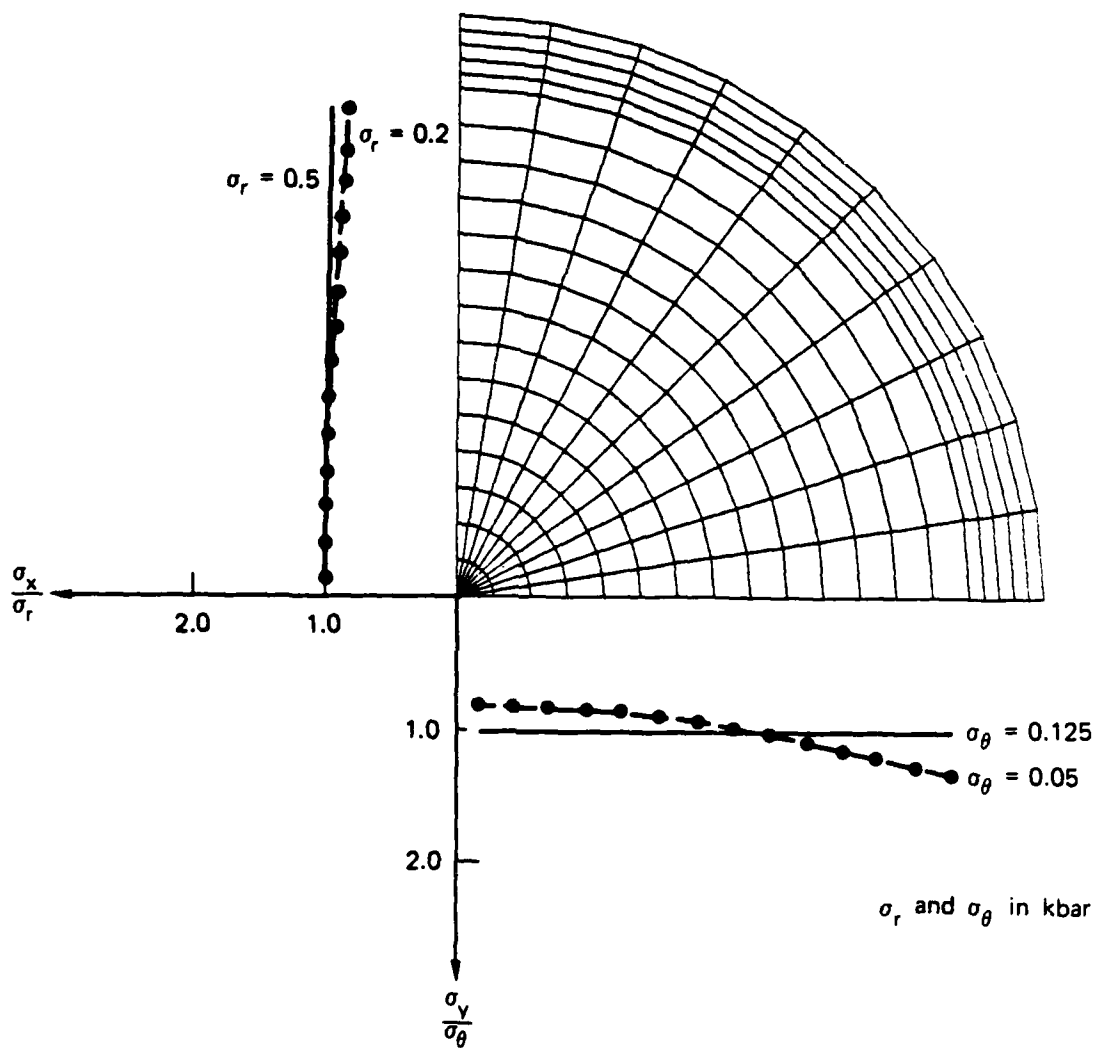stresses along sliding interface.

14

Figure 8. Comparison of Mohr-Coulomb solution against exact solution--
shearing stresses along θ_1 = 49.5°.

JA-314532-16A

15

Figure 9. Normalized stress at gage planes with sliding interface for $\sigma_r/\sigma_\theta = 4$.

JA-314532-17A

16

Figure 10. Normalized stress at gage planes with bonded interface for $\sigma_r/\sigma_\theta = 4$.

17

for either interface condition, but deviates significantly from the free-field outside of this region for the free-sliding interface value. Therefore, a gage in this plane should be restricted to the central core region. A similar condition does not exist in the case of the σ_θ stresses, which vary from the free-field stress by as much as 60% even in the central region of the core for the sliding interface.

(2) Most significantly, for both elastic and elastoplastic conditions, the bonded interface improves both ratios, especially σ_x; in fact, plasticity results in a ratio of 1.0 for both orientations (Figure 10).

(3) For the bonded interface, the maximum shear stress calculated in the salt at the inclusion boundary was approximately 0.14 kbar (14 MPa), which greatly affected the choice of annulus material since a material with a strength exceeding this value is required to prevent shear failure and equivalent slip motion at the annulus.

2.2 SALT HE EXPERIMENT SIMULATION BY PUFF CODE CALCULATIONS.

To guide selection of gage locations and recording equipment sensitivities and for post-experiment comparison with measurements, we generated stress histories at several ranges in the test bed with the PUFF finite difference code. The calculations simulated 77 kg (170 pounds) of high-explosive packed to a density of 0.97 g/cm^3 in a 53.34-cm-diameter (21 inch) cavity in the salt. The material model outlined in Reference 6 was used without simplification because the explosive produced pressures up to 30 kbars (3000 MPa). Because we did not have dynamic tensile strength data for salt, we performed two sets of calculations: one with a low tensile failure (0.03 kbar, 3 MPa), which permitted fracture, and the other with a sufficiently high failure (0.5 kbar, 50 MPa), to prohibit tensile fracture. Wave forms of the resulting radial stress, tangential stress, and radial velocity at two radii in the plastic region (2.0 and 4.2 m) and at two radii in the elastic region (6.0 and 9.0 m) are shown in Figures 11 through 14. The most notable effects of the difference in tensile strength on the stress are the magnitude and duration of the tensile stress. The effect on the radial velocities is that the lower tensile strength results in a greater outward displacement; i.e., the magnitude and duration of the inward velocity are decreased.

18
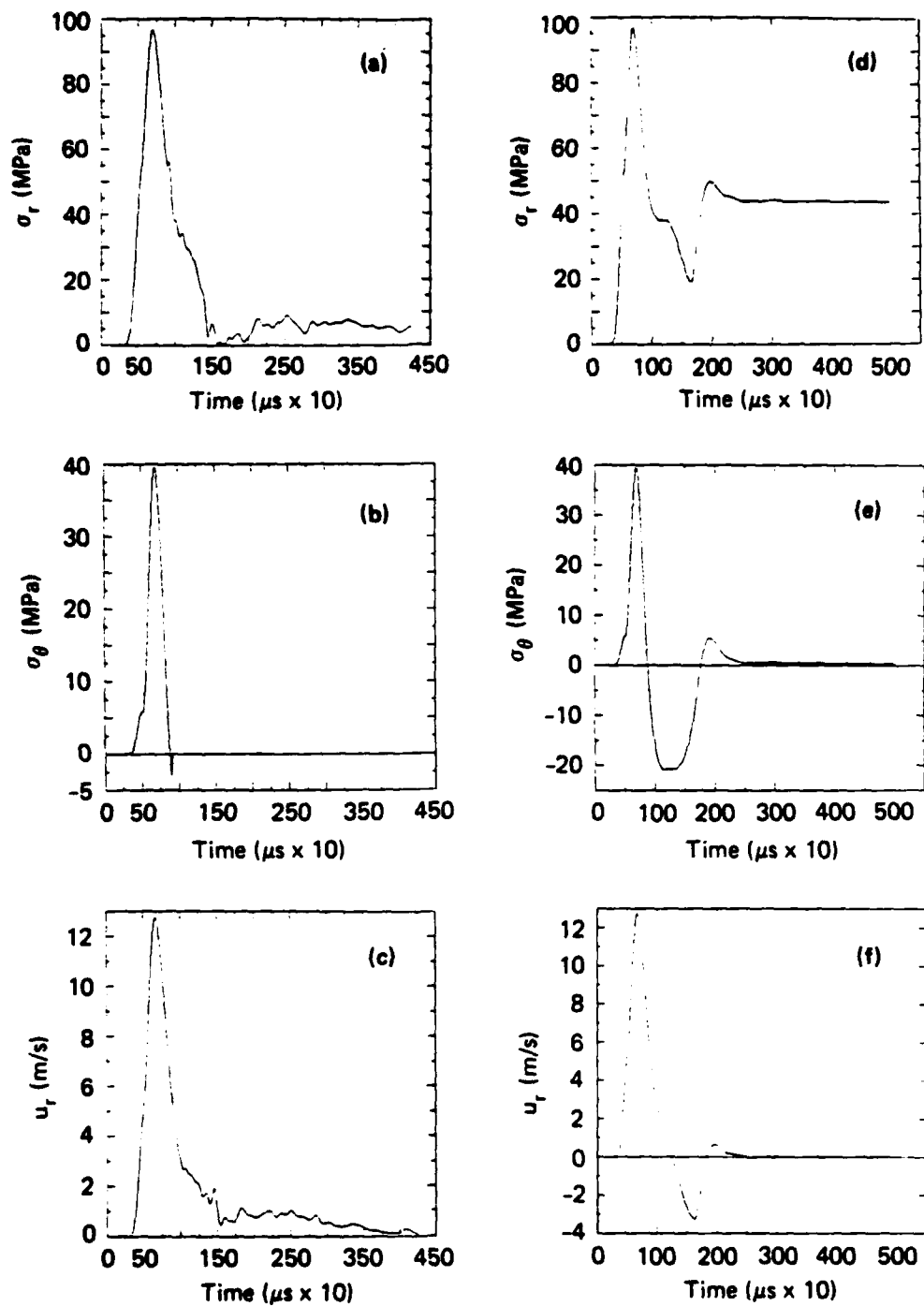
Figure 11. Calculated σ_r, σ_θ, and u_r tories at 2.0-m radius [tensile strength = 0.03 kbar (3 MPa), (a), (b), :); tensile strength = 0.5 kbar (50 MPa), (d), (e), (f)].

19
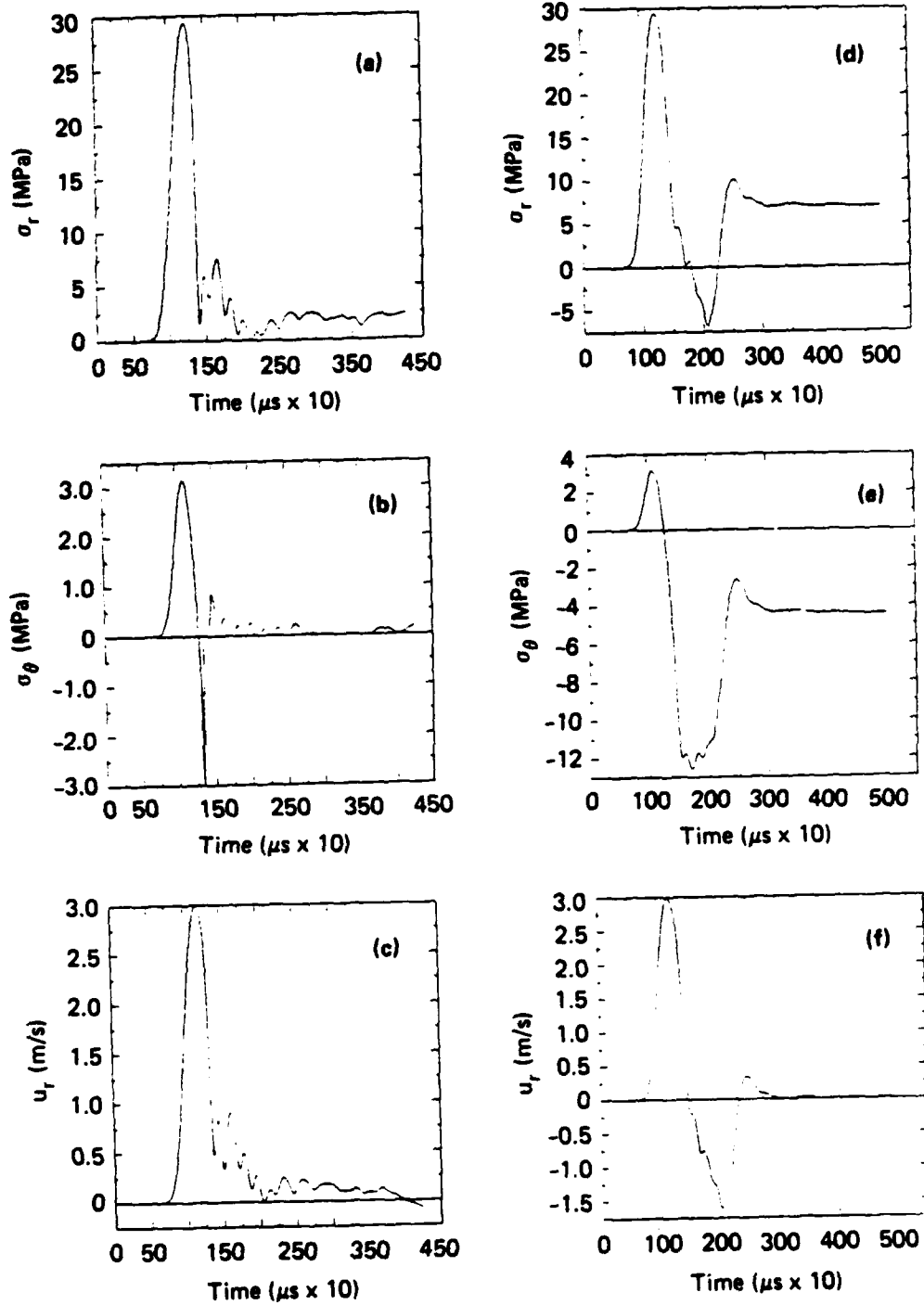
JA-4460-3

Figure 12.   Calculated σ_r, σ_θ, and u_r histories at 4.2-m radius [tensile strength = 0.03 kbar (3 MPa), (a), (b), (c); tensile strength = 0.5 kbar (50 MPa), (d), (e), (f)].

20
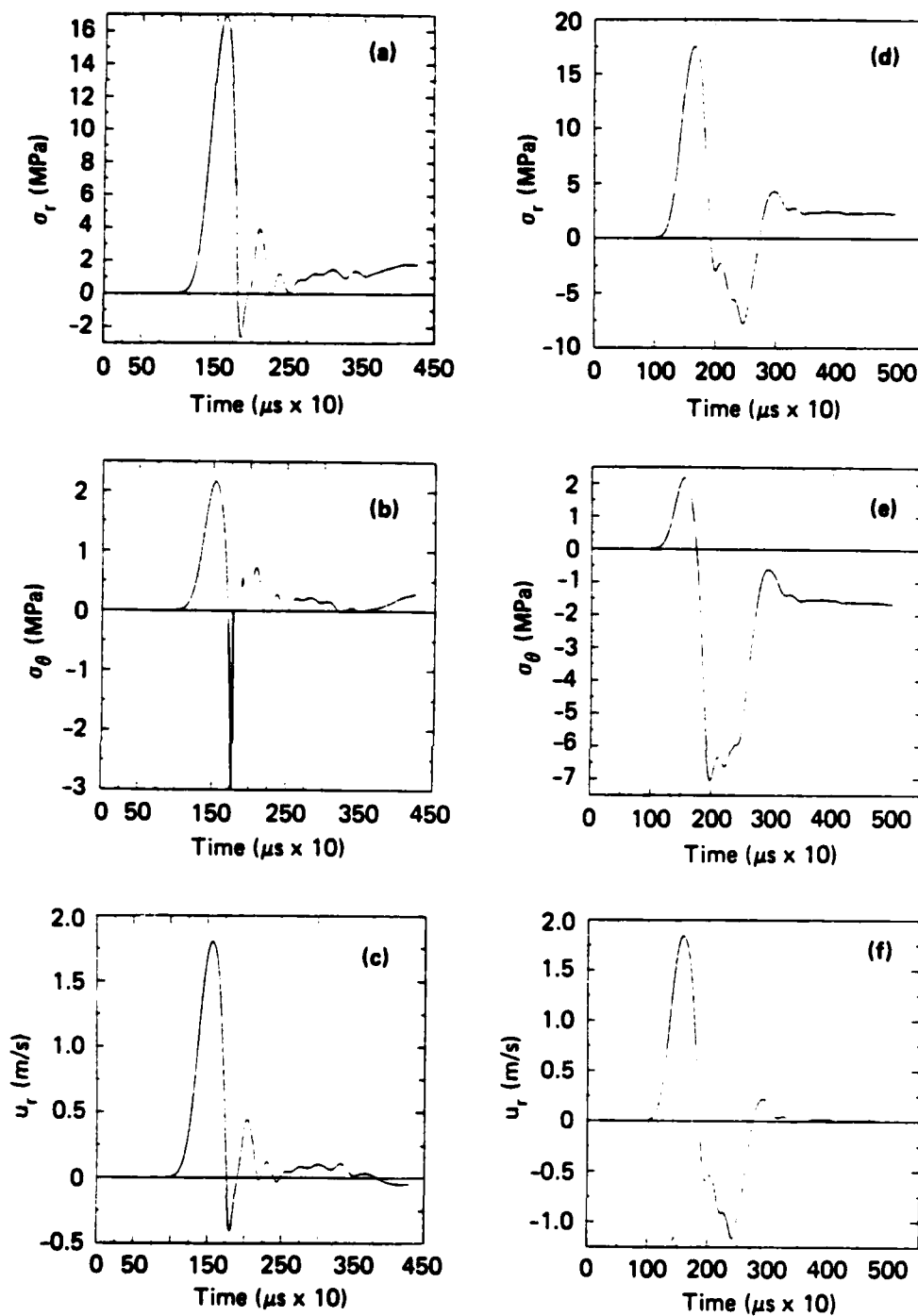
Figure 13. Calculated σ_r, σ_θ, and u_r histories at 6.0-m radius [tensile strength = 0.03 kbar (3 MPa), (a), (b), (c); tensile strength = 0.5 kbar (50 MPa), (d), (e), (f)].

21
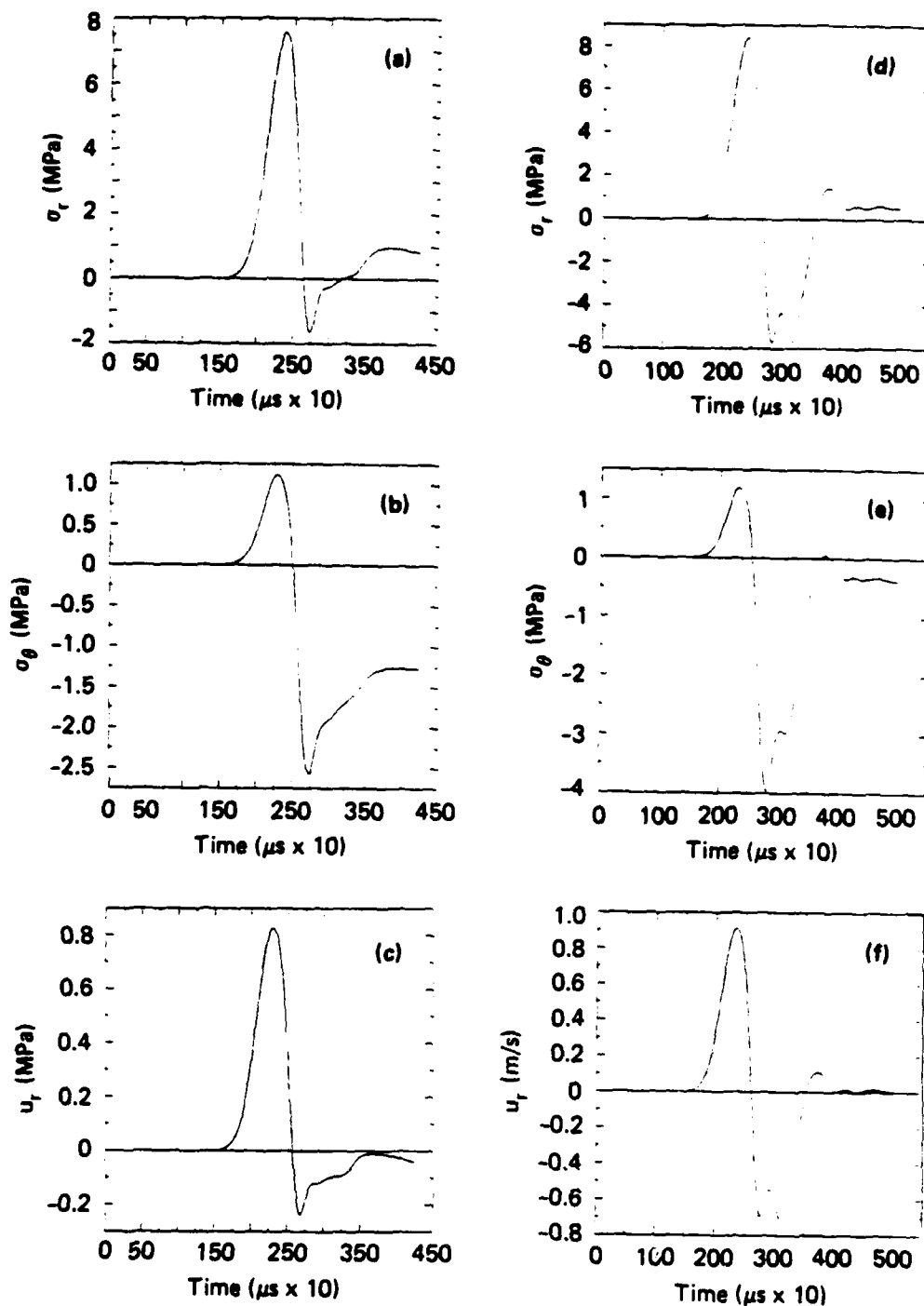
JA-4460-5

Figure 14. Calculated σ_r, σ_θ, and u_r histories at 9.0-m radius [tensile strength = 0.03 kbar (3 MPa), (a), (b), (c); tensile strength = 0.5 kbar (50 MPa), (d), (e), (f)].

SECTION 3

LABORATORY TESTS

Two types of laboratory tests were performed: static calibration of stress gages and static shear strength testing of salt and of salt-epoxy bonds. The results of these tests are discussed below.

3.1 GAGE CALIBRATION.

The stress gage chosen for the salt measurements was the steel-Teflon-ytterbium flatpack gage developed for DNA. This gage, shown in Figure 15, provided the desired geometry of a thin planar inclusion and satisfied the criterion that the inclusion modulus be higher than that of the surrounding medium. The compression modulus of this gage is approximately 600 kbar (60 GPa), which is three times that of salt. Because prior use of this gage (Ref. 3) had indicated that the response of the ytterbium piezoresistant sensor was not well understood during the unloading portion of the stress wave, we performed a laboratory calibration of each gage.

The large size of the gage (1.2 m long x 6.25 cm wide) necessitated construction of a special high-pressure chamber, capable of containing the entire gage and reaching pressures to several kbars. The chamber, shown in Figure 16(a) and (b), consists of a thick-walled (5.7 cm) high strength steel cylinder (198 cm long with double 0-ringed plugs at each end). The calibration procedure consisted of inserting a 1.21-m-long gage into the chamber, recording the initial resistance of the ytterbium sensor on a Cimeron Model 6583 multimeter (accuracy of ±0.001 ohm) and measuring the gage temperature with a Micro Measurements model ETG-50D nickel, resistant temperature gage (resolution of 0.5°F), mounted on the flatpack pressure gage. The fluid pressure was increased in ~25-MPa steps and monitored by a Heise Model H.40711 pressure gage (accuracy of ±0.03 MPa).

Typical calibration data and resistance change (corrected for temperature change) as a function of applied hydrostatic pressure (kbar) are shown in Table 2 and in Figure 17 for three of the gages. Also shown are the static uniaxial strain response as reported by Gupta[8] and the hydrostatic response measured by DeCarli.[9] The response of the ytterbium foil in the flatpack is closer to the uniaxial strain compression response, although the load applied to the flatpack is hydrostatic.

From these results, we concluded that our configuration of the flatpack gage responds primarily to the stress normal to its major surfaces, i.e., in the present

23
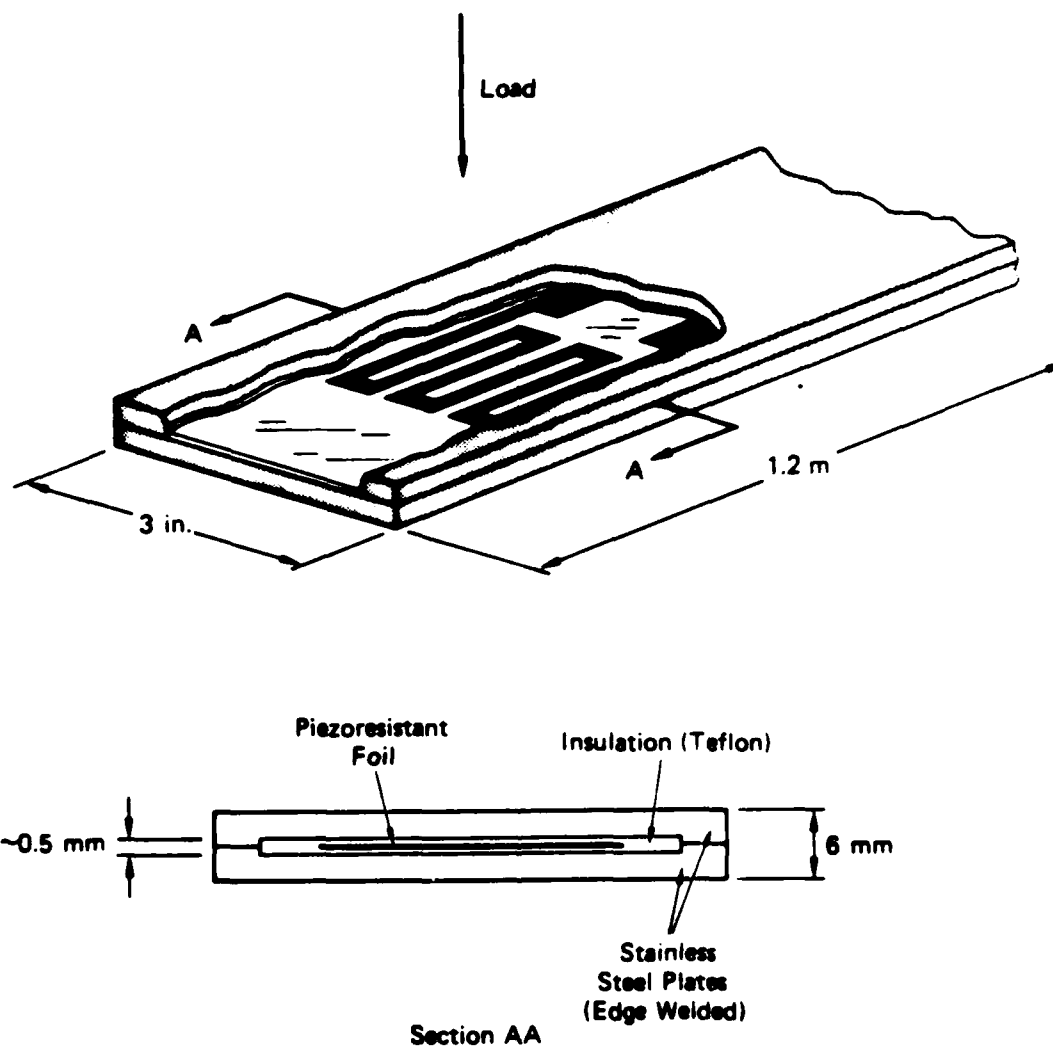
Figure 15. Flatpack stress (pressure) gage.

JA-4459-39B

Gage*

Oil line

Pump,
air driven
21 MPa max

Intensifier for range
above 21 MPa up to
51.7 MPa (safe
maximum for vessel)

Pressure vessel

*Heise precision bourdon tube
gage is used to measure
chamber pressure
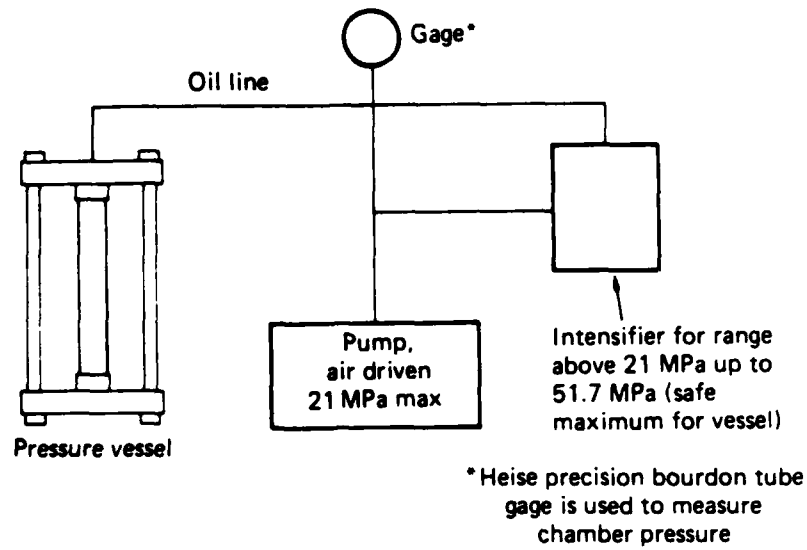
(a) Schematic of overall system.

Oil inlet

Electrical
feedthroughs (12)

O-ring sealed plug

8-inch-OD, 3-1/2-inch-
ID, 103 MPa yield
strength steel

6.5'

2-inch-diameter tie
rods, 4135 steel H.T.
to upper plate

O-ring sealed plug

2-inch-thick,
12 x 12 inch
lower plate
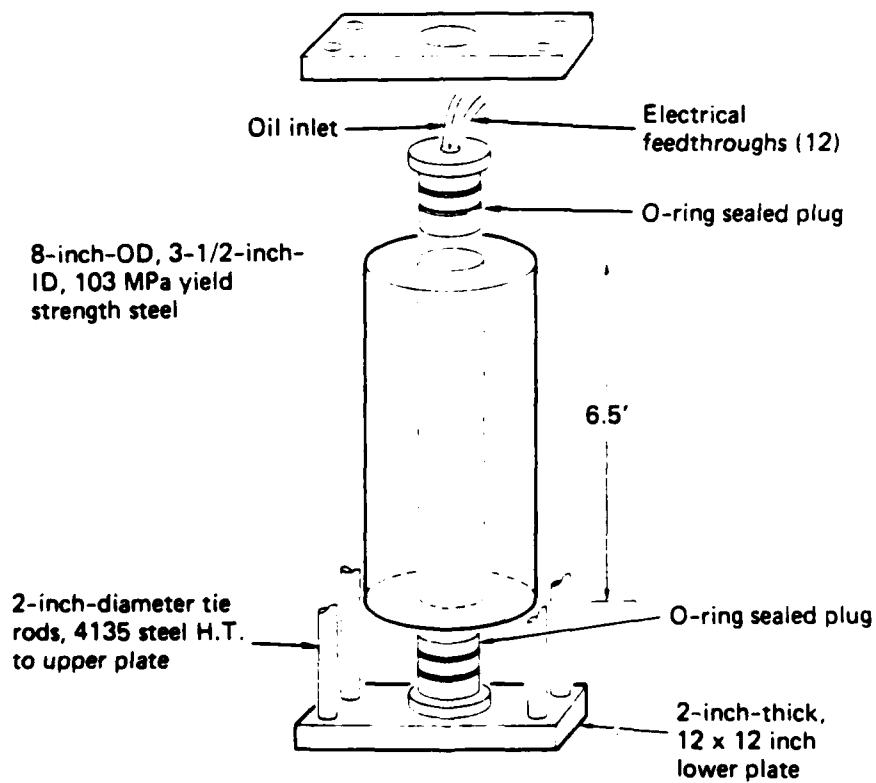
(b) Detail of pressure vessel.

JA-4460-6

Figure 16.   Gage calibration system.

25

Table 2. Calibration data for salt flatpacks.

Pressure (MPa)	(psi)	Uniaxial strain[a]	Relating resistance change, $\Delta R/R_o$			
			Hydrostatic pressure			
			Gages 1-2	Gage 9	Gage 3	Foil gage[b]
1.53	2,218	--	0.0[c] / 0.00756 / -8.5[d]	0.0 / 0.00747 / -8.7	0.0 / 0.00794 / -2.9	--
2.5	3,625	0.010914	--	--	--	--
5.0	7,250	0.022185	--	--	--	--
5.33	7,729	--	+10.9 / 0.0287 / <1	0 / 0.26 / -8.7	+7 / 0.0296 / +4	--
7.5	10,875	0.03248	--	--	--	--
9.2	13,344	--	--	--	--	0.056
10.0	14,500	0.047825	--	--	--	--
10.1	14,650	--	+8.8 / 0.054 / 0	-2 / 0.0503 / -6.8	+8.4 / 0.0568 / +5.2	--
12.5	18,125	0.058179	--	--	--	--
15.0	21,750	0.071446	--	--	--	--
15.62	22,650	--	+11.4 / 0.086 / +2.9	+6.2 / 0.081 / -3.8	--	--
17.5	25,375	0.083803	--	--	--	--
18.7	27,075	--	+13.6 / 0.105 / +5	+9.1 / 0.0996 / -3.8		--
19.9	28,855	--	--	--	--	0.131
20.0	29,000	0.098098	--	--	--	--
17.0	24,650	--	--	--	--	0.111
10.0	14,500	0.053166	+19.4 / 0.059 / -9.3	+14.1 / 0.0557 / +3.1	--	--
0	15	0.000540[b]	-0.00035	-0.00089	--	-0.0007

[a]TERRA TEK Data (Ref. 8, uniaxial, static).

[b]P. DeCarli (private communication).

[c]Departure from linear.

[d]Departure from 0.054 Ω/Ω/kbar.
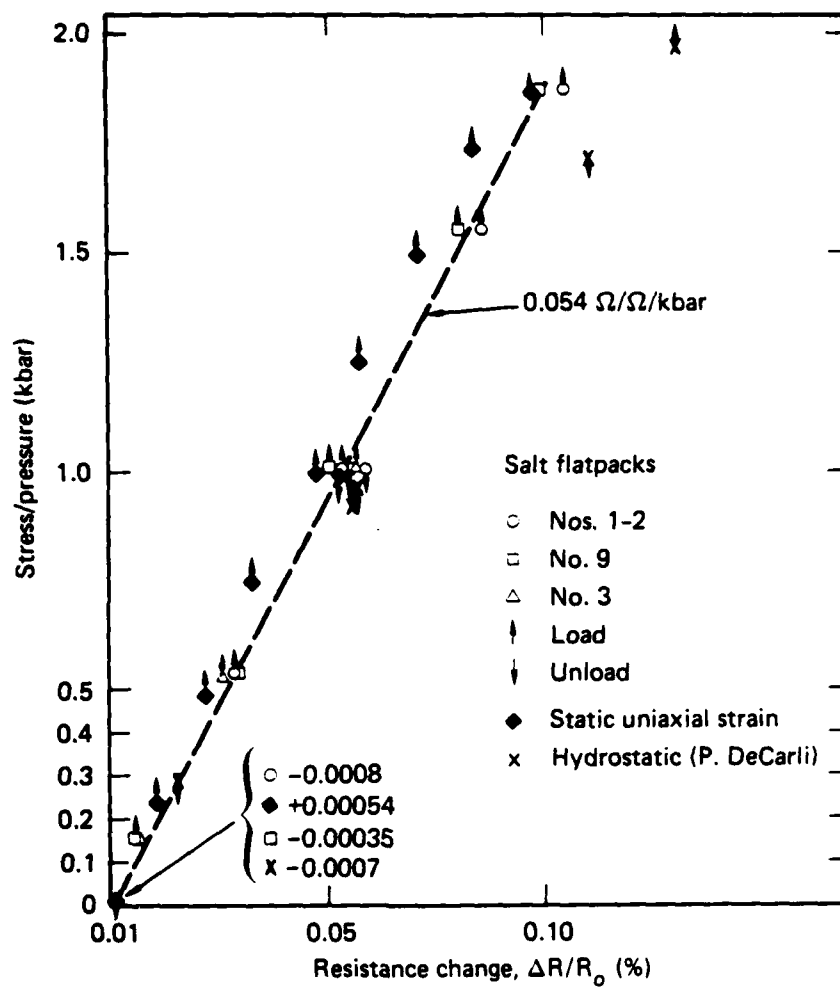
Figure 17.   Response of salt flatpack gages.

application to the x and y stresses in the salt cores, and not to the lateral
stresses, except as these are coupled to the normal stress in the surrounding
medium.

Because all the salt gages responded within the data spread shown in the figure
for the three gages and because the response was linear (±10%), we used one calibra-
tion value of $0.054 \pm 10\%$ $\Omega/\Omega/kbar$ for all the salt gages over the range of our
measurements. (Similar hydrostatic tests of a Kapton-encapsulated ytterbium element
in the flatpack configuration show that the response of the ytterbium is closer to
the hydrostatic response of unencapsulated ytterbium.)

As can be seen from the data of Figure 17, the ytterbium resistance returned to
the prestressed value (within <0.1%) on release of pressure. This behavior is
consistent with the static uniaxial strain data of Ref. 8, but is inconsistent with
the dynamic (shock) uniaxial strain data of Ref. 8. The favorable comparison of
loading response between our data and those of Ref. 8 indicates that the ytterbium
foils in each case are in similar states of tensorial stress and strain during
compression, i.e., uniaxial strain. However, differences in unloading indicate that
the states obtaining upon static (slow) release of stress differ from the dynamic
uniaxial (probably due to time-dependent stress relief within the foil).

In the proposed salt measurements, the unloading time was expected to be
intermediate between the static and shock cases, which introduces considerable
uncertainty in the unloading or relief portion of our data. Because of the higher
accuracy of our static calibration data, we used the static data in our conversion
of resistance to stress.

3.2 SHEAR STRENGTH MEASUREMENTS.

To assess the adequacy of epoxy bonding of the salt cores to the native salt,
we performed static shear strength tests on salt specimens bonded by the slow-cure
epoxy to be used in the core installation. Our criterion for acceptance of a
bonding material was that its shear strength must be greater than the calculated
shear stress at the location of the measurement. Specimens of the native salt (4 x
2 x 2 inches) were cut into 2 x 2 x 2 inch samples, joined by the epoxy (Hysol 2039
with 3719 activator) to form 2 x 2 x 4 inch units, and shear loaded in a Baldwin
Model BET 120k shear strength tester. We also measured the shear strength of the
salt. Shear strength of the salt was measured as 0.3 kbar (30 MPa), and that of the
bond was 0.16 kbar (16 MPa). Shear strength of the epoxy was obtained from the
manufacturer's literature as 0.3 kbar (30 MPa). The limit of the bonding of the

28

core to the native salt was therefore the salt-epoxy bond, which was low but acceptable because the epoxy also satisfied our requirement of a sufficiently slow cure-time (2 hours) to allow for installation of the gage-core assembly at the bottom of the 62-m drill holes.

SECTION 4

DEVELOPMENT AND IMPLEMENTATION OF FIELD TECHNIQUES

4.1 GAGE AND CORE DESIGN.

An unassembled gage-core combination is shown in Figure 18. Rough cores were obtained from the salt bed in Gran Saline, Texas, machined into cylinders, cut into hemicylinders, and milled to accommodate the steel flatpack stress gage. Because the maximum length of core obtainable was only 30 to 35 cm, four hemicylinders were used per gage. To satisfy conclusion (1) of our inclusion calculations (see page 12), the core diameter was made 8.89 cm, which resulted in the gage occupying <50% of the core diameter. Because the stress-sensitive region of the gage is the area of the ytterbium foil in the gage, the region of measurement was actually about 30% of the core radius.

Two methods of assembling the gages and cores were used. In one, completed before to receipt of inclusion calculations conducted by A. Florence in an independent effort, the gages were bonded to the cores with a high shear strength epoxy (Hysol 2039). Florence's analysis indicated that a slip interface between a thin planar inclusion such as the flatpack gage and the surrounding medium caused less perturbation to the free-field stress than a bonded interface. Therefore, our second method consisted of introducing a slip plane of sticky Kapton between the steel gage and salt core. The two conditions formed additional parameters in our test matrix.

4.2 TEST MATRIX.

The primary parameters we wished to address in our test matrix were the radial and tangential stresses at several ranges in the salt. However, to assess the significance of differences between the two at a given range, it was also necessary to examine the following:

(1) The reproducibility of measurement within a gage in the salt core, i.e., sensor-to-sensor reproducibility.

(2) The reproducibility of the core emplacement method, i.e., gage-to-gage comparisons.

The test matrix shown in Table 3 was used to evaluate these parameters. Velocity and acceleration measurements were made by Physics Applications, Inc., under separate contract to DARPA. Calculated values of σ_r were obtained from the PUFF simulations. The calculated tangential stresses at the chosen radii were lower than desirable for the flatpack gages, but were necessitated by the restricted range of measurement of the velocity and acceleration gages.

30
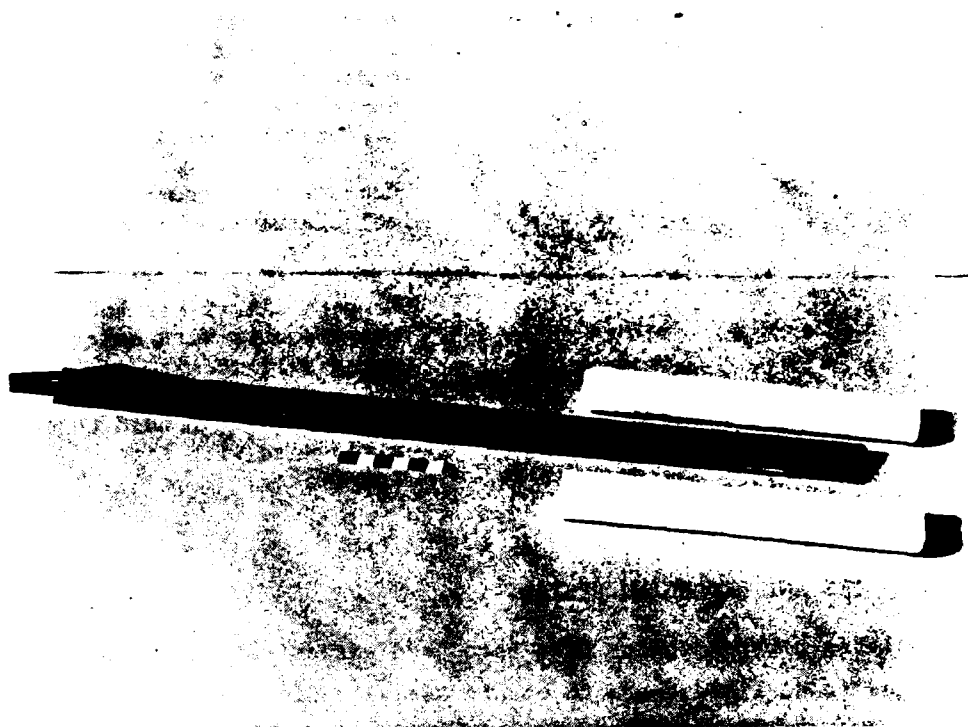
JP-4460-8

Figure 18.   Flatpack gage-salt core (unassembled).

31

Table 3. Test matrix for salt stress measurements.

Parameter	Gage/Hole Numbers	Evaluation Method
Sensor reproducibility (gage inclusion in salt core)	All	Two sensors per gage.
Emplacement reproducibility (salt core in salt medium)	1S1 vs 1S2	Compare 2 σ_θ's at high σ_r.
	2S2 vs 2S3	Compare 2 σ_r's at each of two ranges.
Validity of <u>in-situ</u> σ_r and σ_θ	Three gages at each range	Compare measured values of $(\sigma_r - \sigma_\theta)$ and $(\partial\sigma_r/\partial h)_t$ with measured velocity using momentum conservation equation and Lagrange analysis.
		Compare σ_θ measured with σ_θ calculated from σ_r and velocity.
		Compare all stress and velocity measurements with calculations using salt models.
Slip plane at gage interface		Compare gages bonded to core with gages with Kapton interface.

4.3 GAGE POWER SUPPLIES AND RECORDING SYSTEM.

Pulsed high voltage power supplies have been used extensively with ytterbium flatpack stress gages in HE field tests to obtain adequate signal-to-noise ratios at very low stresses. Because these supplies require rather precise synchronization with the source detonation and such synchronization was not available on the salt tests, we chose to power the ytterbium gages from DC sources (12 V wet cells) and rely on downhole and uphole amplification to obtain adequate signals. Noise levels equivalent to <10 bars (1 MPa) were achieved by using differential mode operation at both locations, as shown in the schematic of Figure 19. The downhole differential amplifier eliminated common mode noise originating at the gage or between the gage and the first amplifier. The uphole amplifier eliminated common mode noise on the cable system that transmitted data to the recorders.

Noise rejection tests were performed and showed that the system was capable of >25 dB common mode rejection from 50 Hz to 200 kHz, and that bridge signals as low as 5 mV could be recorded easily. In addition to the common mode tests, we measured
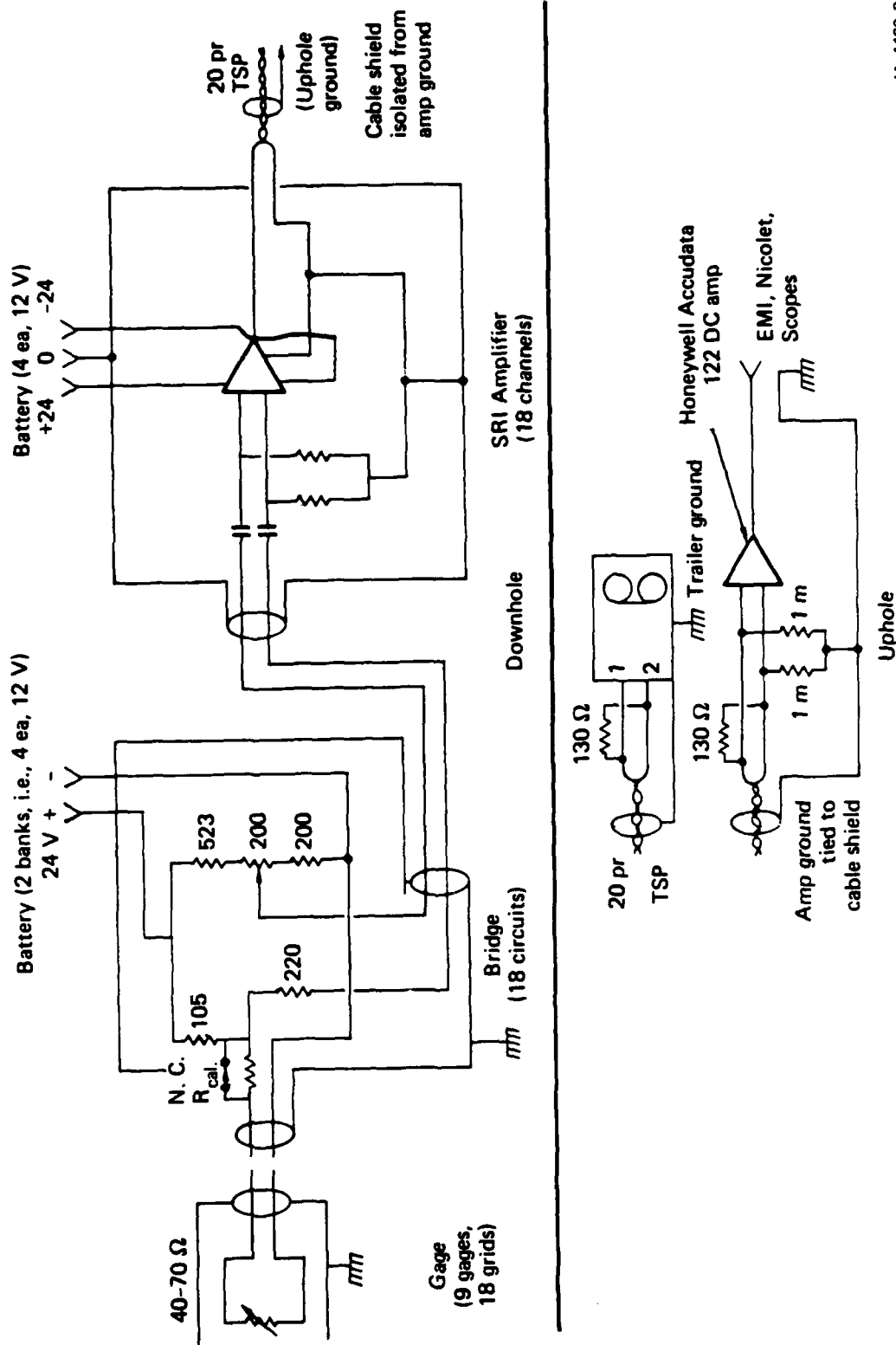
32

Figure 19. Schematic of recording system.

JA-4460-9

33

the frequency response of the data transmitting system by means of downhole signal injection, and we measured channel-to-channel cross-talk, which was less than 15 dB. The frequency response, shown in Figure 20, was entirely adequate for transmitting the expected stress waveforms without distortion.

The DC power supplies contained relay-activated resistance-insertion calibration on each channel. However, these were not used because the contact resistance of the solid state relays was larger than the calibration resistance, which was equal to the peak resistance change as determined from our gage calibration and the predicted peak stress (PUFF calculation).

4.4 GAGE EMPLACEMENT PROCEDURE.

To achieve a bond between our core assemblies and the borehole surfaces, we designed and constructed fixtures capable of placing approximately one-half gallon of mixed, uncured epoxy at the bottom of each borehole before to gage installation. The quantity of epoxy was chosen to fill the annulus between the core and native salt and to extend approximately 5 cm above the core as shown in Figure 21. The epoxy insertion fixture, diagrammed in Figure 22, consisted of two cylindrical chambers separated by a thin Mylar diaphragm. The lower chamber was open at the bottom. Mixed but uncured epoxy was placed in the upper chamber; the fixture was then lowered to the bottom of the borehole by means of the 1/2-inch-diameter PVC pipe. Upon reaching the bottom of the borehole, the diaphragm was ruptured by the pointed end of the pipe, and the epoxy drained when the fixture was withdrawn. The gage-core assembly was then lowered into the borehole by means of the RG22U cables.

Measurement of gage alignment was attempted by a removable 1/2-inch-diameter PVC pipe extending to the surface and marked to indicate the direction perpendicular to the gage plane. This system was not satisfactory because it was difficult to rotate the core assembly at the bottom of the 62-m borehole. At the time of gage emplacement, we estimated that the uncertainty in alignment was ±20°. Shot data, however, indicate the uncertainty to be more like ±90°, which is large enough to compromise the major objectives of the experiment. (Measurements of actual gage orientations were to be made by PAI personnel using borehole TV cameras).

Two additional problems were encountered during gage installation:

(1) The boreholes were not vertical but tended to spiral, which increased the difficulty in gage alignment and therefore the uncertainty in gage orientation.

(2) One hole was overdrilled by approximately 1.9 m; therefore, the gage in this hole was below the plane of measurement of the other gages, and the stress wave was incident at an angle of 65° rather than at 90° as planned.

34
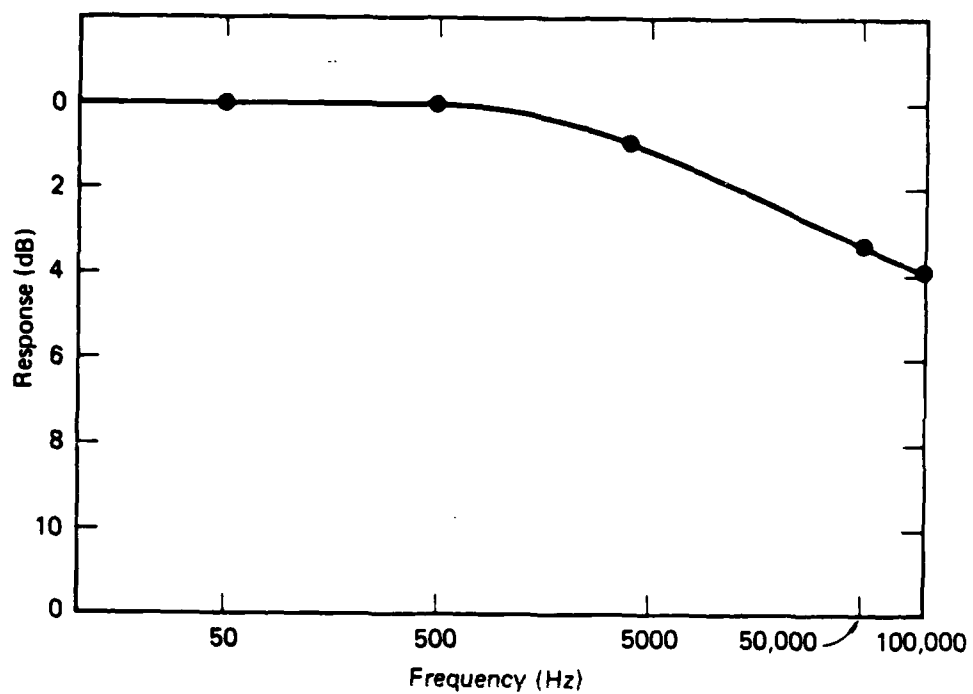
JA-4460-10

Figure 20. Frequency response of amplifiers and ~ 1600 feet of TSP cable, terminated in 130 Ω.

35
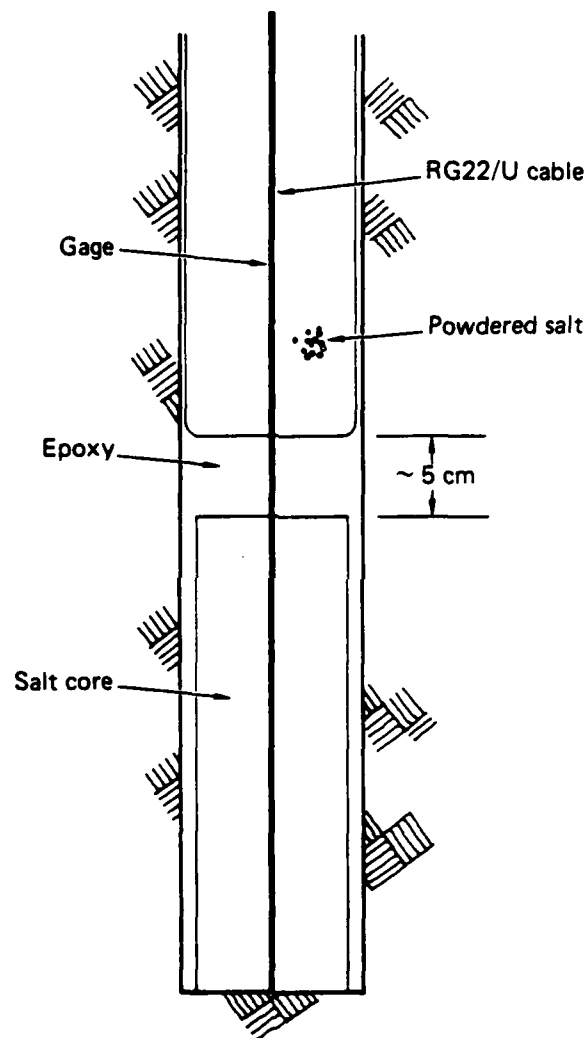
Figure 21. Schematic of epoxy bonding.

1/2-in.-ID PVC
pipe ~ 64 m long

Stop on 1/2-in. pipe

Mixing chamber

2-in.-ID
PVC pipe

Mylar diaphragm

Standoff chamber

JA-4460-12

Figure 22.   Epoxy insertion fixture.

37

SECTION 5

DATA REDUCTION AND ANALYSIS

Voltage-time records (raw data) obtained from the 18 piezoresistant sensors fielded are shown in Appendix B. The records are similar in waveform, except one sensor in the tangentially oriented gage at 9 m radius (gage 7, grid 1), which agrees with its companion sensor during stress loading, but disagrees upon unloading by showing an oscillatory waveform. The reason for this behavior was not determined. Most of the records are characterized by an initial baseline shift of a few milli-volts (downhole value) occurring at the time of explosive initiation. Because in most cases the shift appeared to be constant before stress arrival, we measured all voltage changes and hence resistance and stress changes with respect to the shifted baseline.

Voltage was converted to stress by using resistance substitution calibration values obtained before the shot and our laboratory-derived stress-resistance sensi-tivity of $0.054 \pm 10\%$ $\Omega/\Omega/\text{kbar}$ for both loading and unloading. This constant-sensitivity data reduction procedure for ytterbium sensors in a flatpack gage differs from previously used procedures that invoke both a nonlinear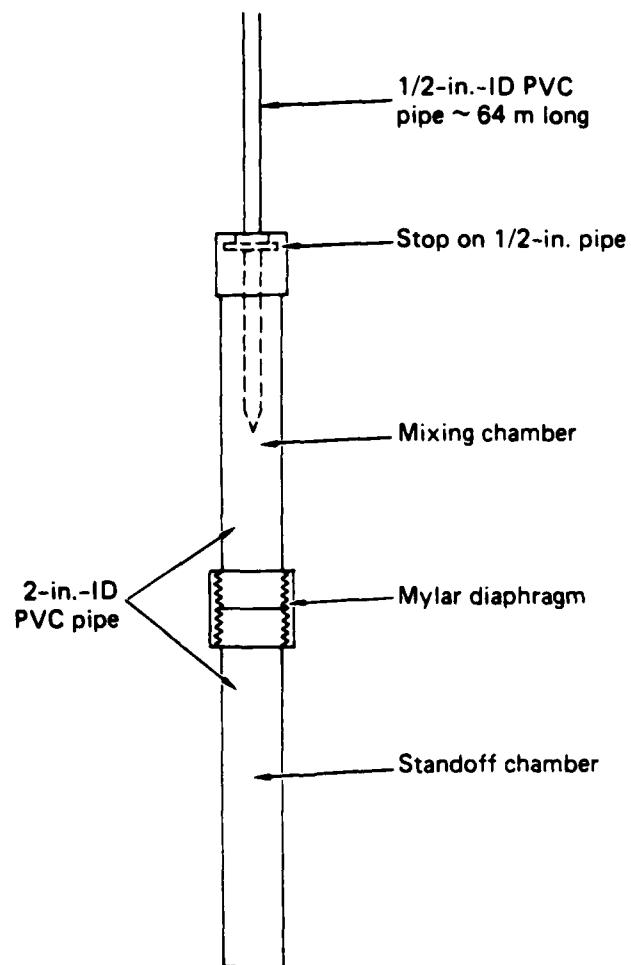 loading curve and a shock-induced change in stress-free resistance procedure that results in a large residual resistance and a large baseline correction throughout the stress profile. Because the bounds on our calibration sensitivity encompass the load and unload data, we believe that the single value is justified. The stress profiles so obtained are shown in Figures 23 through 31.

These profiles exhibit several interesting features:

(1) All are characterized by a relatively slowly rising loading wave, followed by an unloading wave that appears to become tensile before a return to preloaded stress.

(2) Many of the records show a precursor of approximately 10-bar (1 MPa) magnitude that does not change amplitude with range.

(3) There is not a systematic difference between peak stresses from gages supposedly oriented to measure radial stress and those oriented to measure tangential stress, indicating that the desired orientations may not have been achieved.

(4) Peak stresses differ by as much as 50% and arrival times by as much as 40% for gages supposedly at the same radial distance from the source.

Because of this last feature of the data, we used the distance-arrival time data as determined from the foot of the precursor and from the foot of the main
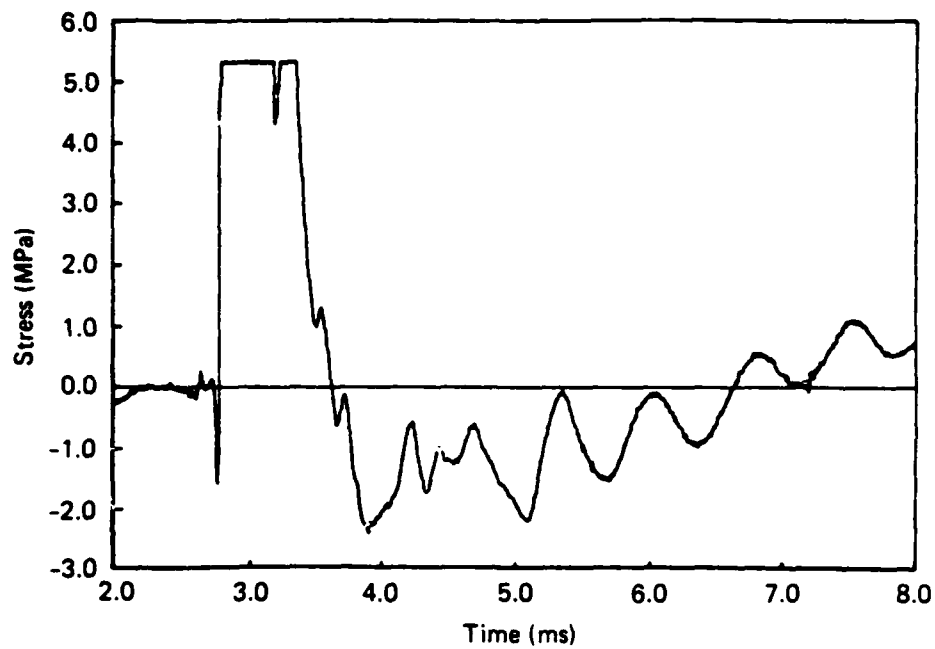
(a) 4.2 m (4.4 m) σ_θ, gage 10, grid 1.
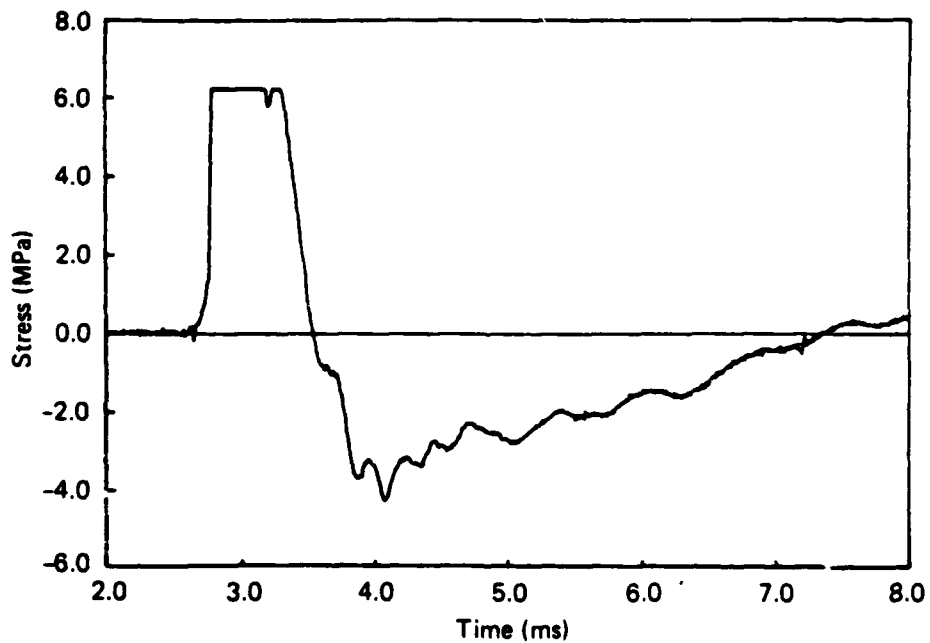
(b) 4.2 m (4.4 m) σ_θ, gage 10, grid 2.

JA-4460-14

Figure 23. Stress histories for hole 1S1.

39
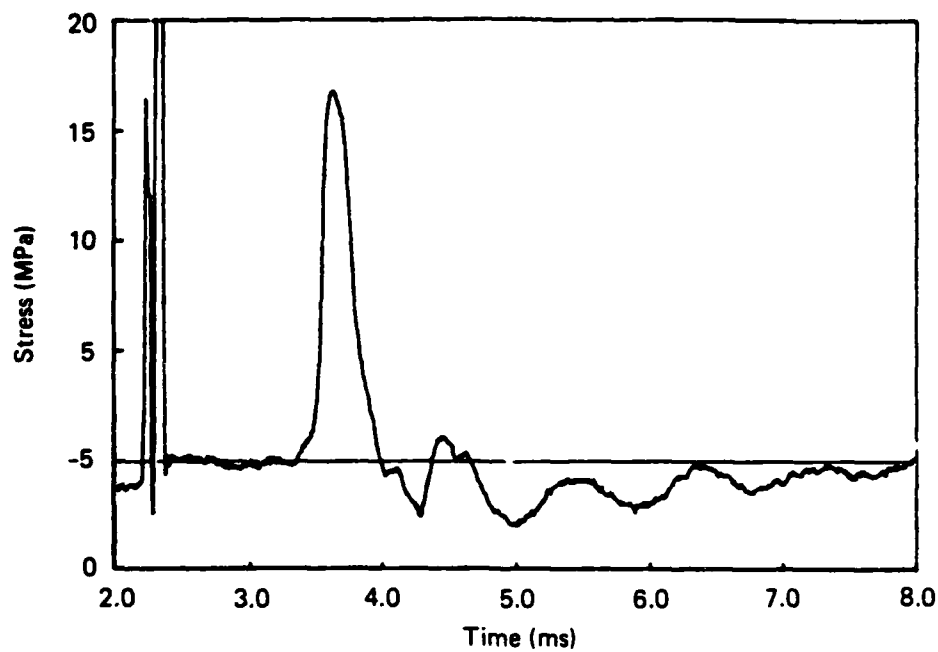
(a) 4.2 m (4.4 m) σ_r, gage 6, grid 1.
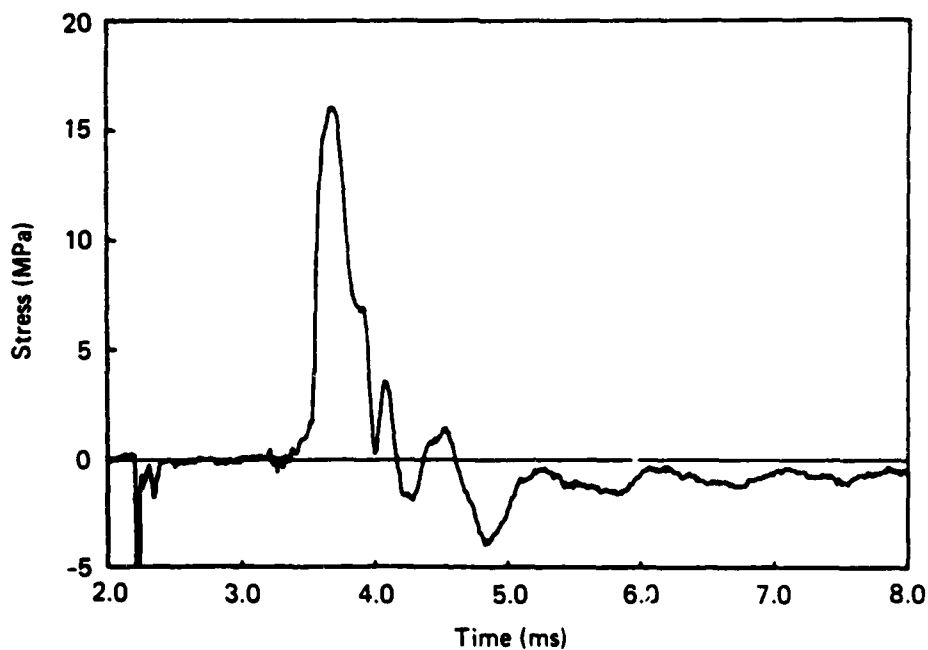
(b) 4.2 m (4.4 m) σ_r, gage 6, grid 2.

JA-4460-15

Figure 24.   Stress histories for hole 1S2.

40
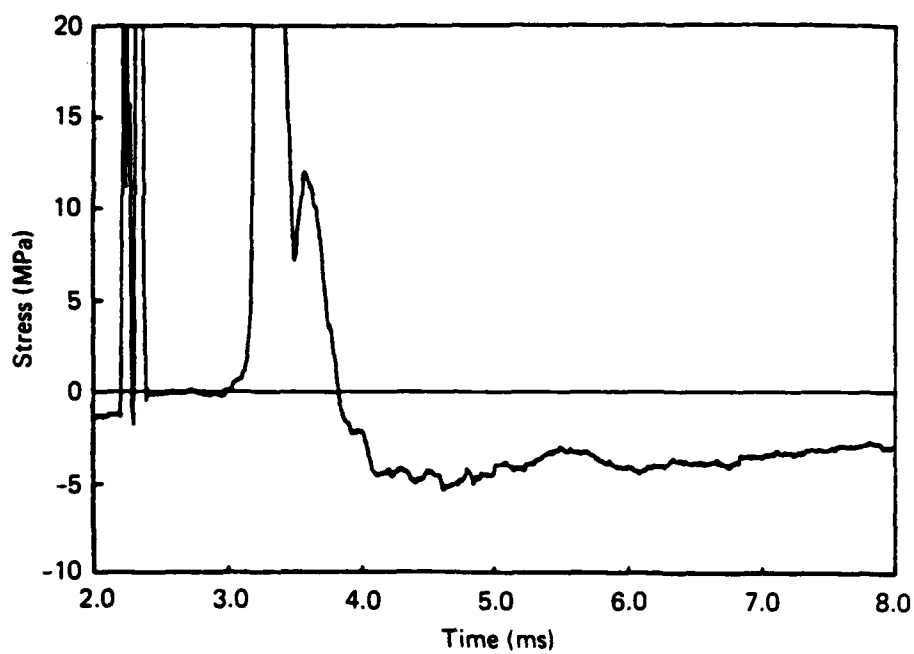
(a) 4.2 m (3.65 m) σ_r, gage 8, grid 1.
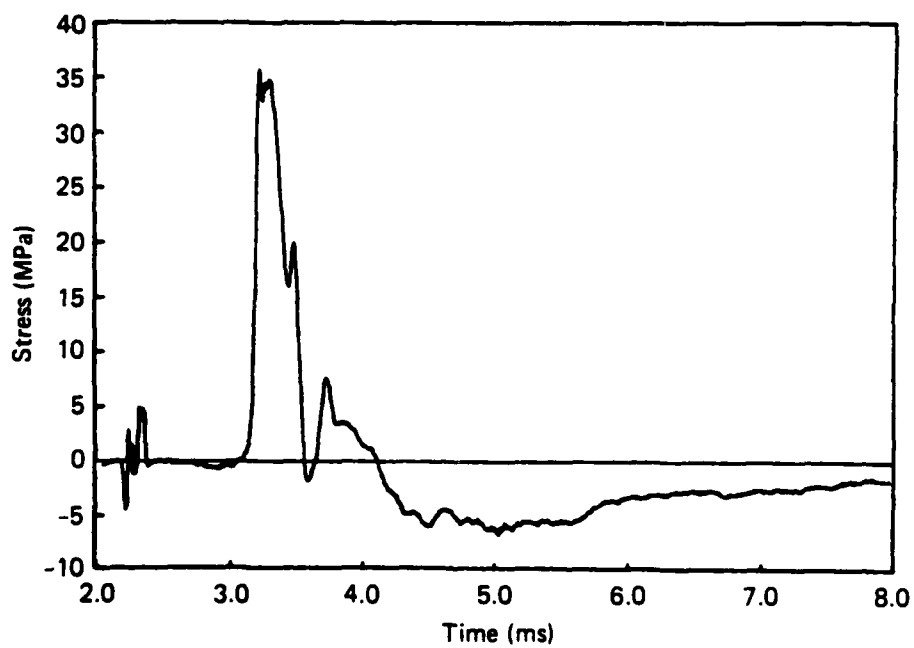
(b) 4.2 m (3.65 m) σ_r, gage 8, grid 2.

JA-4460-16

Figure 25.   Stress histories for hole 1S3.

41

(a) 6.17 m (5.4 m) σ_θ, gage 12b, grid 1.

(b) 6.17 m (5.4 m) σ_θ, gage 12 b, grid 2.
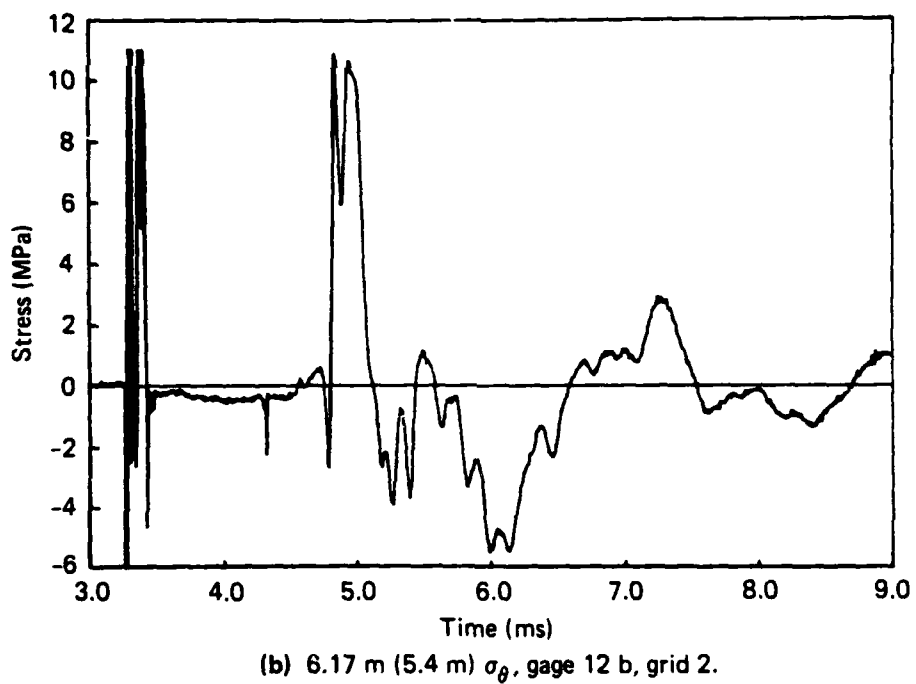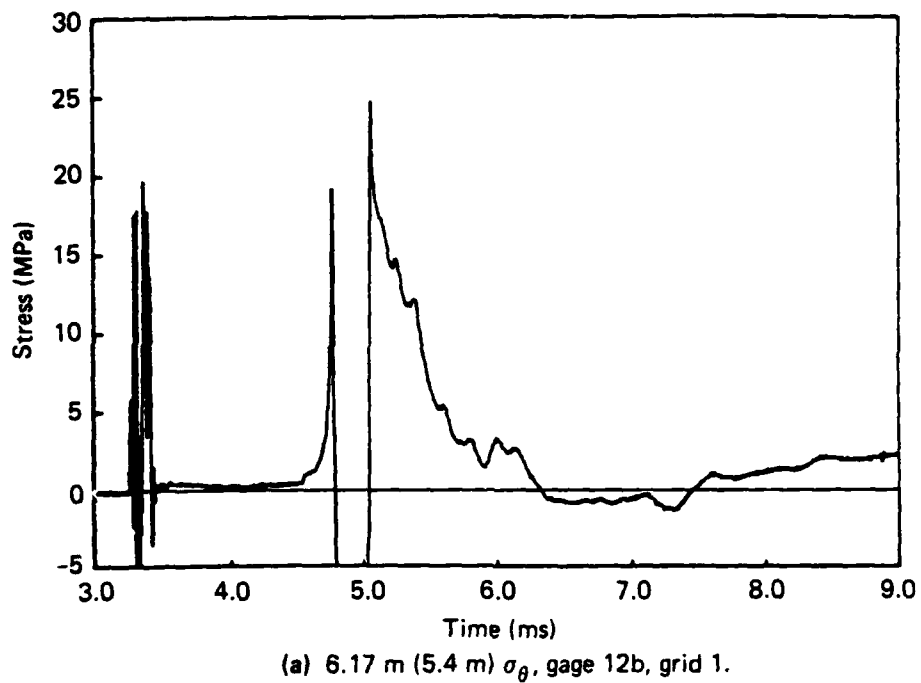
JA-4460-17

Figure 26.   Stress histories for hole 2S1.

42
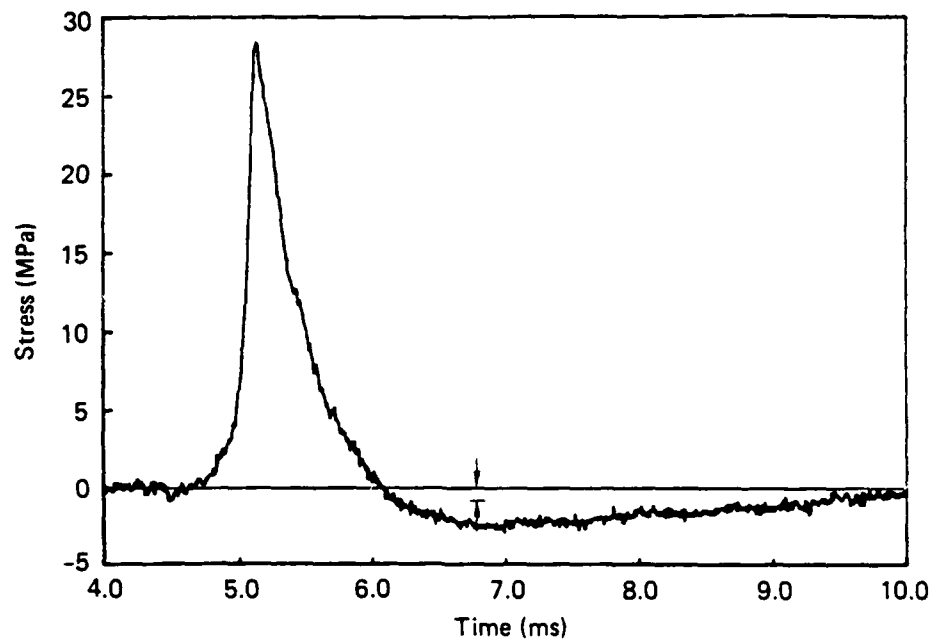
(a) 6.17 m (6.3 m) σ_r, gage 11, grid 1.
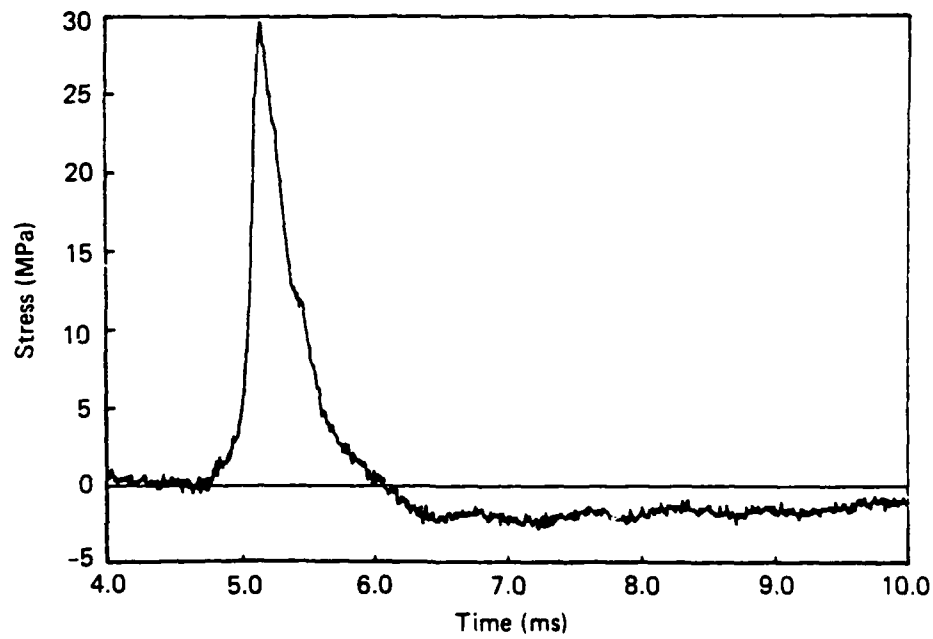
(b) 6.17 m (6.3 m) σ_r, gage 11, grid 2.

JA-4460-18

Figure 27.   Stress histories for hole 2S2.

43
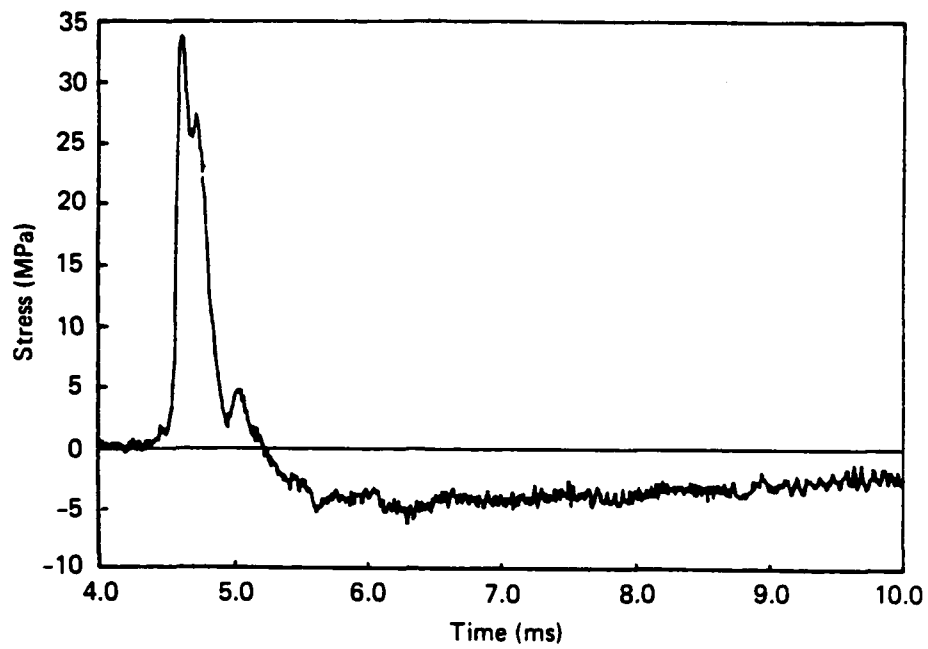
(a) 6.17 m (4.6 m) σ_r, gage 4, grid 1.
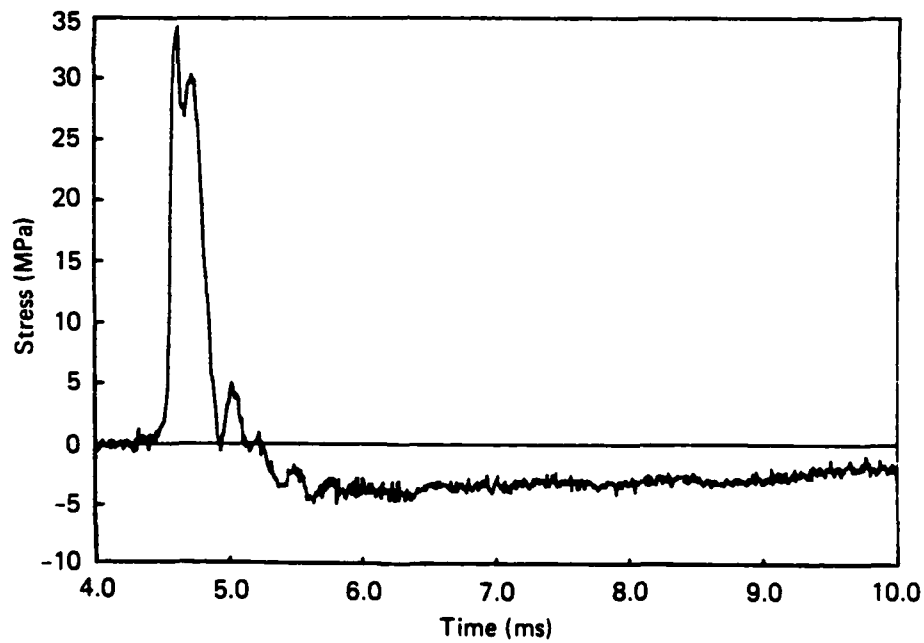
(b) 6.17 m (4.6 m) σ_r, gage 4, grid 2.

JA-4460-19

Figure 28. Stress histories for hole 2S3.

44
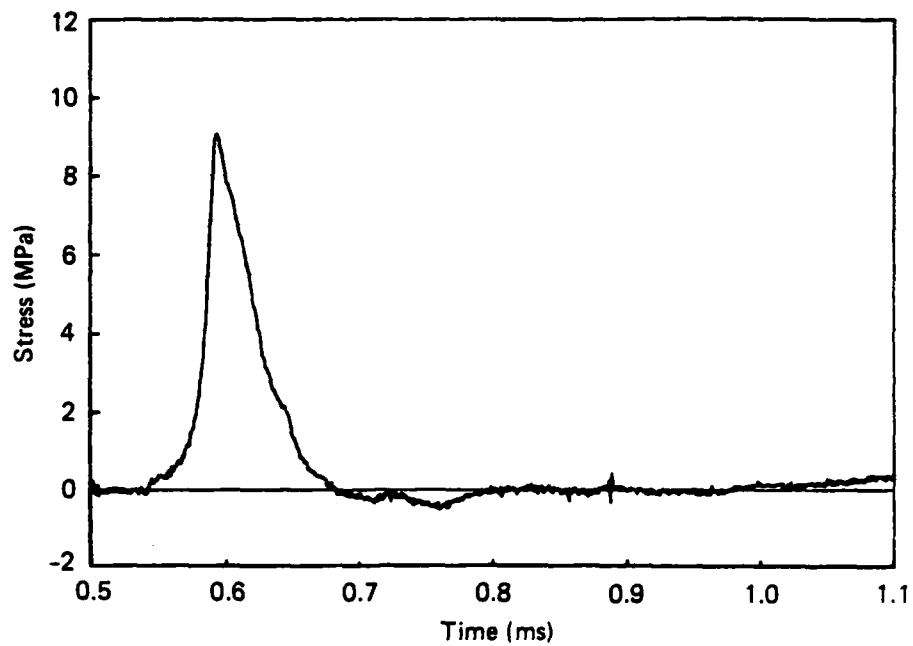
(a) 9.07 m (9.07 m) σ_θ, gage 7, grid 1.
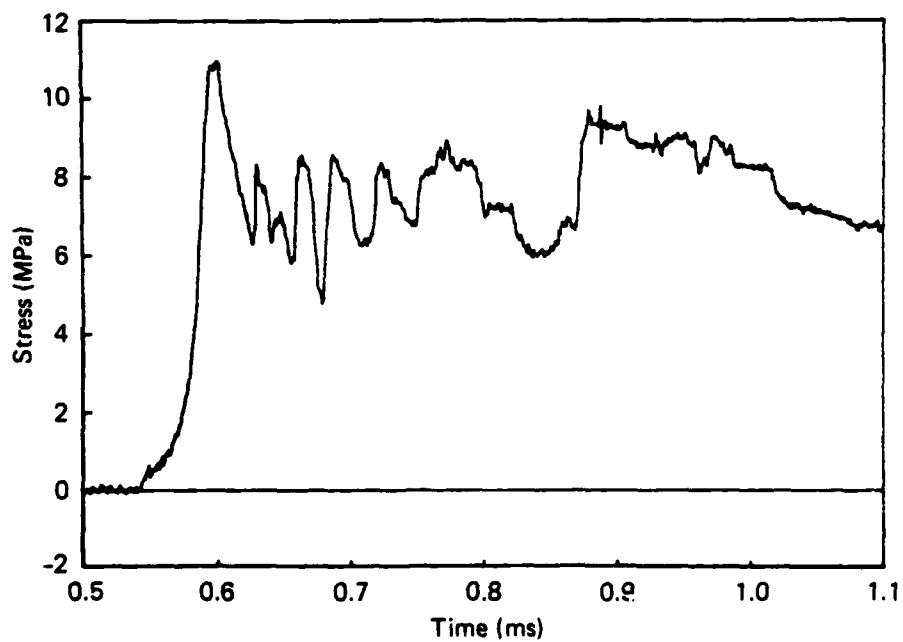
(b) 9.07 m (9.07 m) σ_θ, gage 7, grid 2.

JA-4460-20

Figure 29.   Stress histories for hole 3S1.

45
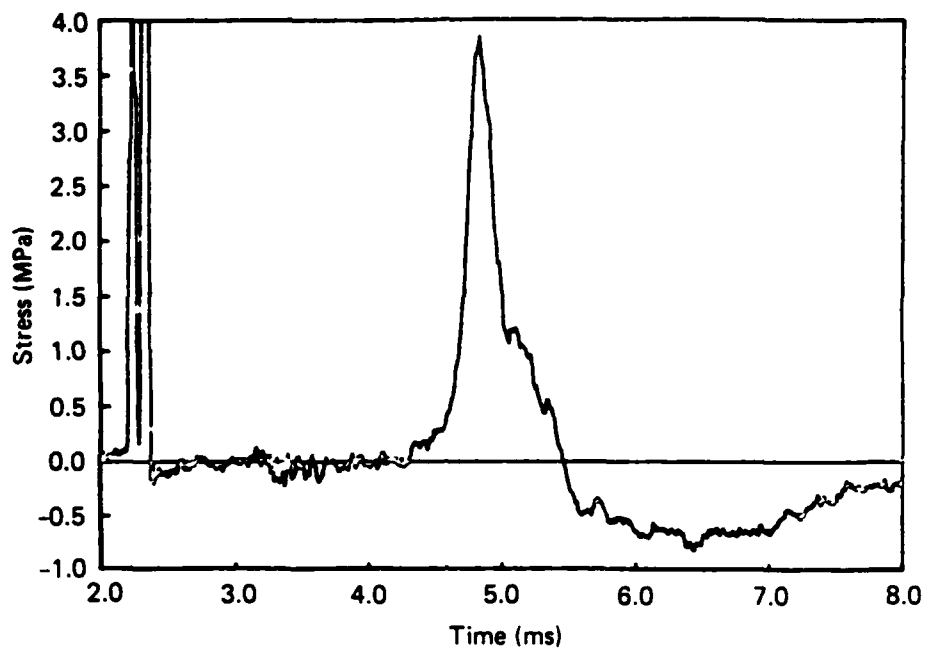
(a) 9.07 m (9.07 m) σ_r, gage 1, grid 1.
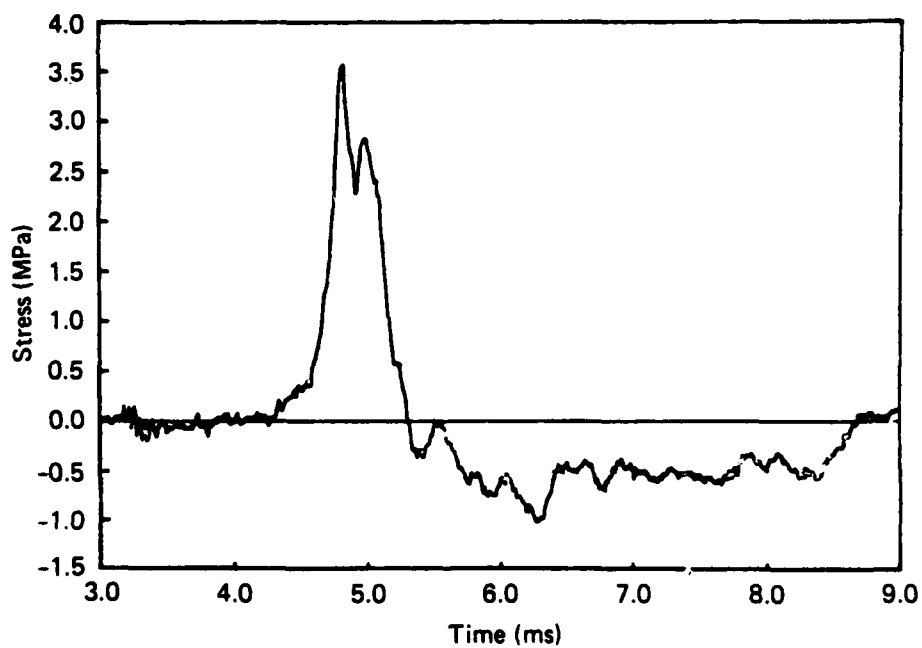
(b) 9.07 m (9.07 m) σ_r, gage 1, grid 2.

JA-4460-21

Figure 30.   Stress histories for hole 3S2.

46
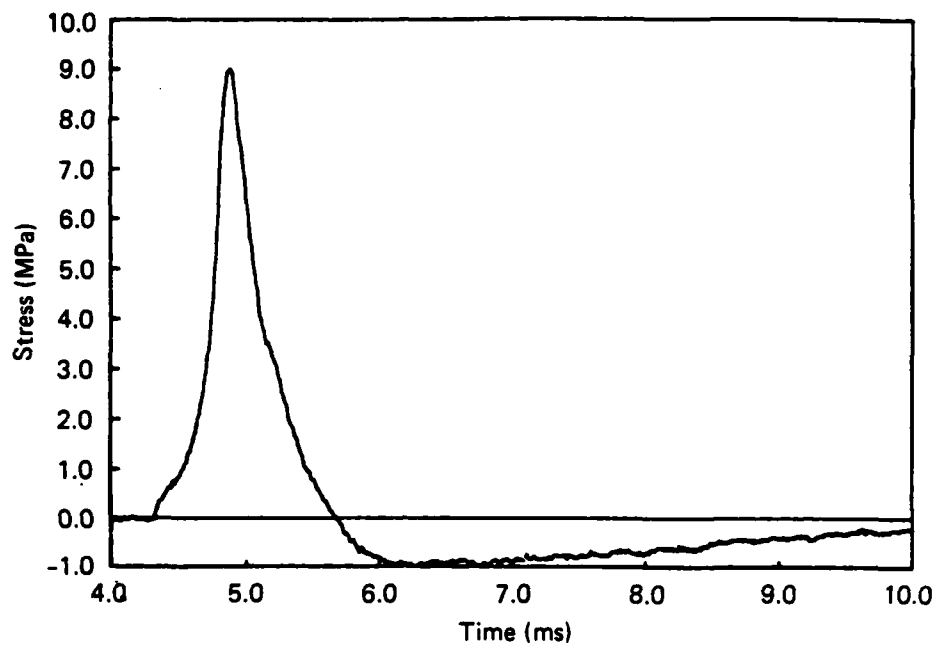
(a) 9.07 m (9.07 m) σ_r, gage 2, grid 1.
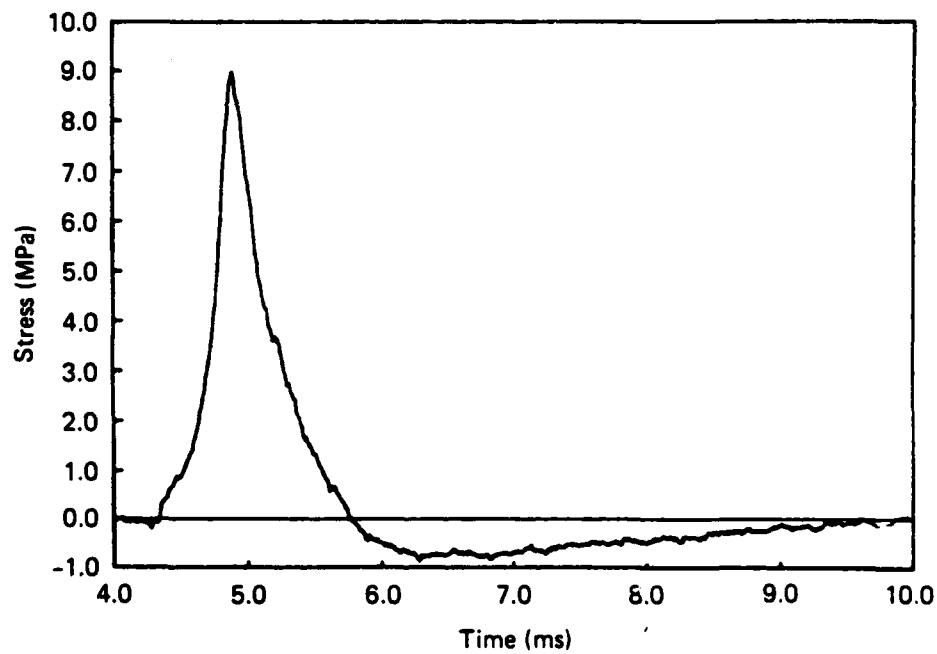
(b) 9.07 m (9.07 m) σ_r, gage 2, grid 2.

JA-4460-22

Figure 31.   Stress histories for hole 3S3.

47

compressional wave to establish the probable actual location of each gage. These data are shown in Figure 32. The corrected radial distances are at the tip of the arrows, which indicate the direction of the correction. The largest correction is required for gage No. 4 in hole 2S (see Figure 28), which instead of being at a radial distance of 6.17 m was actually at 4.6 m. The holes at the greatest radial distance appear to be the most accurately drilled. Because of the uncertainty in gage orientation, it is not possible to obtain values of stress gradient and stress differences and compare these with velocity data. Qualitatively, the waveforms are remarkably similar to those calculated by the PUFF code (see Figures 11 through 14). However, the validity of the apparent tensile portion of the measured waveforms is doubtful and deserves discussion.

The uniaxial strain tensile responses of ytterbium and of the flatpack gage have not been measured. Because of this lack of data and because we could not extend the static calibration to the tensile region, we used our compression sensitivity calibration of $0.054 \pm 10\%$ $\Omega/\Omega/kbar$ to convert resistance change to stress regardless of the sign of the change. By so doing, we have assumed that the observed decrease in resistance is due to a tensile stress applied normal to the flatpack gage and is not a manifestation of some other phenomenon that also produces the negative resistance change in ytterbium, e.g., bending-induced tensile strain, which has been observed in earlier UGT experiments involving fiberglass flatpacks.

Bending-induced resistance change does not appear to be a reasonable explanation in the current salt experiment for three reasons. First, bending deformation of the gage can be estimated if we assume the gage flows with the salt and displaces from a position along a chord to the spherical shock to an arc. The resulting elongation of the flatpack would produce a strain about of 4×10^{-5}, which from Gran's uniaxial stress-tensile strain data for ytterbium[10] would result in a change in resistance of the same sign as that observed, but an order of magnitude lower. Second, all gages show a negative change in resistance, which could occur in bending only if all the ytterbium sensors in the flatpacks were located on the tensile strain side of the neutral axis of the gage, a highly unlikely possibility. Third, the flatpack has evolved from fiberglass to steel to eliminate bending-induced resistance changes.

It is also possible that the apparent negative resistance is really only a decrease from a preshot biased value resulting from the horizontal component of the lithostatic pressure. (Most of the gages were installed six months before the experiment; therefore, the salt might have been able to flow and redistribute the
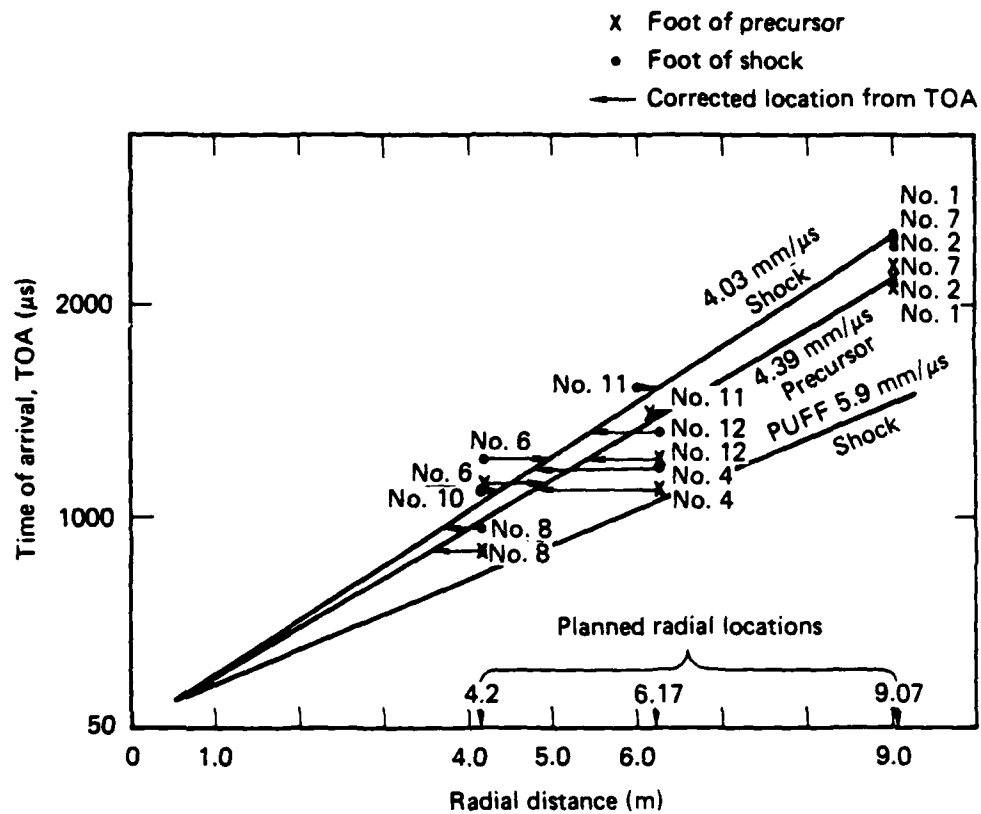
Figure 32. Time of arrival data.

lithostatic stresses.) At the experiment depth of approximately 800 feet (744 m),
the horizontal component would be about 0.01 kbars (1 MPa). If a bias stress
existed, our compression sensitivity calibration would be applicable, and assuming
that the gages cannot respond to a tensile stress (some were coupled to the salt
cores by a slip plane of sticky Kapton tape incapable of supporting tensile stress),
the maximum reduction in stress from the bias or preshot value could be only 0.01
kbar (1 MPa). The records yield an average "tensile" stress of 0.04 to 0.05 kbar (4
to 5 MPa); therefore, lithostatic stress does not appear to be a good explanation
for the observed "tensile" stress. We can only conclude that either

(1) A combination of bias stress, bending, and tensile stress produced
     the observed change, or

(2) The tensile stress measurement is valid and we can compare the
     measurements with the calculated values.

Calculated and measured peak tensile stresses are listed in Table 4. Also
shown are the durations of the tensile phase. In general, the "measured" stresses
are much larger and of longer duration than the calculated stresses. Although the
amplitude difference could be due to the use of the 0.05 Ω/Ω/kbar calibration
factor, the duration difference appears to be real and inexplicable.

Table 4. Tensile stress amplitude and duration, calculated versus observed.

Radial distance (m)	Peak tensile radial stress (MPa)		Duration (μs)	
	Calculated	Observed	Calculated	Observed
3.65	--	0.5	--	>4000
3.65	--	0.64	--	>3800
4.2	0	--	0	--
4.6	--	0.54	--	>4000
4.9	--	0.37	--	>3700
6.0	0.026	--	138	--
6.3	--	0.24	--	>4000
6.3	--	0.24	--	>4000
9.0	0.162	--	556	--
9.07	--	0.79	--	>2000
9.07	--	1.0	--	>3300
9.07	--	1.0	--	>4000
9.07	--	1.15	--	>4000

SECTION 6

CONCLUSIONS AND RECOMMENDATIONS

Gage orientation uncertainty prevented our achieving the major objective of the test and one of the secondary objectives, gage-to-gage comparison. However, the uncertainty does not affect a comparison of the response of two sensors in one gage, which appears to be excellent: compare the record of Figure 25(a) with that of Figure 25(b) and Figure 31(a) with Figure 31(b). The significance of the reproducible response is that variations in waveform due to sensor nonreproducibility and gage-core interaction differences can be eliminated. That is, if we could determine gage orientations, we could proceed to a comparison of gage-to-gage response and finally to comparing the remaining parameters of our test matrix (stress gradient and stress difference).

Records with very low noise levels (equivalent to less than a few bars) resulted in high resolution waveforms that appear to satisfy the objectives of the experiment during the loading portion of the waveforms. That is, the quality of the data during loading would be high enough to determine stress gradients and stress differences if gage orientations were known accurately. The veracity of the data during unloading is questionable and could probably not be used in an analysis of gradients and stress differences. The loading data show a precursor of approximately 10 bars (1 MPa).

The experiment successfully evaluated one of the remaining parameters of the test matrix in that two sensors in one gage responded in the same manner. The response of gage-core combinations in separate drill holes could not be evaluated.

The actual locations of the gages could be established from the time-of-arrival data. However, gage orientations are too uncertain to permit calculation of stress quantities that are required for comparison with velocity data.

Although tensile stresses appear to have been measured, the validity of the measurement is doubtful.

The finite element analysis of the core-medium interaction indicates that the measurement of free-field tangential stress is difficult and depends more strongly on the coupling between the core and free-field medium than does the measurement of radial stress. This analysis also indicates that the size of the gage is important.

Because of the unusually high quality of the waveforms obtained in this experiment and because of the high integrity of the medium, we recommend that

51

posttest gage locations and orientations be determined and that the comparison of stress gradient, stress difference, and velocity be completed. Successful completion of this effort will provide the ground motion community with the only experimental assessment of the validity of in-situ stress measurement in divergent flow, particularly tangential stress measurement.

SECTION 7

LIST OF REFERENCES

1. J. T. Rosenberg, P. S. DeCarli, G. Falconer, and D. D. Keough, "In-Situ Constitutive Relations of Soils and Rocks, Spherical Field Tests and LASS Results for Pre-Dice Throw II Materials; LASS Error Propagation Analysis," SRI International Final Report, Contract DNA001-76-C-0113 (April 1977).

2. R. Mak, "Stress Gage Inclusion Analysis," Poulter Laboratory Technical Report 006-82, SRI International (March 1983).

3. P. S. DeCarli and D. D. Keough, "Adaption of the Ytterbium Flatpack Stress Gage to Low Soil Stress Measurment," SRI International Final Report, Contract DNA001-80-C-0142 (July 1982).

4. A. L. Florence, L. E. Schwer, T. Cooper, J. T. Rosenberg, and D. D. Keough, "Inclusion Effects on Stress Measurement in Rock and Soil," SRI International Final Report, Contract DNA001-83-C-0279 (April 1984).

5. Y. M. Gupta and G. Privitzer, "Compression and Shear Wave Propagation in Salt and Granite," SRI International Final Report DNA 5058F (August 1979).

6. Private Communication with Lynn Seaman, SRI International.

7. C. J. Maiden and S. J. Green, "Compressive Strain Rate Tests on Six Selected Materials and Strain Rates from 10^{-3} to 10^4 inch/inch/second," General Motors Corporation Report TR65-26 (May 1965).

8. Y. M. Gupta and D. F. Walter, "Piezoresistance Response of Ytterbium Under Static and Dynamic Loading," SRI International Technical Report, Contract F49620-81-K-002 (April 1982).

9. Private Communication with P. S. DeCarli, SRI International.

10. Private Communication with J. K. Gran, SRI International.

APPENDIX A

COMPUTATIONAL AND EXPERIMENTAL PROGRAM FOR VERIFICATION
OF DYNAMIC IN-SITU FREE-FIELD STRESS MEASUREMENTS

J. Thomas Rosenberg

BACKGROUND

This Appendix presents an overview of the dynamic in-situ stress measurement problem as it applies to DNA objectives and outlines a systematic interdisciplinary multiagency approach to the problem. An increasingly urgent need exists in major Defense Nuclear Agency programs for reliable in-situ stress history measurements in geologic materials loaded by aboveground, surface, and underground detonations. The measurements are needed for a broad range of study materials, stress amplitudes, strain rates, deformation geometries, and material response regimes. Nevertheless, for virtually none of these environments is a reliable and validated stress measurement capability now available.

Four major reasons for this lack are suggested below:

- The necessity of stress measurements is not always appreciated. A mistaken notion has persistently reappeared in the DNA community that the mechanical state of a dynamically loaded continuum can be meaningfully defined without recourse to stress measurements. Instead, internal mass motion histories (or their equivalents such as displacement, acceleration, or strain histories) sometimes augmented by boundary conditions are used in an attempt to validate or optimize wave code calculations that then provide stress information. As discussed later in this section, this procedure is invalid; stress measurements are unequivocally necessary in DNA programs.

- Stress measurement capabilities of use to DNA have not already been developed in other research areas. The environments of interest to DNA are uncommon except in military and mining applications because they are generated by large amplitude detonations and their related effects, but by little else, and because they generally occur within large masses of undisturbed in-situ geologic material. Because these environments differ qualitatively from those in research areas within the civil engineering, geophysics, and shock wave physics disciplines for which workable stress measurement capabilities already have been developed, there is no simple carryover or extrapolation to the DNA environments. Thus to obtain a dynamic in-situ stress measurement capability, DNA needs to support a development program for that purpose.

- The problem has been judged intractable by some parts of the DNA community. Until recently, many members of the DNA community have considered the development of a useful dynamic in-situ stress measurement capability unachievable because of the technical difficulty of various parts of the problem and, more important, the lack of well-developed solution techniques for addressing them.

- The problem has not been attacked with a well-funded systematic multiagency program. Distinctly different skills and capabilities are required to develop and validate stress measurement capabilities for DNA applications. Since these skills do not reside with a single contractor, since the problem is so complex and because the cost of DNA programs such as UGT tests, STP, and CARES that will be adversely affected by inadequate stress measurements approaches 10^8 dollars., a coordinated interdisciplinary multiagency multiyear program is necessary.

56

NEED AND RELEVANCE

NEED FOR DYNAMIC IN-SITU STRESS MEASUREMENTS IN DNA APPLICATIONS.

Many current and long-standing DNA programs require specification of the
mechanical state at points within a dynamically loaded continuum. By definition this
implies quantification of both the stress and strain tensors at the points of
interest. The question sometimes arises as to whether the required stress informa-
tion can be obtained from the presumably more easily acquired strain information.
The fundamental structure of continuum mechanics does not permit the determination
of the stress tensor within a body solely from knowledge of the strain tensor
everywhere nor from knowledge of the strain tensor augmented by boundary conditions.

The three methods that we know for determining stress are (1) measuring stress
directly, (2) making use of established constitutive relations, or (3) applying
empirically determined stress scaling relations. Because neither constitutive nor
scaling relations of sufficient reliability already exist for most materials of
interest, and because neither are derivable directly from theory, implementation of
any of these three approaches in DNA programs requires the prior development of a
stress measurement capability.

As an example of the importance to DNA of developing a stress measurement
capability, consider the problem of generating material properties for in-situ site
materials. For more than twenty years, efforts to use wave propagation calculations
to predict ground shock environments induced by conventional or nuclear explosions
have been unsuccessful. The problems are attributed to various deficiencies in the
material properties and models used in the calculations. As a result DNA contrac-
tors have devoted considerable attention to procedures for developing adequate
material property data bases and methods for modeling them in numerical calcula-
tions. It is now fairly widely acknowledged that such models must either be based
on, or validated with, in-situ tests and that loading and deformation rates in such
characterization tests should simulate or span those of interest. The strain path
approach goes a step further and recommends that the experimental data base
characterizing the material be generated along paths in strain space that simulate
those to be calculated, in which case a material model is not strictly needed at
all. However, in light of our preceding arguments, not one of these improved
modeling approaches can be implemented without prior development of a reliable
dynamic in-situ stress measurement capability.

A commonly used modeling approach that we believe is unlikely to succeed is to model a particular site material, in the absence of stress data, by computationally simulating an actual in-situ test at the site and iteratively adjusting the constitutive relation until the measured particle motion is adequately reproduced by the calculation. Unfortunately, the stresses predicted in such a computational procedure are not unique. The model may, therefore, be expected to adequately describe the motions (not the stresses) in tests like the one used to generate it, but it is highly unlikely to accurately predict stress or motions under other test conditions.

Stress quantification is unequivocally necessary to specify the mechanical state of a continuum. All known means for accomplishing this require dynamic in-situ stress measurements. Since many DNA programs inherently require such mechanical state determinations, the need for stress measurements in DNA programs is established.

NEED FOR A DNA INSTRUMENTATION PROGRAM.

A DNA program to develop capabilities to measure dynamic in-situ stresses is now necessary because of current measurement inadequacies including:

- Lack of proven measurement systems or accepted measurement guidelines for applications such as the bidirectional flows beneath near-surface detonations or spherical flows near contained detonations.

- The data are often not reproducible.

- The measurement system is not calibrated or validated in the measurement environment.

- Measurements often show unrealistic properties such as features not correlatable to expected stress profiles, large variations from amplitude-range trend lines, peak stresses greater than driving pressure, and large late time amplitudes violating impulse considerations.

A general program to develop and validate dynamic in-situ stress measurement capabilities is directly relevant to DNA programs such as CARES, STP, deep basing, and UGTs.

58

To define the stress measurement problem addressed by the program, we first
list a number of stress measurements relevant to DNA applications and recommend some
practical objectives for a DNA stress gage development program. Second, we describe
an idealization of, and nomenclature for, the components of a stress measurement
system. Third, we cite the key problems that we believe need to be addressed in the
development of stress measurement systems adequate for DNA applications.

RECOMMENDED SCOPE.

DNA applications require dynamic in-situ stress measurements in an immense
range of environments, that is, for various study materials, deformation geometries,
peak stresses, strain rates, and material response regimes. Table 5 lists some of
the specific measurements and environments of interest to DNA and indicates the
range of values that can be assumed by the various parameters.

Table 5. Free-field stress measurements and ground shock
environments of interest to DNA.

Measurement			Environment		
Stress Type	Deformation	Material	Peak Stress (GPA)	Strain Rate (s^{-1})	Material Response
Principal (no shear stresses)	One-dimensional . Uniaxial . Cylindrical . Spherical	Sandy soil (dry and wet)	10^{-3} (150 psi to 10^2 (1 MPar)	Static to 10^6	Elastic Hydrodynamic
Normal shear (stresses)	Two-dimensional . Axisymmetric . Plane strain	Clays (wet and saturated) Tuffs (dry and wet)			Elastic/plastic Elasto/visco-plastic
Shear	Three-dimensional . Finite sizes . Reflections (geologic interfaces, structures, ...)	Grouts (dry and wet) Dome salt Granite Other hard rocks			

59

We impose two initial constraints that eliminate some of the measurements and environments in Table 5 from consideration in this program. First, the free-field stresses must be compressive before and during the period for which they are to be measured. Neither the measurement systems nor the experimental techniques considered here are suitable for tensile stress measurements. Without evidence to the contrary, it should be assumed that tensile stresses preceding the measurements will alter the installation or otherwise compromise the measurement system response. The second constraint is introduced for efficiency of research and exposition. The stress history profiles are limited to the simplest shape of interest: a monotonically increasing compression followed by a monotonic, but not necessarily total, release. More complex or cyclic profiles will be introduced explicitly if necessary.

In the following subsections we further limit the large number of specific environments in Table 5 to be studied. The approach is to select from the list in the table four materials, three stress ranges, and two strain rates.

Two additional factors that influenced our recommendations concerning the scope of the investigation are the relative tractabilities of the technical problems and the nature of the specific measurement systems to be investigated. Certain cases of interest in Table 5 are strongly recommended for exclusion as being beyond present capabilities. The measurement systems emphasized here are based on *piezoresistance* transducers because of their adaptability to the full range of environments in the table.

Measurements.

Development of a capability to measure principal stresses should be the first priority because of their relevance and because of the severe measurement complications that are added if shear stresses also act on the measurement plane. Normal stress measurement on planes containing shear stresses are recommended for later study in a more limited set of environments (see below). Shear stresses should be excluded because they require different measurement and testing techniques and, in the free-field, can be derived from a set of successful principal stress measurements. A separate shear stress program may be considered if promising shear stress transducers become available.

The one-dimensional deformation geometries in Table 5 are assigned the highest priority because of their importance and their relative tractability. Two- and three-dimensional strain geometries, however, should be excluded as targets for a

60

validated experimental measurement capability (but may be included in computational studies and gage evaluation experiments). These geometries are presently intractable because of the difficulty of verifying measurements and the complication of rotation of principal stress axes that is often induced by the interaction of the measurement system with incident stress wave.

Uniaxial strain should be the baseline one-dimensional case because one stress component (the axial principal stress) can be independently determined dynamically and statically, providing the foundation for measurement system development and validation (see Suggested Program). It is also recommended as the appropriate case for initial development of non-principal normal stress measurement technqiues.

Despite their importance in DNA applications, spherical and cylindrical strain should be considered after uniaxial strain because only partial validation is possible (see Suggested Program). Since spherical and cylindrical strain add very similar complexities to the stress measurement probiem, but spherical strain has one less independent stress component making it somewhat simpler to validate, we assign cylindrical strain the lowest priority of the one-dimensional strain deformations.

The measurements recommended for inclusion in a free-field stress measurement development program are summarized in Table 6. The selected quantities are of great importance to DNA programs, include the principal features complicating the excluded measurements, and are presumed to be more amenable to validation than the excluded quantities. Successful development of techniques for measuring these quantities will provide an appropriate foundation for attempting the other measurements.

Table 6. Recommended scope of free-field stress measurements.

Deformation Geometry	Stress Component	Priority
Uniaxial strain	Axial	1
	Transverse	2
	Non-principal normal	4
Spherical strain	Radial	3
	Hoop	3
Cylindrical strain	Radial	5
	Hoop	5
	Axial	5

61

Environments.

To decrease the size of test matrix by identifying a manageable number of constitutive response classes spanning the environments in Table 5, we first consider the test material. The following four geologic classes contain most of the materials of interest: dry granular soils, wet compactable soils, low strength silicate rocks or rock simulants, and low porosity hard rocks and minerals. Because these classes differ qualitatively in the mechanical properties that are expected to affect stress measurement, we recommend that at least one material be selected from each to class for a measurement development program.

We recommended that the investigation be limited to the following materials: (1) dry rained sand (low cohesion, high initial compressibility, high hysteresis, easily handled), (2) wet clay or drilling mud (low shear strength, decreased compressibility and hysteresis, care required to avoid local compaction, moisture loss), (3) MINI JADE or other grout (moderate strength, compressibility, and hysteresis; care required to avoid bubbles, nonuniform cure), and (4) dome salt (moderate strength, low compressibility and hysteresis, fairly easily handled).

A few general factors affecting the selection of peak stress amplitudes and strain rates at which to load these materials are cited here. Consider first peak stress amplitudes. Each of the suggested materials is to some extent porous and thus may be modeled as having an elastic, a crush up, and a fully compacted phase. Some phases may be negligible such as the elastic phase of rained sand, and others may be further subdivided because of effects such as silicate phase transformations. Of the three phases, the crushup region where stresses are near and above the elastic limit, and where material strength effects are dominant, is especially challenging and should receive special attention.

Strain rate dependent can occur in either the test material or the gage. Therefore, at least two rates should be investigated. One should be quasi-static so that strain rates are low enough that (1) static calculations and properties apply and (2) simple mechanical loading devices can be used to generate them. The second strain rate should be greater than or equal to the maximum expected in DNA applications to determine whether dynamic effects are important and require further study. Extremely high rates can be achieved in small-scale laboratory or field experiments, and more realistic rates can be achieved in moderate-scale or larger field experiments.

In summary, the many environments in Table 5 can be effectively surveyed by a fairly manageable number of specific cases. This number is roughly estimated as 24:

4 materials x 3 stress ranges x 2 strain rates. This is the number of cases of interest for each measurement quantity selected from the first part of Table 5.

STRESS MEASUREMENT SYSTEM COMPONENTS AND TERMINOLOGY.

The components of a piezoresistant free-field stress measurement system are described below and shown in Figure 33. We assume a test material M (also the native or matrix material) in some specified initial state. Boundary conditions applied to M induce a free-field stress everywhere within and, in particular, at some point P where we wish to measure the amplitude history of one or more of its components. The free-field stress at P is called σ_{ij}^M (P,t), and an individual principal free-field stress component at P is called σ_i^M (P,t).
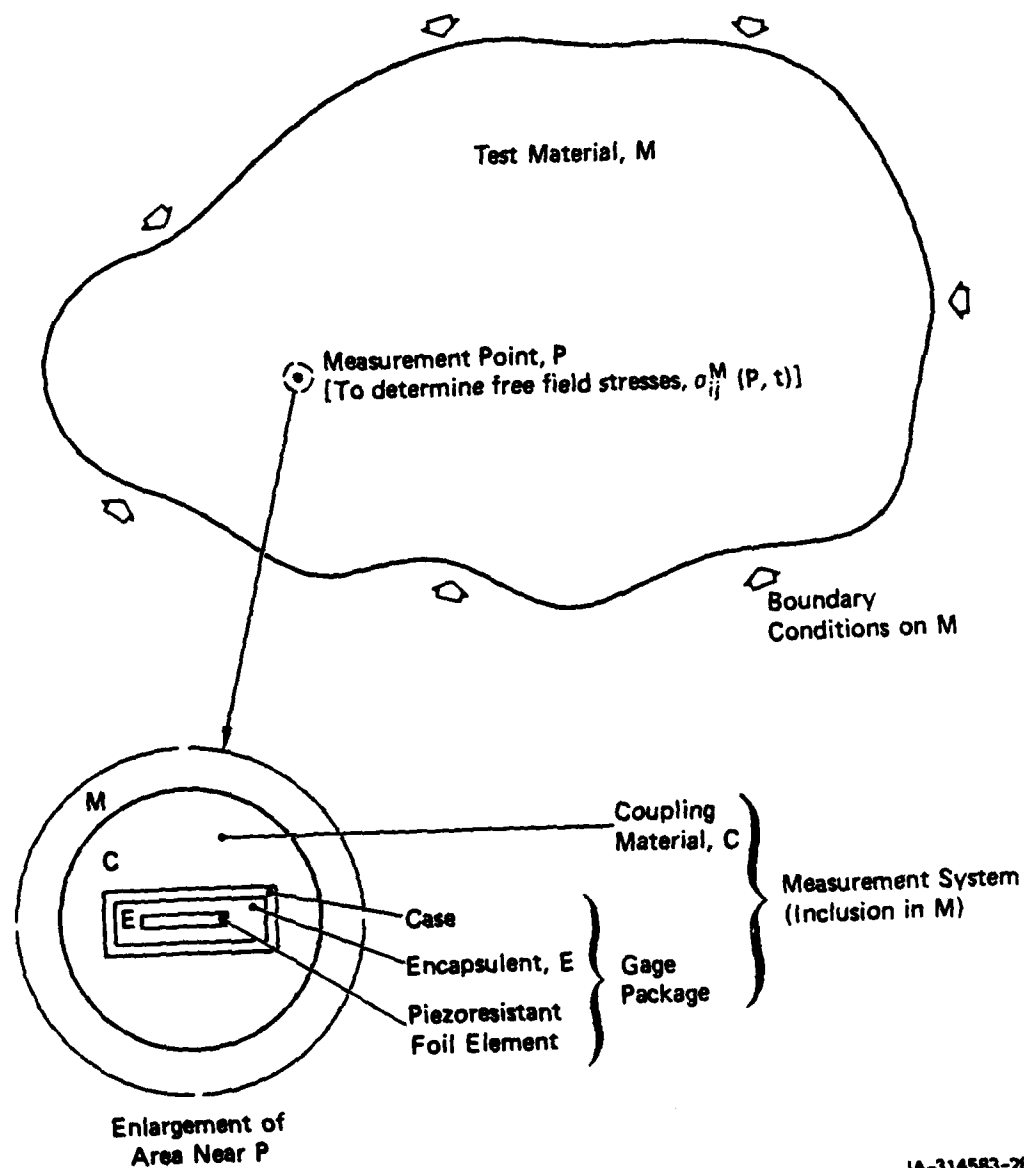
Stress Measurement System.

To perform a stress measurement at P, we must disrupt M, usually removing considerable native material, and insert a complex stress measurement system, or inclusion as shown in the enlargment in Figure 33. Figure 33 is a plane section perpendicular to an axis extending through P from some physical access point on an external surface of M. The stress measurement system is composed of two parts, a stress gage package and a coupling material, discussed separately below.

For DNA purposes, the external boundary of the inclusion in M has only two interesting shapes in the plane of Figure 33: a circle, as shown, or a highly oblong rectangle. The circle is of interest because it is eminently practical in the field to drill an access hole with this cross section. A requirement for any other shape usually greatly complicates implementation problems for in-situ field tests of any significant size. The oblong rectangle is of interest because, given our current understanding of inclusion effects, it apparently generates the smallest and most calculable perturbations to the free-field stress in many cases and thus offers the greatest hope for a successful measurement. In three dimensions, then, the two inclusions of primary concern are a circular cylinder in a long borehole or a rectangular slab in a long slot where length is measured in the direction perpendicular to the plane of Figure 33.

Coupling Material and Gage Package.

The stress measurement system consists of a gage package and a coupling material. The coupling material may be back-filled native material, grout, or anything else that is practical to handle, reliably fills the gaps between M and the gage package, and has appropriate stress transmission properties.

63

Figure 33. Schematic section of free-field stress measurement problem (above) and stress measurement system components (enlargement, below).

JA-314583-28

64

The gage package consists of a case, an encapsulent (insulator), and a piezo-resistant foil (transducer, sensor or active element). The case (1) controls the stresses and strains transmitted to the transducer (for example, minimizes lateral strains and generates uniform loading), (2) produces desirable mechanical properties (such as a high compressive modulus) for the overall gage package, and (3) promotes measurement survival. The encapsulent provides electrical isolation for the piezo-resistant foil and controls the type of deformation applied to it (for example, causes the foil deformation to be hydrostatic or uniaxial strain). The transducer may be a single piezoresistant material or a strain-compensating composite of several materials. Although the transducer may have various planar shapes, for present purposes it is adequately modeled as shown in Figure 33, that is, a linear ribbon or foil lying in the plane on which the normal stress is to be measured.

Additional Terminology.

Relating the resistance change of a piezoresistent element in a particular gage package design to one component of the local stress on the element or the surrounding package is called foil or gage package calibration, respectively, in this report. The ratio of a component of the local stress within an inclusion to the (hypothetical) free-field value of that component at the same point is called the registration factor. For successful development of piezoresistant free-field stress measurement systems, both gage calibration and registration factor problems must be successfully addressed.

KEY TECHNICAL PROBLEMS.

The six steps required for the successful development of a free-field stress measurement system as follows:

(1) Specification of required measurement accuracy.

(2) Solution of the registration factor problem, that is, quantifying the free-field stress modifications caused by each component of the measurement system and then designing the system so that these result in a sufficiently well behaved overall registration factor.

(3) Solution of the calibration problem, that is, designing the system so that a component of the local stress in the transducer can be determined from the transducer resistance change.

(4) Solution of the implementation (or engineering) problem, that is, translating the theoretical solutions of the registration factor and calibration problems into specific hardware and construction methods.

65

(5) Validation, that is, testing the measurement system in environments of interest and quantifying its performance characteristics and accuracy.

(6) Documentation of results, that is, putting the program results into an accessible updatable format to facilitate both the application of developed principles and standardized tests to new measurement environments and the incorporation of later developments into measurement system design.

Steps (2) through (5) are basic technical requirements common to any free-field stress measurement system development process. Steps (1) and (6) are requirements added to maximize the efficiency of the development process and usefulness of the results. It is important to differentiate among the four basic technical requirements, steps (2) through (5), so that proposed stress measurement development efforts can be evaluated in terms of which part of the problem they address and the extent to which they contribute to the overall solution.

Of the four steps (2)-(5), we assign the registration factor problem, step (2), first priority on the basis that if the local stress at the transducer cannot be related to the free-field stress, then solving the calibration problem, Step (3), is pointless. The converse is false; if the piezoresistance calibration problem cannot be solved, the registration factor problem remains vital since other transducers exist.

The solution of the registration factor problem is expected to be a function of the test material and deformation geometry. However, the solution of the calibration problem is expected to be independent of both the test material and deformation geometry because the case and/or encapsulent control the stress and strain fields in the transducer. Both registration factor and calibration are expected in general to be functions of loading amplitude and history. Thus, at the outset we must expect the overall transfer function to be sensitive to material (class) and amplitude/history and possibly to deformation geometry. Rate dependence, if important, is expected to affect the registration factor through inertial or material property effects; piezoresistance is not expected to be rate dependent. Discussions of the technical problems associated with these six development steps follow.

Accuracy Requirements.

Because the free-field stress gage development problem is so complex, measurement accuracy requirements must be established at the outset to prevent the development of either unacceptably coarse or unnecessarily precise measurement systems. The two required steps are to identify a representative set of expected

66

DNA stress measurement applications and to determine the measurement accuracy required to meet the application objectives. No unduly difficult technical problems are expected although significant effort may be required. For example, if the intended program objective is material model development or differentiation, generic calculations to establish the magnitude of stress prediction discrepancies between candidate models may be necessary.
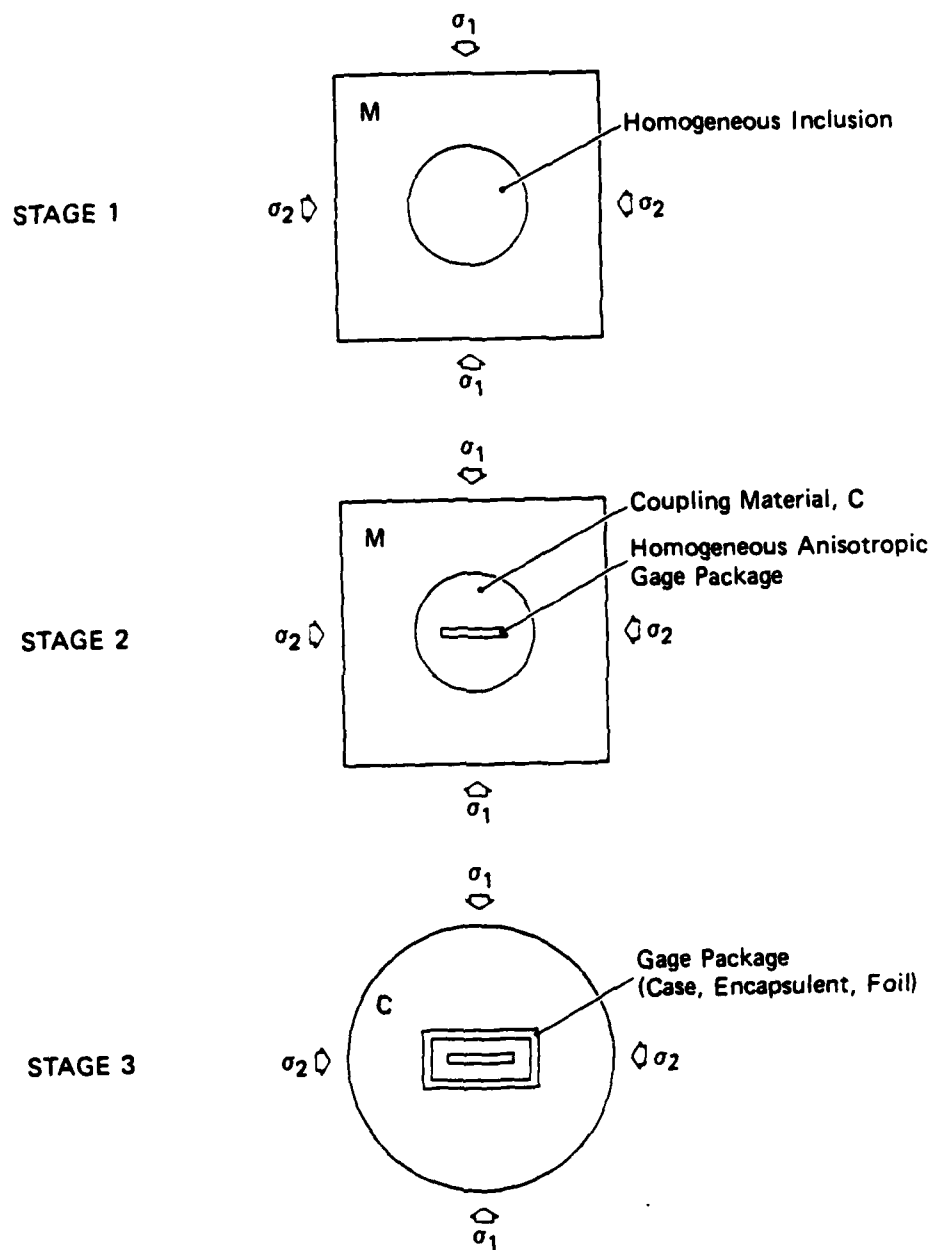
Registration Factor.

The objective is to design the parts of the measurement system to have mechanical response such that the normal stress (assumed to be the output controlling quantity) in the gage element is uniquely, and if possible, conveniently relatable to the corresponding component of the free-field stress. The ideal, of course, is a constant registration factor with a value of 1. However, even in static low amplitude soil stress measurements this ideal is not attainable; instead, a high-modulus high-aspect-ratio inclusion is used to achieve a registration factor that is sensibly constant with respect to variations in load amplitude and test material (that is, is well-behaved) at the expense of significant overregistration (nonunitary registration factor).

Less desirable, but workable, is a variable but well-behaved registration factor. Registration factors that, within one class of test material, are multi-valued functions of the free-field normal stress or are strong functions of more than one component of the free-field stress are too environment-specific to be of practical use to DNA. The registration factor problem is difficult because (1) the properties of geologic test materials are highly variable and hysteretic during a load-release cycle and thus do not maintain constant relationships to the properties of the structural materials used in the measurement systems (2) registration factors are strong, but unknown and hard to control, functions of the boundary conditions, and (3) possible rate dependences of material or structural response must be considered.

In addressing the registration factor problem, it is convenient to model the stress measurement inclusion in three stages of increasing detail starting with a macro view (see Figure 34):

Stage (1)   Homogeneous inclusion in test material (that is, a uniform inclusion with the averaged mechanical properties of the coupling material and gage package).

Stage (2)   Homogeneous gage package (that is, a uniform inclusion with the averaged mechanical properties of the gage package) in the coupling material within the test material.

67

STAGE 1

STAGE 2

STAGE 3

σ_1

M

Homogeneous Inclusion

σ_2

σ_2

σ_1

σ_1

M

Coupling Material, C

Homogeneous Anisotropic
Gage Package

σ_2

σ_2

σ_1

σ_1

C

Gage Package
(Case, Encapsulent, Foil)

σ_2

σ_2

σ_1

JA-314583-29

Figure 34. Three stages for modeling stress measurement system as an
inclusion in native material M.

Stage (3) Gage package components in coupling material.

In stage (1), we can study the effect on registration factor of (1) inclusion shape, (2) effective inclusion mechanical properties, and (3) inclusion-matrix interface properties. The last is especially difficult, both computationally and experimentally. Recent work at SRI has indicated that, for elastic inclusions, a welded interface is necessary for a well behaved registration factor, but if the inclusion goes plastic, this condition may not be necessary. The homogeneous inclusion results provide a basis for developing an inclusion design that has acceptable registration factor properties and is feasible for field use; for example, variations of registration factor with position in the inclusion must be minimized near potential measurement points.

In stage (2), the same type of considerations apply to the gage package. In addition, we must evaluate the possible perturbations on the stage (1) results caused by the nonuniformity of the measurement system. The objective is to deter-mine those gage package properties, such as anisotropic strength, that will decouple the registration factor as much as possible from the various undesirable dependences cited previously.

In stage (3), the individual gage package components are designed subject to the overall constraints established in stage (2). At this point the problem is effectively decoupled from the test material M so we are effectively also addressing part of the package calibration problem. In fact, requirements imposed by the transducing characteristics of piezoresistant foils should be explicitly included at this point. For example, it would greatly simplify the calibration problem, discussed next, if the encapsulent were a fluid so that the applied stresses are equal and the piezoresistance hysteresis observed in uniaxial strain deformations is minimized. The objectives are to identify desirable encapsulents, to design for simplified stresses and strains in the piezoresistant transducer, and to address the usual registration factor considerations of shape, material properties, and interface conditions.

Calibration.

The technical problems of calibration lie in two areas: development of adequate piezoresistance functions for gage materials of interest (fundamental studies) and determination of gage package designs and associated analysis methods for which local normal stress can be determined from the gage resistance change (calibration). The first area, fundamental studies, requires evaluation of the

69

parametric coefficients in the piezoresistance equation relating resistance change to stress, strain, temperature, and history. The key unsolved technical problems are determination of the deformational history dependence of the terms in the resistance change equation and quantification and validation of the coefficients.

The second area, calibration, presents three technical problems. The first is to determine under what conditions the foil resistance change is dominat ¹ by, or directly relatable to, local normal stress. Two examples are believed to be hydrostatic loading and uniaxial strain (in foil). If no such conditions are found, it still may be possible to proceed by using multiple sensors to evaluate the additional local strains or stresses that are required to relate resistance change to normal stress. The second problem is to develop engineering designs to achieve these conditions, and the third is to provide procedures for calculating the normal stress from the resistance change.

Implementation.

Implementation includes both (1) translating the designs developed in solving the registration factor and calibration problems to practical working hardware and (2) developing emplacement procedures and tools. Thus, measurement systems must be good mechanical analogs of the developed design: gage packages must be electrically reliable in expected loading environments and not excessively expensive to fabricate, and emplacement procedures and tools, must be practical in field environments.

Problems that have been encountered in previous work can be expected to recur here. These include electrical survivability, especially at cable junctions or other discontinuities in high stress applications; variable resistance junctions (not piezoresistant effects) in low stress applications; baseline shift of unknown origin; characterization of encapsulent; development of test material slot cutting tools, if this shape inclusion is necessary; and control of coupling material uniformity at depth, in the vicinity of the gage package. In addition, static and dynamic load tests intended to validate aspects of implementation such as survivability have been too mild in some cases and have introduced extraneous features (such as nonuniform loads) in other cases.

Validation.

Validation refers to proof-of-measurement, that is, verification in the environments of interest that the stress measurement system measures the desired free-field stress component to within a specified degree of accuracy. This is

70

probably the most difficult technical problem of all because it requires calibrated test environments (ones in which a free-field stress component is known). Such environments are generally unavailable. Even for the environments recommended for this investigation (Table 6), only the axial stress, under uniaxial strain deformations, can be independently determined by appropriate motion measurements. Our approach to this problem is presented in the section, Suggested Program.

A second validation problem is to determine sensitivity to nonideal loads and conditions. Fxamples include nonhomogeneous explosive sources such as HESTs, misoriented gages or loading direction, bending, dimpling, cross axis sensitivity, and sensitivity to inherent local inhomogeneities characteristic of specific test materials.

The final validation problem is to verify that the displacement behavior of the measurement system and its internal components in time-dependent motion fields is Lagrangian. It is assumed that the measurement system moves with the surrounding particles and that the internal components retain their initial relative positions. These assumptions need to be examined to validate both system performance and subsequent data interpretation.

Documentation.

Documentation is included as a problem to ensure that three problems that can limit the development program usefulness are recognized and addressed. These problem areas are access, generalization, and updating.

Access refers to the procedures that will be necessary to obtain the program results. Since a multiagency program is envisioned, a single document unifying the results is highly desirable.

Generalization refers to the problem of relating program results developed for specific environments to other environments of future interest. To facilitate such extrapolations or interpolations (1) development approaches and validation tests should be standardized and described adequately to permit their use in future work and (2) results should be presented, when possible, in terms of underlying parametric dependences as well as for the specific conditions under which they were generated.

Updating refers to the process for incorporating later findings. Since ultimate solutions, even to the component parts of the problem, are not expected, the results should be reported in modular form to permit later findings to be easily added.

SUGGESTED PROGRAM

The program for developing the free-field dynamic in-situ stress measurement capability is presented in terms of the six development steps described above. The six steps, with their associated problems, are summarized in Table 7.

SET ACCURACY REQUIREMENTS.

An early task in a unified stress measurement development program is to specify the accuracy necessary for present and foreseeable DNA purposes. This can be accomplished by (1) identifying DNA programs with free-field stress requirements, (2) calculating the stress accuracy needed to satisfy the objectives of these programs, and (3) developing a set of measurement requirements, for example, by material class, amplitude range, and so on, that encompasses the results of (2).

DETERMINE INCLUSION REGISTRATION FACTORS.

Finite element codes now calculate structure-medium interactions including realistic interface conditions such as finite strength, slip, and friction. Therefore, and because parameter studies can be performed more effectively with numerical than with physical experiments, the major tool recommended for this step is a finite element structural code. However, because of the approximations involved in such calculations, analytical solutions and experiments must be closely integrated with the code calculations to produce credible results. In addition, a few large finite difference calculations are recommended as part of the finite element validation process.

Task 1 - Finite Element Calculations.

The stress measurement system can be modelled in the three stages given in Table 7. In Task 1, each of these stages is addressed by a series of two-dimensional finite element parameter variation calculations, taking into account the deformation geometries, classes of matrix material, and measurement system parameters of interest. The limitations to the range of applicability of such two-dimensional calculations due to three-dimensional effects must be explicitly determined. Most interactions will probably be adequately described by quasi-static calculations (inertial stresses negligible), but the upper bound on free-field deformation rates for validity of this approximation should be established, and dynamic finite element or difference calculations should be performed where

Table 7. Summary of free-field stress measurement system development steps and problems.*

Steps	Tasks and expected problems			
1. Set accuracy requirements	Identify representative applications • Inclusiveness • Future needs	Establish stress measurement accuracy requirements for each applications • Interpretation • New calculations	Set accuracy requirements • Unification	
2. Determine inclusion registration factors	Solve homogeneous inclusion in matrix • Shape • Average properties • Matrix/inclusion interface strength/slip • Residual stresses • Separation • Spatial variation • Rate dependence • Matrix material • Validation	Solve inhomogeneous inclusion in Matrix • Package shape • Average package properties and anisotropy • Package/coupling material interface strength/slip • Spatial variations • Rate dependence • Perturbations to homogeneous inclusion results • Matrix material dependence • Validation	Solve gage package in coupling material • Case design (anisotropy) • Encapsulent properties • Foil stress/strain • Spatial variations • Rate effects • Coupling to calibration requirements • Validation	Solve for Overall measurement system • Reduce idealizations to overall design • Calculate registration factor for overall design • Validation
3. Solve calibration problem	Develop and quantify fundamental understanding • Stress/strain coefficient quantification • History dependence • Hysteresis • Validation	Use piezoresistance information to solve calibration • Desirable foil environment • Required measurements • Data reduction procedure • Validation/expected accuracy		
4. Implement	Translate results of steps 2 and 3 to engineering • Sensor development • Material selection • Construction procedures • Overall transfer function	Test component performance • Survivability • Qualitative behavior	Develop emplacement techniques • Hardware • Coupling material • Procedures	
5. Validate for intended applications	Perform uniaxial strain tests (static/dynamic) • Dynamic source • Motion measurements • Test bed uniformity • Transverse stresses	Extend to divergent one-dimensional strain • Analyses (FE, FD) • Dynamic consistency tests • Stress resolution	Test sensitivity to nonideal conditions • Gage misorientation • Bidirectional loading • Multiple loading • Local inhomogeneities	Test for overall and internal velocity equilibration • Non-Lagrangian data • Survivability
6. Document Program results	Put results in an accessible reference • Unification of individual reports	Cast results into forms facilitating generalization to untested conditions • Find underlying parametric dependences • Fully document recommended development procedures (standardization)	Make reference document easily updatable • Develop modular report format	

*See Problem section for expanded discussion.

73

necessary. Whenever possible, analytic solutions should be developed and used to check the code.

Code calculations of dedicated experiments, whether or not these simulate free-field stress measurement systems, are vital to validate the finite element machinery: codes, modeling assumptions, and material properties. The basic piezo-resistance equation should be incorporated into the finite element calculations so that the expected foil resistance changes can also be predicted and used in solving the calibration problem. The objectives of Task 1 are to identify mechanical measurement system designs with well behaved registration factors, to develop predictive relationships for registration factor as a function of measurement system design parameters, and to analytically and experimentally validate the finite element codes used to accomplish this.

Task 2 - Static Registration Factor Experiments.

Static or quasi-static experiments should be designed and performed both to simulate the measurement system design cases of interest and to test the relevant capabilities of the finite element code. Experimental environments that would not be appropriate for free-field stress measurements, but that do test the various capabilities of the code and also permit credible measurements, are a promising approach. Strain measurements on structural material surfaces and pressure measurements in fluid cavities are the two suggested diagnostic tools. Triaxial loading machines can be used to generate both (1) environments of interest from Table 5, such as uniaxial matrix strain, and (2) other environments useful for testing the code, such as triaxial stress. The uniaxial matrix strain case is especially important because, under static conditions, no stress gradients exist in the matrix in axial or transverse directions, and each of these stress components can be independently measured at the loading surfaces. This provides an absolute validation environment (static) for both axial and transverse stresses of great use in the validation tasks described later.

Task 3 - Dynamic Registration Factor Experiments.

High rate uniaxial strain (matrix) experiments analogous to the quasi-static experiments in Task 2 should be performed to experimentally evaluate the importance of dynamic effects. These can be efficiently performed in small scale using labo-ratory gas gun experiments, in moderate scale using 8- to 12-inch-diameter (0.2 to 0.3 m) explosive shots or larger gas guns, or in intermediate-seal test site tests such as dilute explosion HESTs.

74

SOLVE CALIBRATION PROBLEM.

Task 1 - Fundamental Piezoresistance Studies.

Work on developing a fundamental understanding of piezoresistance was initiated at SRI by D. D. Keough and Y. M. Gupta (now at Washington State University) and is continuing at both locations. Key problems were discussed in the section on calibration.

Task 2 - Calibration Problem.

Task 1 naturally culminates in the ability to identify foil environments for which the sensor output can be related to an individual component of applied stress. The key step is then to determine which of these environments can be made compatible with the registration factor requirements and thus are appropriate to DNA's free-field stress measurement problems. This task is most effectively addressed by coordinated efforts between the contractors performing fundamental piezoresistance studies and those performing the finite element inclusion calculations.

IMPLEMENTATION.

Three tasks are required to translate the registration factor and calibration solutions to hardware: develop engineering designs and models, test field performance, and develop emplacement tools and procedures.

Task 1 - Develop Engineering Designs and Models.

Translating the solutions of the registration factor and calibration problems into physical gage packages (coupling materials and emplacement are discussed in Task 3) requires first that sensors with necessary transducing and data transmission capabilities be designed and fabricated. Previous flatpack work at SRI indicates that it will be necessary to consider strain and temperature compensation, foil forming and shaping procedures, material and dimensional uniformity, and foil/foil and or foil/cable junction properties and fabrication processes. Next, an encapsulent material satisfying the requirements of both the registration factor and the calibration solutions must be obtained, and design and fabrication procedures must be developed that also satisfy required interface conditions. Finally, case design, material, and assembly procedures, again satisfying the registration factor solution requirements in material properties and in interface conditions, must be developed.

As part of this task, various laboratory proof tests such as hydrostatic loading, strain and temperature compensation verification, environmental suscepti- bility, (destructive) quality assurance checks, and small-scale dynamic loading are likely to be necessary. For the final prototype gage packages, the resultant transfer function (registration factor x calibration) should be calculated and compared with available experimental results (hydrostatic tests and small-scale laboratory and field tests).

Task 2 - Evaluate Component Performance.

Field tests larger than those performed in developing the prototype gage packages are required to evaluate component survival and qualitative performance in the environments and times of interest. These may be either dedicated tests or tests of opportunity as long as the loading environments (rates, amplitudes, times, and deformation geometries) are similar to those of interest and no additional deleterious effects are present. For example, a running detonation in a slab of explosive may provide a very useful proof test environment whereas a near surface location in a HEST test in soil probably would not, because of the spatially and temporally nonuniform loads produced by the individual explosive strands in the HEST source.

Many tests address this task, rather than gage validation, in that they generate good testing environments for the gage components but cannot validate the measurement because the test beds are not calibrated (individual free-field stress component histories are not known). These evaluation tests are much less expensive than validation tests and very important to the implementation process, but do not take the place of true validation tests. To emphasize the difference between evaluation and validation tests, we have included evaluation tests (in which absolute stress is unknown) here in the implementation section rather than in the section on Validation.

Both uniaxial and divergent flow field evaluation tests are recommended. Task 2 could be performed at a low cost to the program by making efficient use of DNA/AFWL tests of opportunity.

Task 3 - Develop Emplacement Techniques.

We will need to develop a coupling material as well as procedures for excavating the inclusion cavity and emplacing the coupling material and gage package. Specific requirements depend on the results of the previous tasks.

However, if circular boreholes do not generate satisfactory registration factor characteristics, a slot cutting and filling capability will be necessary. Initial work on this problem for cemented sand matrix material performed by NMERI as part of CIST 23 would provide a good starting point. It will be important to develop techniques for each of the material classes of interest and to take into account the typical inhomogeneities characteristic of the in-situ materials.

VALIDATE FOR INTENDED APPLICATIONS.

Three basic validation steps are suggested: validate specific free-field stress measurement systems in their intended environments, establish sensitivity to nonideal conditions, and test for overall and internal velocity equilibration. This ordering reflects relative importance rather than suggested chronology.

The first step, validation of stress measurements by comparing the measurement with the actual free-field stress history is crucial but is missing from most stress measurement system development proposals, for a very good reason: calibrated test beds are generally unavailable.

The only dynamic calibratable stress testing environment of which we are aware is uniaxial strain deformations. For this case, measurements of mass element motion histories, in conjunction with the partial differential equation expressing the conservation of axial momentum, are sufficient to determine Lagrangian axial stress histories. SRI has been a pioneer in performing such Lagrange analyses and has recently made significant additions to its computational capabilities in this area. The first step (Task 1, below) is thus to perform uniaxial strain, axial stress, validation tests.

The next step of Task 1 is to attempt validation of transverse principal stress measurements in uniaxial strain. The axial stress results from the uniaxial strain test are first used to partially evaluate matrix material constitutive relations and the finite difference and finite element computations performed in other parts of the program (these will have already been tested against other, smaller scale tests in those parts of the program). The partially validated constitutive relations and the two types of codes can then be applied, and iteratively adjusted, to predict the transverse principal stress measurement results in the uniaxial strain validation tests. The transverse stress measurements are not validated by this procedure, but the results are made consistent with the state of the art of computational and modeling capabilities.

A direct transverse stress validation is generally not possible because the transverse stresses are neither known nor usually determinable. (A special case is an elastic matrix material, for which transverse stresses can be calculated.) Validation now requires that constitutive relations be iteratively adjusted against various experiment results. Static uniaxial strain validation results (transverse and axial stresses) from the registration factor task may greatly simplify this problem.

The second recommended validation step, Task 2, is to extend the results to divergent one-dimensional flows. In these cases, the conservation of linear momentum relation does not permit an individual stress component to be precisely determined from measured motion histories, because both radial and hoop stresses contribute to motion and cannot be resolved. Nevertheless, the momentum conservation relation is still a key tool in the recommended validation program.

The suggested approach is first to use the finite element computational capabilities, developed and validated in the registration factor tasks and updated in Task 1 of the validation work, to design radial and hoop stress measurement systems for one-dimensional divergent flow environments. The validity of resulting measurements can then be examined in two ways.

The first is simply to use the best dynamic material models (which will include the uniaxial strain validation test data) in finite difference calculations to estimate the stresses. This is an example of depending on constitutive relations and has well known strengths and limitations.

The second is experimental compatibility validation based on conservation of momentum. Well-controlled one-dimensional spherical tests are performed in which motion histories at various Lagrange positions are measured along with radial and hoop stresses. The motion data are, temporarily, assumed to be correct and are used to determine radial momentum histories at various Lagrange positions, providing an independent evaluation of the radial force histories at the positions through conservation of momentum. The radial force, however, depends on both the radial and the hoop stresses through radial stress gradient and stress difference terms. The two stress component measurement sets are used to evaluate these terms and check for consistency with the motion data using analyses of the type SRI has pioneered and used extensively.

We call this compatibility validation because the results of two stress component measurements are examined together, rather than independently. In principle, such tests allow the possibility of compensating errors in case of

78

agreement with motion measurements; in the case of disagreement, they do not indicate which measurement is at fault.

Both the constitutive model and compatibility validation methods have limitations. Again, as in the case of transverse stress measurements in uniaxial strain, since direct validation is not possible, an iterative approach is the suggested alternative. The results of the two uniaxial and one divergent one-dimensional free-field validation techniques, in conjunction with the measurement system mechanical and piezoresistant modeling studies and their independent static and dynamic tests, provide as wide a base for such boot strapping as is currently possible. Below we describe four tasks to perform the validation steps listed in the first paragraph of this section.

Task 1 - Uniaxial Strain Validation.

Static to moderate strain rate tests should be performed to the maximum stress levels and strain rates available in laboratory testing machines. If end and side wall frictional effects are controlled and external axial and confining stresses are measured, these tests provide calibrated quasi-static test beds for any stress component of interest in uniaxial strain.

Dynamic uniaxial strain field tests with appropriate stress levels and test times are the cornerstone of this task and the whole program. The first step is to develop an appropriate planar source because running detonations in slabs produce two-dimensional flow, and HEST sources (due to their nonuniform explosive distribution) produce spatial and temporal flow oscillations to unknown depths in the test bed. This step may take several forms such as determining valid test depths in specific HEST/test material configurations, the development of satisfactory initiation and explosive distribution configurations analogous to plane wave lens/HE slab systems used in uniaxial strain experiments at smaller scales, or the development of new planar sources such as large gas guns.

Next, appropriate motion measurement gages need to be developed and/or validated for the various ground shock environments of interest. This task is also critical because stress gage validation depends on the credibility of the motion data. Although motion measurements are much simpler, in principle, than stress measurements, there are well known problems with gages such as accelerometer canisters and mutual inductance probes that require a dedicated effort to this program element.

Finally, test design and construction techniques must meet the requirements to ensure uniaxial flow in these validation experiments. Thus dimensions must be adequate to produce the desired uniaxial flow testing durations, and material uniformity requirements must be given high priority in assembling the beds, installing the measurement systems, and performing the tests.

Analysis efforts include the Lagrange analysis for axial stress validation, the updating of constitutive relations and finite element calculations, and iterations with results of other tasks to maximize the accuracy of transverse stress measurement procedures as discussed previously.

Task 2 - Divergent One-Dimensional Strain Validation.

This task was addressed by the effort to perform an initial spherical experiment in dome salt described in the body of this report. The test is termed initial in the context of a stress gage development program in that current measurement systems are being tested, and the program suggested here is expected to result in different designs. Nonetheless, the test is useful not only for evaluating current designs but also to (1) provide experimental data for checking finite element simulations and (2) develop guidance on sources and motion measurements for other spherical validation tests in different materials and with modified measurement systems.

In addition to spherical validation tests, this task requires the analyses discussed under Background. These include finite difference calculations using updated constitutive relations, spherical Lagrange analyses, finite element measurement system simulations, and finally iterations among these.

Task 3 - Sensitivity Tests.

This task to check system sensitivity to nonideal loads can be accomplished by appropriate add-ons to tests in Tasks 1 and 2 above or in the dynamic registration factor tests.

Task 4 - Test For Overall and Internal Velocity Equilibration.

It is assumed that the measurement systems move as would a mass element of the native material at that location in the absence of the measurement system. Because of the inclusion shape and the impedance mismatch between the inclusion and native material, this assumption should be verified. Finite difference computations are recommended as a first step. If the calculations indicate that potential problems exist, then experiments are needed both to define properties, such as interface

80

conditions, needed as input for high fidelity calculations, and to validate the computations.

In addition to the motion of the overall system, it is desirable to examine the internal component motions, for example, to identify possible failure mechanisms or deviations from geometries assumed in the registration factor tasks. Again, finite difference calculations are an appropriate tool. For ease of exposition, these calculations are listed in this task; however, they will probably be initiated earlier in the program in the development and implementation stages.

DOCUMENT PROGRAM RESULTS.

A program of the type described here will generate individual agency final reports and will suggest standardized procedures for developing measurement systems. Therefore, the program should produce a dynamic free-field stress measurement handbook that promotes standardization of development procedures, uses a modular format to facilitate updating, and casts the research findings into relations facilitating applications to new materials.

APPENDIX B

. VOLTAGE-TIME WAVEFORMS

The raw data from the 18 ytterbium stress sensors are presented in Figures 35 through 43. The caption on each figure lists the hole number, the planned radial distance (the probable actual radial distance as determined from TOA data), the flow parameter being measured, the gage number, and the ytterbium sensor/grid number. For example, 1S1, 4.21 m (4.4 m), σ_θ, gage 10, grid 1 designates the first grid of gage 10 oriented to measure tangential stress in hole 1S1 at a planned radial distance of 4.21 meters and an actual distance of 4.4 meters. Voltages shown are those at the output of the uphole amplifiers, which were generally set for a gain of unity.
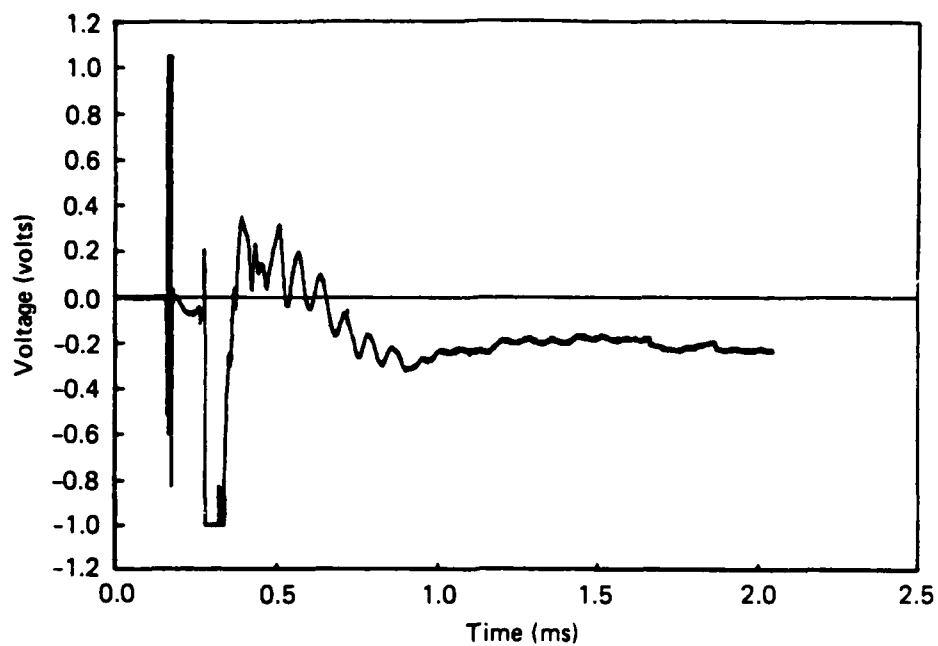
(a) 4.21 m (4.4 m) σ_θ, gage 10, grid 1.
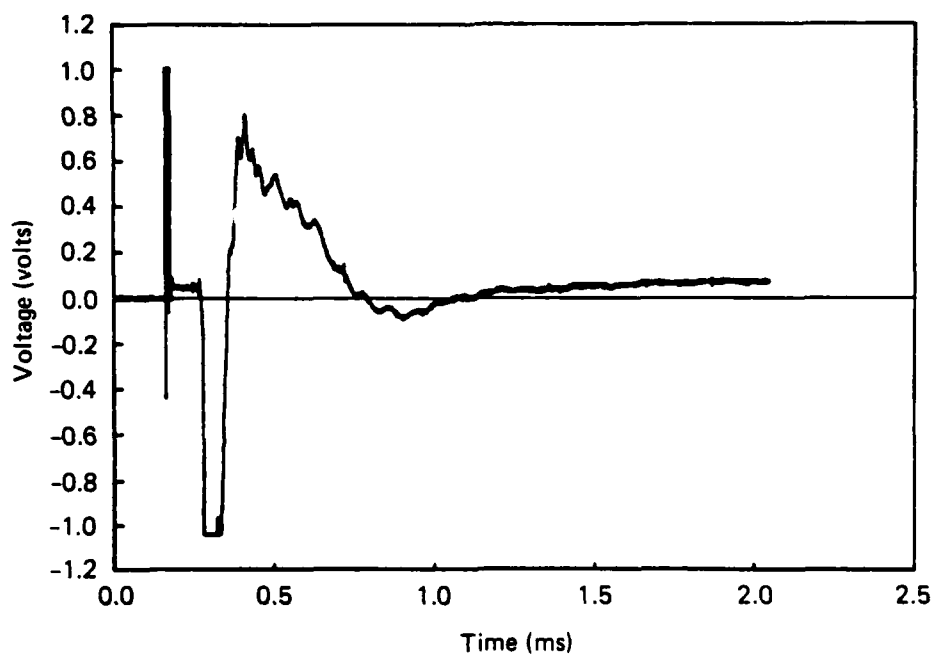
(b) 4.21 m (4.4 m) σ_θ, gage 10, grid 2.

JA-4460-23

Figure 35.   Voltage histories for hole 1S1.

84
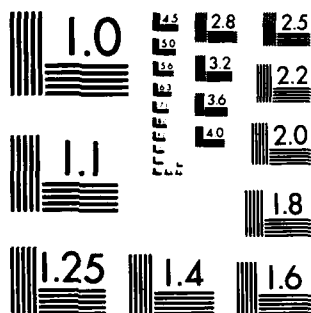
MICROCOPY RESOLUTION TEST CHART
NATIONAL BUREAU OF STANDARDS-1963-A
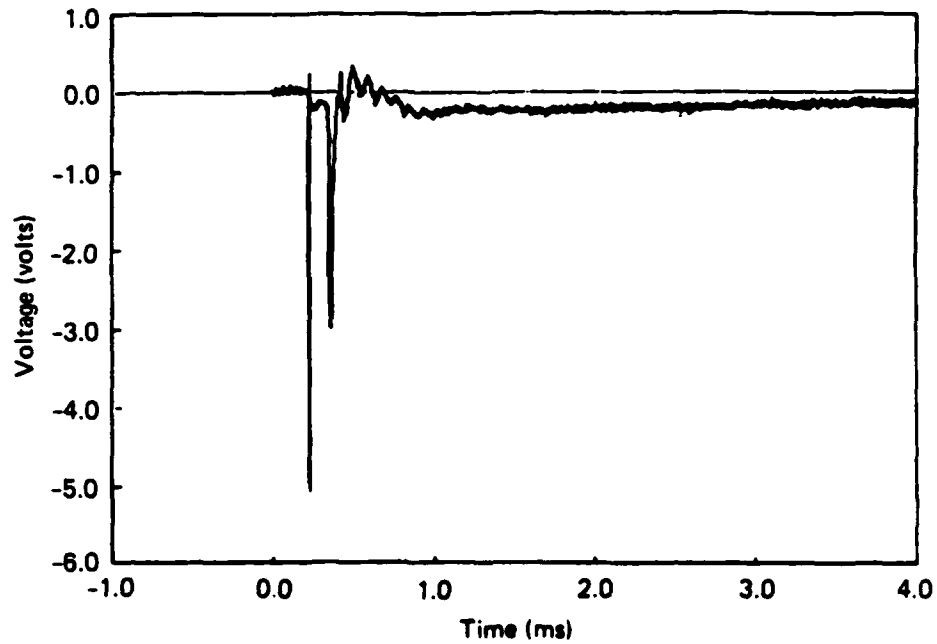
(a) 4.2 m (4.9 m) σ_r, gage 6, grid 1.
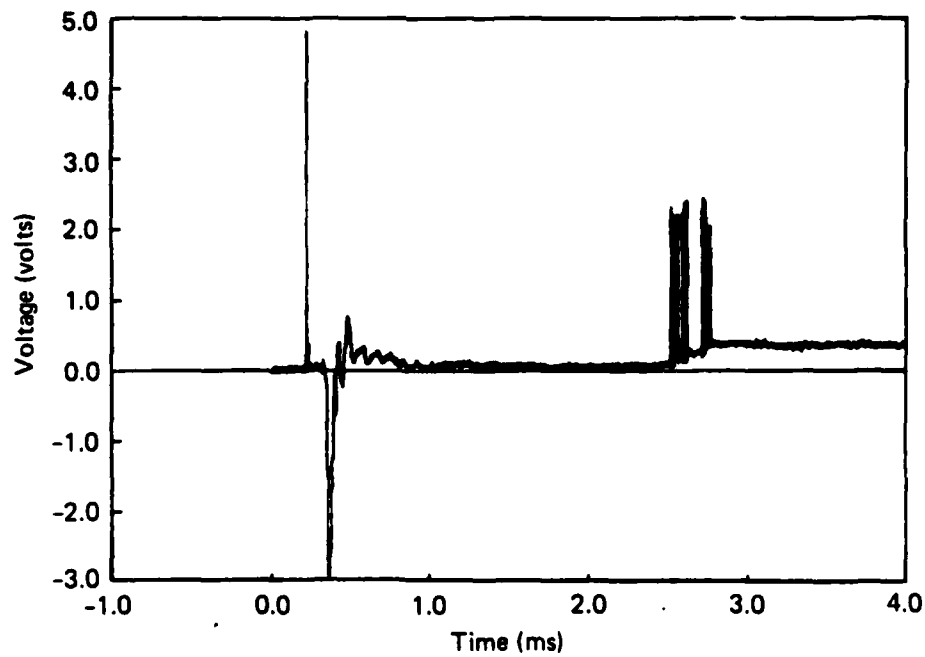
(b) 4.2 m (4.9 m) σ_r, gage 6, grid 2.
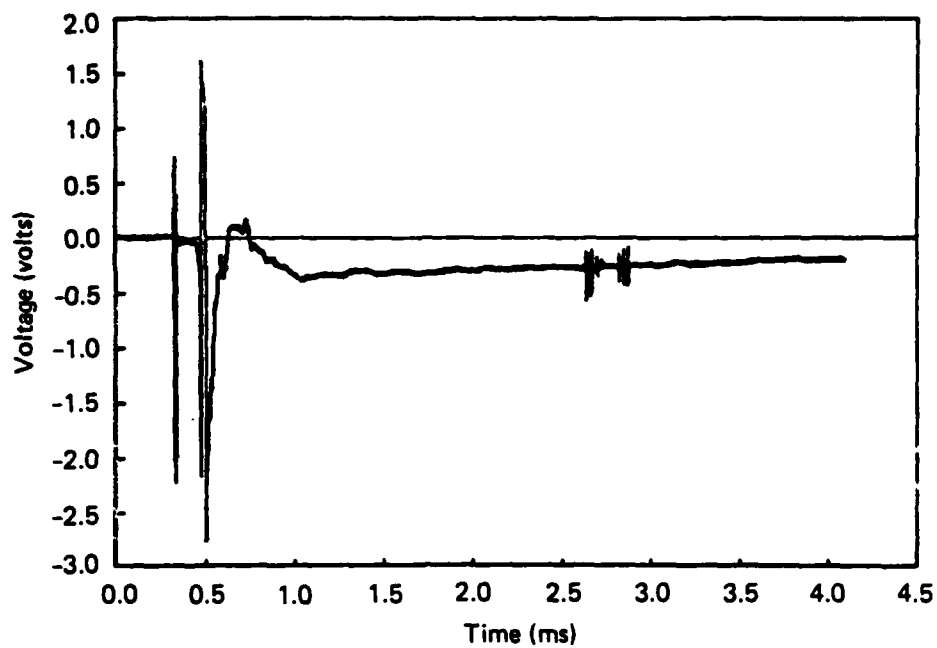
JA-4460-24

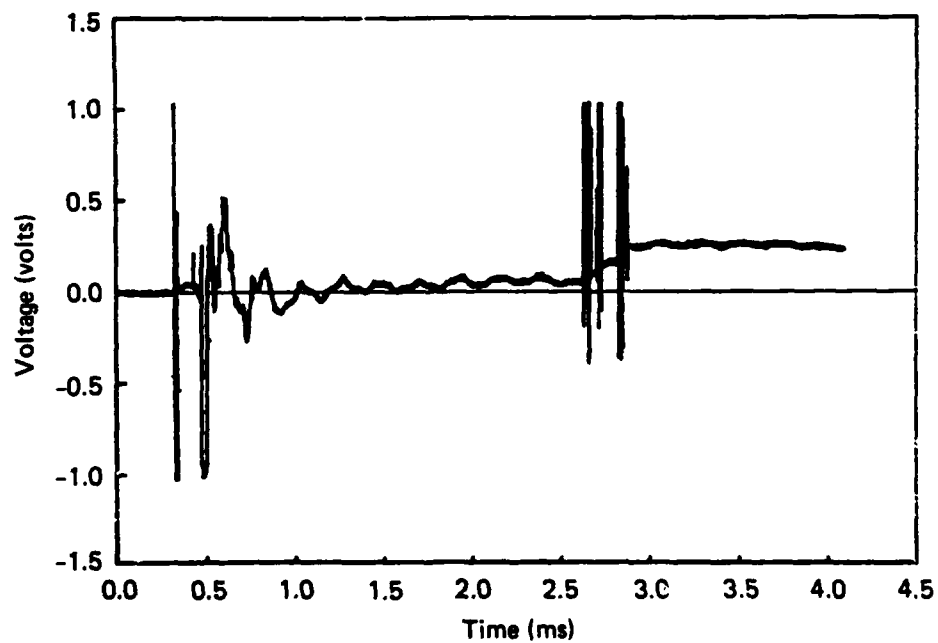Figure 36.   Voltage histories for hole 1S2.

85
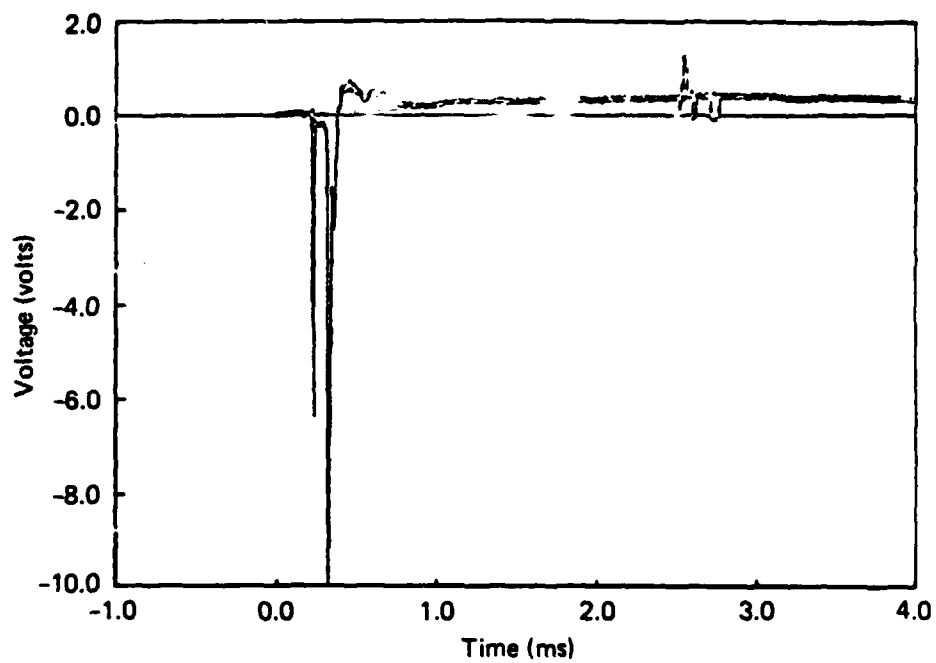
(a) 4.2 m (3.65 m) σ_r, gage 8, grid 1.
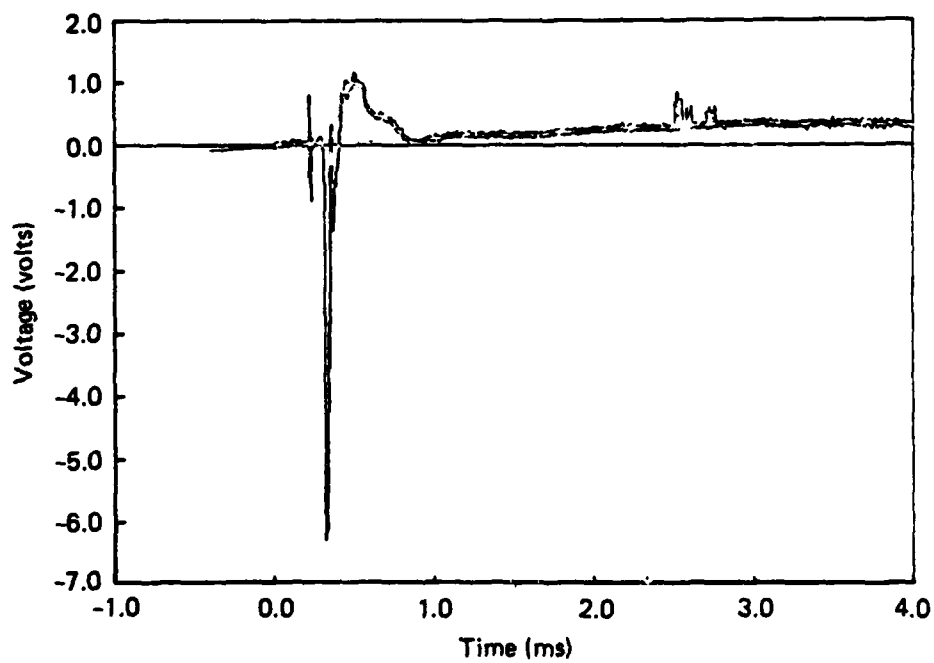
(b) 4.2 m (3.65 m) σ_r, gage 8, grid 2.

JA-4460-25

Figure 37.   Voltage histories for hole 1S3.

86

(a) 6.17 m (5.4 m) σ_θ, gage 12b, grid 1.

(b) 6.17 m (5.4 m) σ_θ, gage 12b, grid 2.

JA-4460-26

Figure 38. Voltage histories for hole 2S1.
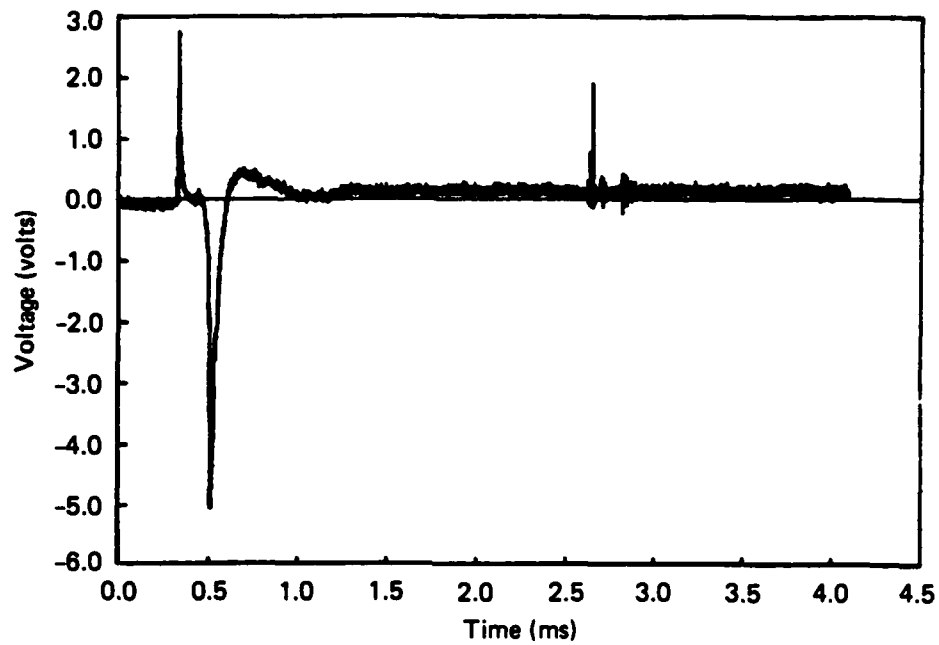
(a) 6.17 m (6.3 m) σ_r, gage 11, grid 1.
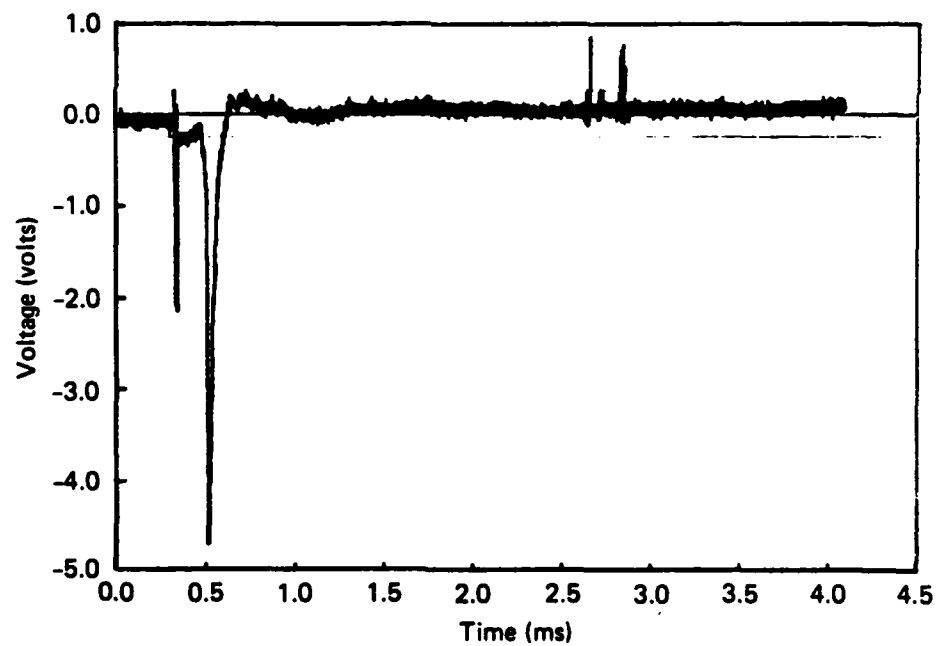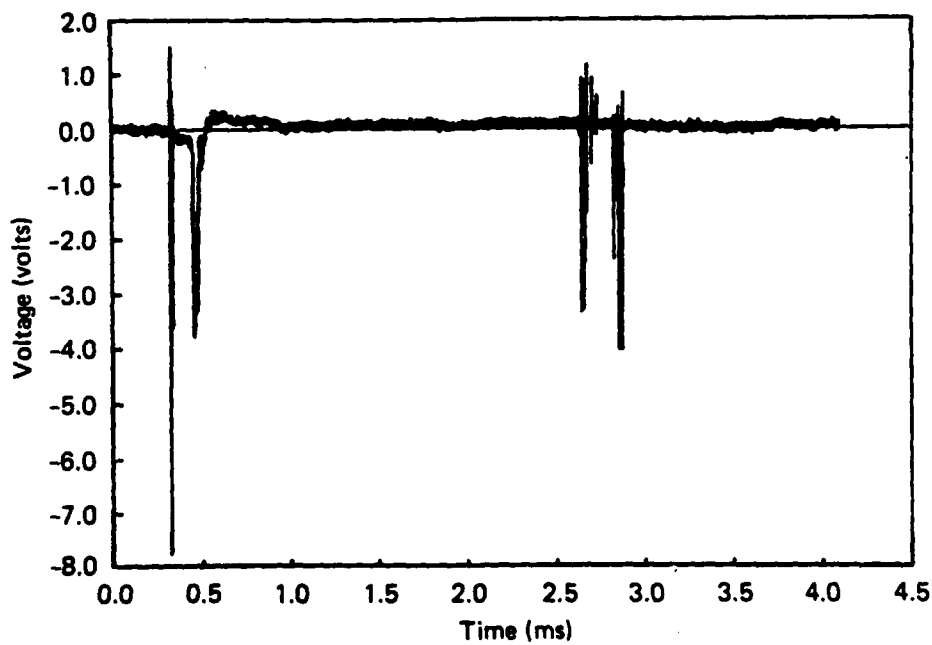
(b) 6.17 m (6.3 m) σ_r, gage 11, grid 2.

JA-4460-27

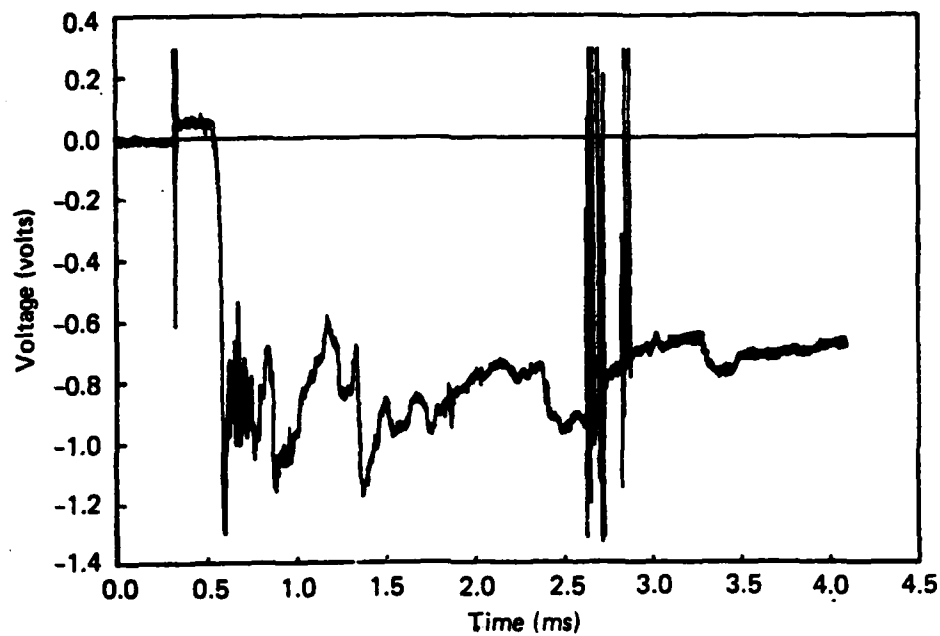Figure 39.   Voltage histories for hole 2S2.
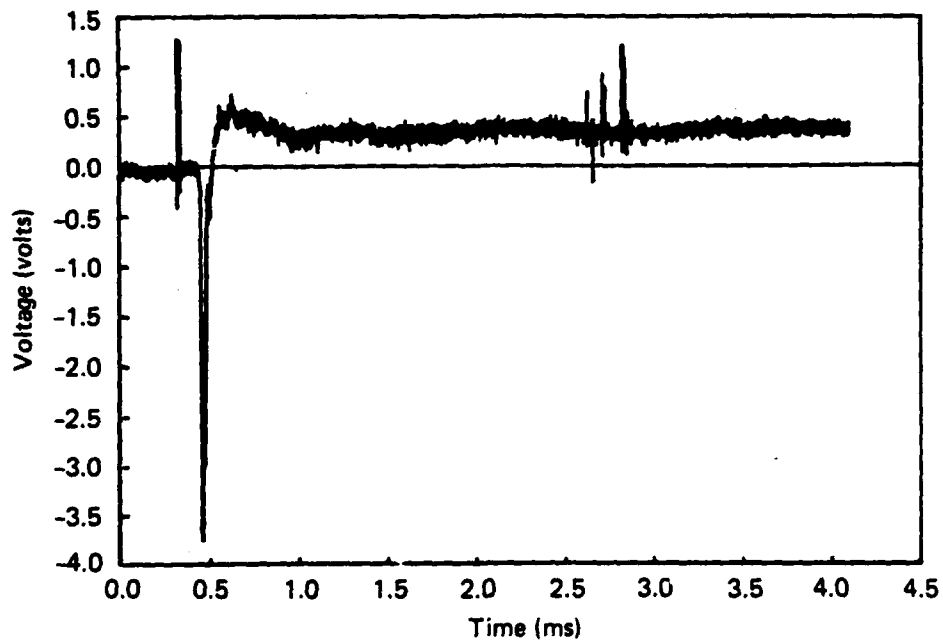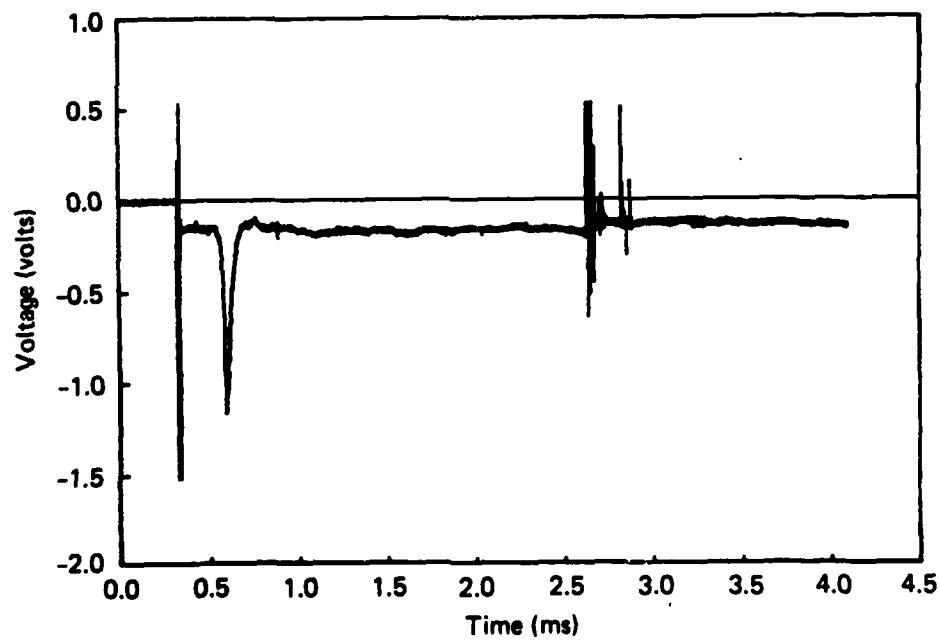
(a) 6.17 m (4.6 m) σ_r, gage 4, grid 1.

(b) 6.17 m (4.6 m) σ_r, gage 4, grid 2.
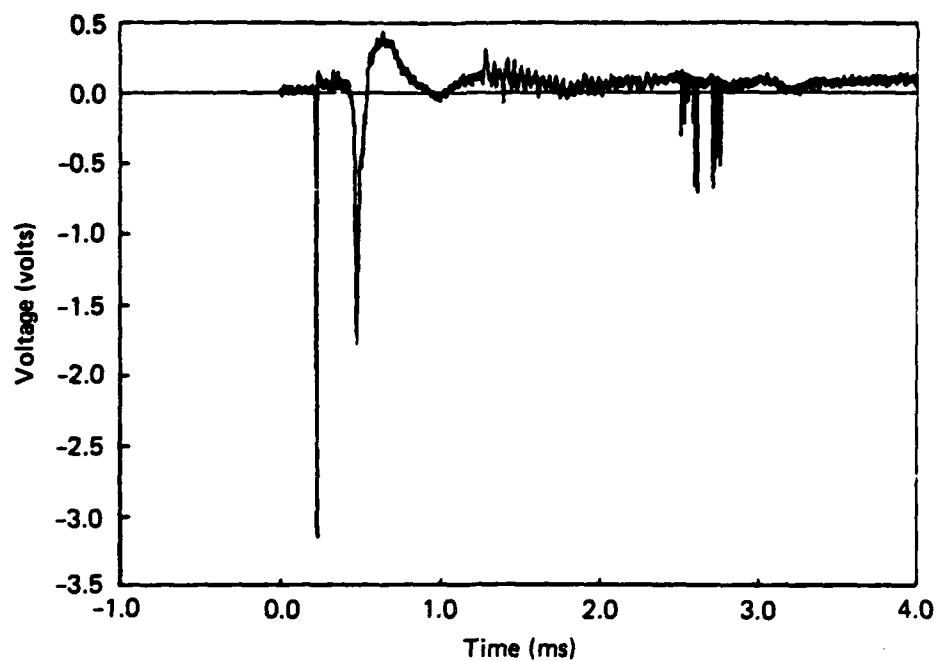
JA-4460-28

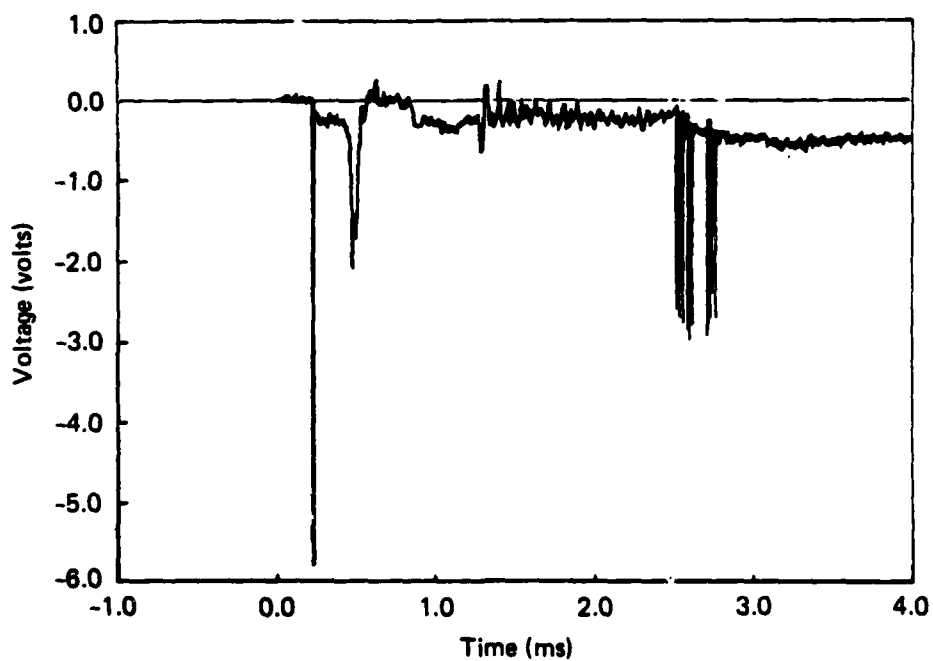Figure 40.   Voltage histories for hole 2S3.

(a) 9.07 m (9.07 m) σ_θ, gage 7, grid 1.

(b) 9.07 m (9.07 m) σ_θ, gage 7, grid 2.

JA-4460-29

Figure 41.   Voltage histories for hole 3S1.

90

(a) 9.07 m (9.07 m) σ_r, gage 1, grid 1.

(b) 9.07 m (9.07 m) σ_r, gage 1, grid 2.

JA-4460-30

Figure 42. Voltage histories for hole 3S2.

91
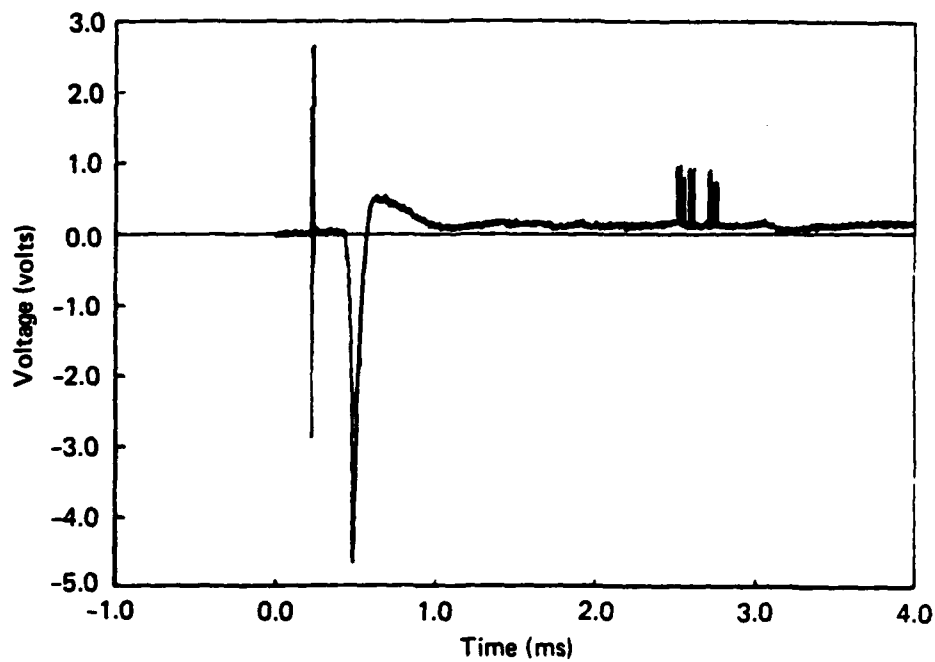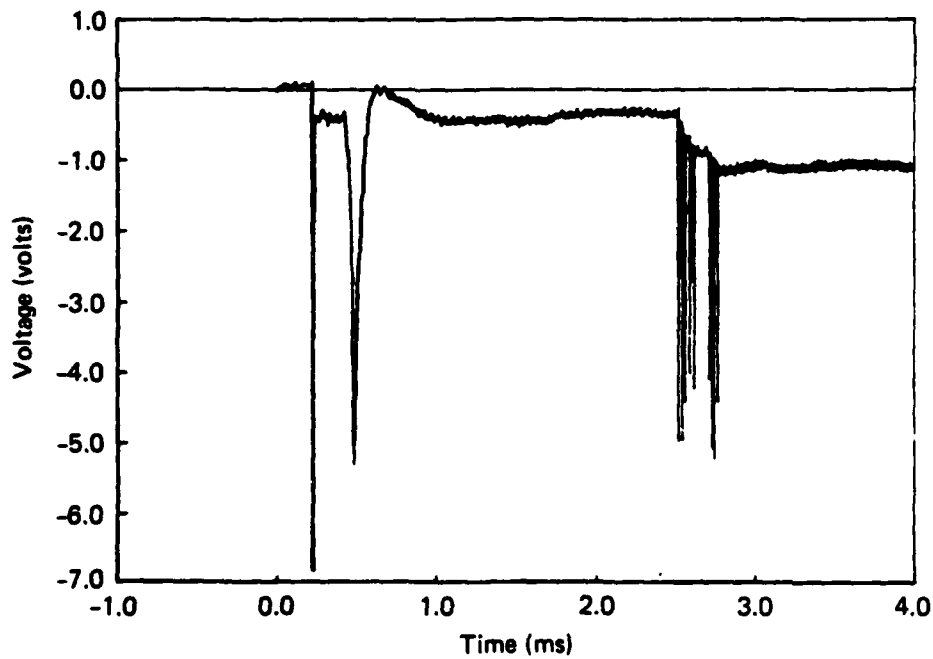
(a) 9.07 m (9.07 m) σ_r, gage 2, grid 1.

(b) 9.07 m (9.07 m) σ_r, gage 2, grid 2.

JA-4480-31

Figure 43. Voltage histories for hole 3S3.

DISTRIBUTION LIST

DEPARTMENT OF DEFENSE

DEFENSE INTELLIGENCE AGENCY
   ATTN: RTS-2B

DEFENSE NUCLEAR AGENCY
   ATTN: SPED
   ATTN: SPWE
   ATTN: TDTR
4 CYS ATTN: TITL

DEFENSE TECHNICAL INFORMATION CENTER
2 CYS ATTN: DD

FIELD COMMAND DEFENSE NUCLEAR AGENCY
   ATTN: FCT
   ATTN: FCTXE
   ATTN: FTTD
   ATTN: FTTD W SUMMA

FIELD COMMAND/DNA
   ATTN: FC-1

UNDER SECRETARY OF DEFENSE
   ATTN: STRAT & SPACE SYS(OS)

DEPARTMENT OF THE ARMY

HARRY DIAMOND LABORATORIES
   ATTN: SCHLD-NW-P

U S ARMY BALLISTIC RESEARCH LAB
   ATTN: SLCBR-SS-T (TECH LIB)

U S ARMY COLD REGION RES ENGR LAB
   ATTN: CECRL-MAILROOM

U S ARMY ENGR WATERWAYS EXPER STATION
   ATTN: D DAY, WESSE
   ATTN: G P BONNER, WESJV-Z
   ATTN: J INGRAM, WESSER
   ATTN: TECHNICAL LIBRARY

U S ARMY MATERIAL COMMAND
   ATTN: DRXAM-TL (TECH LIB)

U S ARMY NUCLEAR & CHEMICAL AGENCY
   ATTN: LIBRARY

U S ARMY WHITE SANDS MISSILE RANGE
   ATTN: STEWS-TE-N K CUMMINGS

DEPARTMENT OF THE NAVY

DAVID TAYLOR NAVAL SHIP R & D CTR
   ATTN: CODE 1770
   ATTN: TECH INFO CTR CODE 522.1

DEPARTMENT OF THE AIR FORCE

AIR FORCE INSTITUTE OF TECHNOLOGY/EN
   ATTN: LIBRARY/AFIT/LDEE

AIR FORCE WEAPONS LABORATORY
   ATTN: NTE
   ATTN: NTED J RENICK
   ATTN: SUL

AIR UNIVERSITY LIBRARY
   ATTN: AUL-LSE

BALLISTIC MISSILE OFFICE
2 CYS ATTN: ENSN

DEPARTMENT OF ENERGY

LAWRENCE LIVERMORE NATIONAL LAB
   ATTN: L-53 TECH INFO DEPT. LIBRARY

SANDIA NATIONAL LABORATORIES
   ATTN: EDUCATION AND TECH LIB DIV

SANDIA NATIONAL LABORATORIES
   ATTN: J S PHILLIPS
   ATTN: TECH LIB 3141 (RPTS REC CLRK)

OTHER GOVERNMENT

CENTRAL INTELLIGENCE AGENCY
   ATTN: OSWR/NED

DEPARTMENT OF THE INTERIOR
   ATTN: D RODDY

DEPARTMENT OF DEFENSE CONTRACTORS

ACUREX CORP
   ATTN: J SAPERSTEIN

AEROSPACE CORP
   ATTN: LIBRARY ACQUISITION

APPLIED RESEARCH ASSOCIATES, INC
   ATTN: J D'ARCY

APPLIED RESEARCH ASSOCIATES, INC
   ATTN: R FRANK

Dist-1

BDM CORP
    ATTN: A VITELLO
    ATTN: CORPORATE LIB(UNCLAS ONLY)

BDM CORP
    ATTN: M WINIARZ

BDM CORPORATION
    ATTN: J MERRITT
    ATTN: LIBRARY

CALIFORNIA RESEARCH & TECHNOLOGY, INC
    ATTN: K KREYENHAGEN

CALIFORNIA RESEARCH & TECHNOLOGY, INC
    ATTN: F SAUER

CUSHING ASSOCIATES, INC
    ATTN: V CUSHING

DEVELCO, INC
    ATTN: L RORDEN

GENERAL RESEARCH CORP
    ATTN: E STEELE
    ATTN: R PARISSE

GEO CENTERS, INC
    ATTN: H LINNERUD
    ATTN: L ISAACSON

H-TECH LABS, INC
    ATTN: B HARTENBAUM

IIT RESEARCH INSTITUTE
    ATTN: DOCUMENTS LIBRARY

KAMAN SCIENCES CORP
    ATTN: LIBRARY/B. KINSLOW

KAMAN TEMPO
    ATTN: DASIAC

KAMAN TEMPO
    ATTN: DASIAC

MITRE CORPORATION
    ATTN: J FREEDMAN
PACIFIC-SIERRA RESEARCH CORP
    ATTN: H BRODE, CHAIRMAN SAGE

PHYSICS APPLICATIONS, INC
    ATTN: DOCUMENT CONTROL

R & D ASSOCIATES
    ATTN: J LEWIS
    ATTN: TECHNICAL INFORMATION CENTER

R & D ASSOCIATES
    ATTN: G GANONG

RAND CORP
    ATTN: P DAVIS

RAND CORP
    ATTN: B BENNETT

S-CUBED
    ATTN: D GRINE
    ATTN: LIBRARY

SCIENCE APPLICATIONS INTL CORP
    ATTN: K SITES

SCIENCE APPLICATIONS INTL CORP
    ATTN: TECHNICAL LIBRARY

SCIENCE APPLICATIONS INTL CORP
    ATTN: W LAYSON

SOUTHWEST RESEARCH INSTITUTE
    ATTN: A WENZEL

SRI INTERNATIONAL
  2 CYS ATTN: D KEOUGH
  2 CYS ATTN: D WALTER
  2 CYS ATTN: J ROSENBERG
  2 CYS ATTN: P DE CARLI
  2 CYS ATTN: R MAK
  2 CYS ATTN: A L FLORENCE

TELEDYNE BROWN ENGINEERING
    ATTN: D ORMOND
    ATTN: F LEOPARD

TERRA TEK, INC
    ATTN: S GREEN

TRW INC
  2 CYS ATTN: N LIPNER
    ATTN: TECH INFO CTR,DOC ACQ

WASHINGTON STATE UNIVERSITY
  2 CYS ATTN: PROF. Y GUPTA

WEIDLINGER ASSOC
    ATTN: J ISENBERG

WEIDLINGER ASSOC., CONSULTING ENGRG
    ATTN: T DEEVY

WEIDLINGER ASSOC, CONSULTING ENGRG
    ATTN: M BARON

LMED

8